From Molecular Medicine and Surgery (MMK), K1
Karolinska Institutet, Stockholm, Sweden

INTERPLAY BETWEEN MITOCHONDRIA, PRIMARY CILIUM, DIABETES AND ITS COMPLICATIONS

Noah Moruzzi

Karolinska Institutet

Stockholm 2017

Cover**:** Picture composition showing primary cilia and mitochondria in mouse inner medullary collecting duct cells (top left), primary cilia in kidney tissue (middle) and mitochondria in human dermal fibroblasts (bottom right), Noah Moruzzi.
All previously published papers were reproduced with permission from the publisher.
Published by Karolinska Institutet.
Printed by AJ E-Print AB

ISBN 978-91-7676-494-7

Interplay between mitochondria, primary cilium, diabetes and its complications
THESIS FOR DOCTORAL DEGREE (Ph.D.)

By

Noah Moruzzi

Principal Supervisor:
Professor Kerstin Brismar
Karolinska Institutet
Department of Molecular Medicine and Surgery
Division of Growth and Metabolism

Co-supervisor(s):
Dr. Jacob Grünler
Karolinska Institutet
Department of Molecular Medicine and Surgery
Division of Growth and Metabolism

Dr. Michael Tekle
Karolinska Institutet
Department of Molecular Medicine and Surgery
Division of Growth and Metabolism

Dr. Ismael Valladolid-Acebes
Karolinska Institutet
Department of Molecular Medicine and Surgery
Division of Growth and Metabolism

Dr. Christian Bergamini
University of Bologna
Department of Pharmacy and Biotechnology
Division of Bioenergetics

Opponent:
Professor Placido Navas
University Pablo de Olavide
Department of Molecular Biology and Regenerative Medicine

Examination Board:
Associate Prof. Jorge Ruas
Karolinska Institutet
Department of Physiology and Pharmacology
Division of Molecular and Cellular Exercise Physiology

Professor Per-Ola Carlsson
Uppsala Universitet
Department of Medical Cell Biology
Division of Islet Transplantation and Beta-Cell Regenerative Medicine

Professor Anita Aperia
Karolinska Institutet
Department of Woman´s and Children´s Health

Till min familj

To my family

Alla mia famiglia

ABSTRACT

Diabetes is one of the major health problems of the 21st century. Dysfunction of the insulin secreting pancreatic β-cell together with insulin resistance is central to the pathogenesis of type 2 diabetes mellitus (T2DM). The cause of the disease and the underlying mechanisms linking hyperglycemia to diabetes complications are still unclear. This thesis is focused on two cellular organelles, the mitochondrion and the primary cilium, and their role in the pathophysiological mechanisms of diabetes and its complications.

In the first paper, we studied the effect of hyperglycemia on cell biology and energy metabolism in human primary fibroblasts and endothelial cells. Acute hyperglycemia triggered a metabolic switch from mitochondrial respiration to aerobic glycolysis, which was persistent after prolonged exposure together with reduced ATP/ADP ratio without increase in reactive oxygen species (ROS). An acute decrease in mitochondrial transmembrane potential and cellular proliferation with changes in cytoskeletal reorganization was linked to the increased osmotic pressure induced by hyperglycemia.

In the second and third papers we investigated the effect of hypoxia, a common feature in diabetes, and hyperoxia in pancreatic islets. Here, we found deleterious effects on mitochondrial content, respiration and glucose-stimulated insulin secretion. Preconditioning with the K^+_{ATP} channel opener diazoxide enhanced insulin release, HIF-1α and AMPK activation and improved β-cell survival in response to hypoxia.

In the fourth paper, a role for the β-cell primary cilium in diabetes was reported. We found reduced first phase insulin secretion in ciliary defective cells and islets, and impaired glucose tolerance in a ciliopathy mouse model. These results were linked to impaired recruitment of insulin receptor A to the cilium, necessary for proper insulin signaling. Mitochondrial respiration and glucose uptake was unaffected by cilia impairment. Additionally, *in vivo* evidence of ciliary morphology alteration in the GK rat, a model of T2DM, supported a relationship between ciliary defect and T2DM.

Preliminary results show that decreasing intracellular ATP and increasing mitochondrial ROS production impaired cilia morphology and/or number in two different cell types. Further, cilia were decreased in number with altered morphology in the kidneys of a mouse model of T2DM with diabetic nephropathy, characterized by increased ROS and altered mitochondrial metabolism.

Finally, a reduction of 60-80% in mtDNA content (reported in diabetes) did not affect mitochondrial metabolism, respiration and energy production in two different cell types.

In summary, mitochondrial dysfunctions during diabetes and its complications are most probably due to a combination of hyperglycemia and other factors such as hypoxia, depending on the cells and tissues involved. A proper ciliary/basal body function is necessary for insulin release and signaling in β-cell. Cilia morphology and number can be affected by mitochondrial dysfunction/ROS and thus related to diabetic complications such as diabetic nephropathy.

LIST OF SCIENTIFIC PAPERS

I. Moruzzi N, Del Sole M, Fato R, Gerdes JM, Berggren PO, Bergamini C, Brismar K. Short and prolonged exposure to hyperglycaemia in human fibroblasts and endothelial cells: metabolic and osmotic effects. Int J Biochem Cell Biol. 2014;53:66-76.

II. Ma Z, Moruzzi N, Catrina SB, Hals I, Oberholzer J, Grill V, Björklund A. Preconditioning with associated blocking of Ca2+ inflow alleviates hypoxia-induced damage to pancreatic beta-cells. PLoS One. 2013;8(7):e67498.

III. Ma Z, Moruzzi N, Catrina SB, Grill V, Björklund A. Hyperoxia inhibits glucose-induced insulin secretion and mitochondrial metabolism in rat pancreatic islets. Biochem Biophys Res Commun. 2014;443(1):223-8.

IV. Gerdes JM, Christou-Savina S, Xiong Y, Moede T, Moruzzi N, Karlsson-Edlund P, Leibiger B., Leibiger IB., Ostenson CG, Beales PL., Berggren PO. Ciliary dysfunction impairs beta-cell insulin secretion and promotes development of type 2 diabetes in rodents. Nat Commun. 2014;5:5308.

PUBLICATIONS NOT INCLUDED IN THE THESIS

I. Bergamini C., Moruzzi N., Volta F., Faccioli L., et al. Role of mitochondrial complex I and protective effect of CoQ10 supplementation in propofol induced cytotoxicity. J Bioenerg Biomembr. 2016 Aug;48(4):413-23.

II. Bader E., Migliorini A., Gegg M., Moruzzi N., et al. Identification of proliferative and mature β-cells in the islets of Langerhans. Nature. 2016 Jul 21;535(7612):430-4.

CONTENTS

LIST OF ABBREVIATIONS

AGEs	Advanced Glycosylated End Products
ATP/ADP	Adenosin Tri-Phosphate/ Adenosin Di-Phosphate ratio
BBS	Bardet-Biedl Syndrome
CoQ	Coenzyme Q10, ubiquinone, ubiquinol
ECAR	Extracellular Acidification Rate
ETC	Electron Transport Chain
FA	Fatty Acids
FAD	Flavin Adenine Dinucleotide
FMN	Flavin Mononucleotide
GLUT	Glucose Transporters
IGT	Impaired Glucose Tolerance
NAD^+	Nicotinamide Adenine Dinucleotide Oxidized Form
NADH	Nicotinamide Adenine Dinucleotide Reduced Form
OCR	Oxygen Consumption Rate
OXPHOS	Oxidative Phosphorylation
PGC1α	Peroxisome Proliferator-Activated Receptor γ Coactivator 1α
ROS	Reactive Oxygen Species
T1DM and T2DM	Diabetes Mellitus Type I and II
TFAM	Mitochondrial Transcription Factor A
$\Delta\psi_m$	Mitochondrial Intermembrane Potential

1 INTRODUCTION

1.1 DIABETES

1.1.1 Epidemiology of Diabetes

Diabetes mellitus (DM) is defined as a group of genetic, metabolic or acquired conditions that manifest with hyperglycemia. The growing diabetic epidemics affect around 347 million people worldwide and can be linked to increased food intake, overweight and sedentary lifestyle. In 2012 diabetes was the direct cause of 12 million deaths (fourth leading cause in Europe (1)) and this figure is predicted to rise by 50% in the coming 10 years. The majority (80%) of death takes place in countries with low or middle income and is mainly due (50-80%) to the cardiovascular complications of diabetes (2). Moreover, chronic diabetes complications are major health issues, especially in those countries with insufficient healthcare to provide awareness and pharmacological aid. In fully developed countries, these complications are better contained but nevertheless diabetes is an extreme economic burden on society. In Sweden the diabetes healthcare uses 8% of the total resources (3). Of special concern is the emerging of adolescent type 2 diabetes mellitus (T2DM) (4), which is associated to the increase in children obesity.

1.1.2 Classification and Diagnosis

Until 2009, the diagnosis of diabetes was based only on plasma measurements of glucose. The cut off levels included fasting glucose >7mM (126mg/dl) or >11mM (200mg/dl) 2h after oral glucose tolerance test (OGTT), or the same concentration in patients with symptoms of hyperglycemia. From 2009, an international committee of experts recommended to add the value of glycosylated hemoglobin (HbA1c) >6.5% (>48 mmol/mol) as diagnosis of diabetes. The advantages are the absence of fasting procedures and the readout of 2-3 months of glycemic history prior the measurement (red blood cells lifespan). However, the cut-off at 6.5% identifies one-third less cases of diabetes than plasma fasting glucose (5).

Depending on the pathogenesis, diabetes mellitus can be classified in:

- Type 1 Diabetes (T1DM), which includes approximately 5-10% of the total number of subjects with diabetes. It is the most common type of diabetes in children or young adults but yearly incidence is more common in adults. The exact cause is not known, however, in most cases an autoimmune reaction is responsible for the destruction of β-cells in the islets of Langerhans leading to insulin deficiency and the need of insulin treatment to survive.

- Type 2 Diabetes (T2DM), which represents the majority of cases (around 90%) of diabetes. It is the result of a progressive defect in insulin secretion and insulin resistance.

- Gestational Diabetes (GDM) occurs between the 24^{th}-28^{th} weeks of pregnancy and affect around 4-7% of the pregnant women in the United States. It is a form of T2DM, which in most cases disappear after delivery. When present, GDM increases the risk of later T2DM onset.

- Other diabetes types dependent on specific causes (genetic defects, pancreatic diseases, tumors and drug or chemically induced diabetes).

In many cases, especially regarding T2DM, the metabolic derangements that culminate with the manifestation of the disease are recognized before the diagnosis. In fact, a category of people whose glucose levels are too high to be considered normal, although not meeting the criteria for diagnosis of diabetes, is classified as prediabetic subjects. Prediabetes is defined with impaired fasting glucose (IFG) with levels ranging between 5.6 and 6.9 mM (100 to 125 mg/dl) or impaired glucose tolerance (IGT) during OGTT 7.8-11mM (140-199 mg/dl). Subjects with IFG and IGT are at high risk to develop diabetes and cardiovascular disease and have often comorbidity with obesity, dyslipidemia and hypertension (5).

1.1.3 Hormone Biology

Glucose homeostasis is regulated by a crosstalk between pancreatic and gut hormones. In a normal adult, the available glucose stores can meet the energy demands for 12-18 hours, while triglycerides stores are considered 100 times larger. In the pancreas, the endocrine portion is responsible for producing hormones, while the exocrine part is secreting enzymes for digestions of macronutrient derived from the diet. The pancreatic Islets of Langerhans are the functional units producing hormones and consist of α, β, δ, pp or γ and ε cells. The β-cells are the majority of the islet cells and secrete insulin, the hormone responsible for metabolism and fuel storage. The ingestion of carbohydrates is capable to induce half of the postprandial insulin release, while another half is facilitated by gut hormones such as glucagon-like peptide-1 (GLP1) secreted by L cells in the intestine, and in small proportions gastric inhibitory peptide (GIP), secreted by K cells in the proximal intestine, which actions are to slow down gastric emptying, decrease glucagon release and reduce food intake (6, 7). The α-cells are responsible for producing the insulin-counteracting hormone glucagon. Its action during hypoglycemia is to promote glucose release from the liver (gluconeogenesis), and to mobilize fatty acids. The balance between insulin and glucagon determinates glucose homeostasis, fatty acid metabolism and protein preservation. Δ-cells are responsible for

secretion of somatostatin, a hormone acting on both α and β cells regulating their secretion. PP or γ-cells are responsible for producing pancreatic polypeptide, which regulates both exocrine and endocrine secretions, and the ε-cells for secretion of ghrelin, a protein that stimulates hunger.

The insulin secretion process begins with the entry of glucose in the β-cells mediated by GLUT2 and its phosphorylation by the enzyme glucokinase. Thus, the glycolysis is enhanced and increases the pyruvate concentration that, in this cell type, cannot be converted to lactate due to the lack of monocarboxylate transporter (8). Due to the low ATP/ADP ratio in resting β-cells, the pyruvate is rapidly metabolized in the mitochondria with increased electron flux and membrane potential. This increases the level of cellular ATP, which closes the ATP-sensitive K^+ channels. The cell then depolarizes resulting in Ca^{2+} influx through the voltage-gated Ca^{2+} channels. This raise of intracellular Ca^{2+} mediates insulin exocytosis. In this process the mitochondria is one of the key components being both responsible for the production of ATP and indirectly inducing synthesis of amplification factors such as cAMP, GTP, long-chain Acyl-CoA, NADPH and glutamate, that stimulate insulin exocytosis (9).

During diabetes condition, the metabolism of liver, muscle and adipose tissue recalls the fasting state. In fact, the low levels of insulin (in T1DM and late T2DM) and the presence of glucagon in the blood raise the level of fatty acids and ketone bodies that are used as fuel by several tissues, while the liver produces glucose to meet the expectations of the brain and other organs which uses it as preferential substrate. However, the low levels of insulin decrease the glucose uptake by muscle and adipose tissues due to the inability to expose their main glucose transporter (GLUT4) to the plasma membrane. Moreover, the presence of glucagon in the blood drives muscle and adipose tissues to release fatty acids and gluconeogenic ammino acids.

Non-insulin dependent cells and tissues (for example vessels and nerves among others) respond in a total different manner not being dependent on the GLUT4 exposure for glucose uptake. Accumulation of glucose, which can pass *via* the GLUT1 transporter, causes damage in these cells probably involving the mechanisms discussed below (see 1.1.5).

1.1.4 Diabetes Complications

Complications of diabetes can be divided in two major categories: acute and chronic or long-term complications. The acute complications are associated with high mortality and are caused by ketoacidosis, dehydration, respiratory infections, seizures or coma, which occur under extreme conditions of hypoinsulinemia and hypoglycemia or hyperglycemia. The

chronic complications, such as nephropathy, neuropathy, cardiovascular events and retinopathy affect tissues not dependent on insulin receptors or GLUT4 for glucose entry and are associated with high medical costs and low life-quality of diabetic patients. Here, due to the possible role of mitochondria and primary cilia in their pathophysiological mechanisms, we focused on the chronic complications of diabetes.

1.1.4.1 Nephropathy

Diabetic nephropathy develops in 30-40% of patients with T1DM or T2DM and is the strongest predictor of mortality in diabetes (10). The risk of chronic kidney disease is 11 fold increased in T1DM and 3 times in T2DM and raises the risk of cardiovascular disease (11). Even though diabetic nephropathy develops years after the first signs of diabetes, kidney hypertrophy and elevated volume of glomerular filtration increase early after the disease onset (12). Tight glycemic control reduces the onset and progression of diabetic nephropathy in T1DM and in lesser extent in T2DM, suggesting different mechanisms of disease progression. Proximal tubular cells and podocytes seem to be the cells affected first in the process. Some of them undergo apoptosis, while the others change shape and size, reorganizing their cytoskeleton to cover the basement membrane (10).

1.1.4.2 Retinopathy

Diabetic retinopathy is the major cause of blindness in working-age adults. In T1DM the majority of cases are presented as proliferative retinopathy while in T2DM as macula edema, which is a breakdown of blood-retinal barrier and leakage of plasma in the macula (13). If followed for 20 years, almost all T1DM patients and 80% of T2DM develop retinopathy (14). 50% of T1DM patients but only 10% of T2DM develop proliferative retinopathy. This number becomes higher in T2DM patients with severe impairment of insulin secretion. Previously classified as microvascular complication, in recent years neuroretinal degeneration has been found to precede the vascular lesions. Since the retina is a complex organ composed of several cell types interconnected by metabolic and signaling pathways (neurons, retinal pigmented, pericytes, astrocytes, Müller, endothelial and glial cells), it is not yet known which type is involved first in the process (15). Early studies pinpointed hyperglycemia as the trigger of diabetic retinopathy leading to selective degeneration of pericytes and subsequent apoptosis of endothelial cells (16, 17). Moreover, clinical studies report a strong association between increased HbA1c and retinopathy (18, 19). However, recent hypothesis indicate that insulin deficiency is a separate risk factor. In fact, the retina as a whole is now thought to be an insulin sensitive tissue and that hyperglycemia can impair the insulin signaling as in the peripheral tissues (15).

1.1.4.3 Neuropathy

More than half of all diabetic patients will develop neuropathy (20). This is a syndrome that causes demyelination originating from Schwann cells, axonal degeneration and involves the endothelium in close relationship with the neurons (metabolic and ischemic roles). Moreover, an inflammatory process is likely to be involved in the development and progression of this complication, especially in T2DM (21). Diabetic neuropathy does not affect only sensory neurons but also the autonomic nerves resulting in cardiovascular disturbances, gastroparesis, diarrhea, bladder atony and impotence. The classical sensory polyneuropathy affects first long sensory distal neuronal fibers and slowly progresses to the proximal ones. This complication can be totally silent and it can be discovered only by chance (foot care) or because of pain. Not all patients develop neuropathy indicating a genetic predisposition such as polymorphism of aldose reductase activity (22). The focal or multifocal neuropathy is seen more frequently in T2DM after 50 years of age and includes oculomotor nerve palsies, truncal neuropathy, muscle weakness and atrophy (21). Patients with IGT display a milder form of neuropathy that is restricted to small fibers compared to diabetic patients showing that its severity correlates with glucose dysregulation or hyperglycemic spikes (23).

1.1.4.4 Cardiovascular Complications

Cardiovascular disease (CVD) is the major cause of death in diabetes. In fact, T1DM and T2DM increase the occurrence of myocardial infarction 10 fold and 5 fold respectively. This risk is cumulative with the metabolic syndrome. Diabetes is also correlated to an increased risk of stroke, which can be predicted by the glucose history levels (24). Moreover, peripheral artery disease during diabetes causes occlusions and pain especially in the lower extremities, and increases the risk of limb amputation.

1.1.5 Mitochondria and Metabolism as Trigger for Diabetes Complications

The pathogenesis of the chronic complications of diabetes is still matter of debate and intensive studies in order to find valid therapeutic approaches to stop or delay their progression (25). The most prominent chronic diabetes complications are retinopathy in T1DM and CVD in T2DM followed by neuropathy and nephropathy.

It is commonly thought that the complications of diabetes arise mainly, but not only, due to the high blood glucose and its accumulation in the cells. However, some cells or tissues might adjust to, or escape from gluco-toxicity, while others might be affected. The primary difference between cell adaptation and crisis might be the expression of different glucose transporters (GLUT). Nearly all tissues express GLUT1, including human β-cells, with

highest concentration in blood and endothelial cells, astrocytes and cardiac muscle (26). It facilitates the diffusion of glucose across the plasma membrane rapidly equilibrating the sugar concentration between the two sides. The regulation of GLUT1 can be transcriptional and post-transcriptional. Glucose deprivation and hypoxia increase the transcription and stability of GLUT1, while hyperglycemia has no effect (27). In contrast, high glucose causes capillary hypoxia (28, 29) and inhibits stabilization of hypoxic inducible factor HIF-1α interfering with the adaptation to hypoxia (30). These conditions can explain some of the diabetes related complications. Pancreatic β-cells in rodents and epatocytes express mainly GLUT2, which has an extremely high Km for glucose. Other insulin sensitive tissues involved in storage (fat) and utilization (muscle) of glucose, express mainly GLUT4, which is transported from the cytosol to the plasma membrane in response to insulin.

The high glucose concentration in the blood and its consequent accumulation in the cells has been postulated to be responsible for the development of the diabetic complications *via* the mitochondria (31). In fact, Brownlee and colleagues suggested that an increase of mitochondrial metabolism derived from the pyruvate delivery into the mitochondria and subsequent raise of mitochondrial membrane potential ($\Delta\psi_m$) induces an overproduction of superoxide anion. The excess of reactive oxygen species (ROS) that escape mitochondria might inhibit directly the enzyme GAPDH or activating the DNA repair enzyme poly (ADP-ribose) polymerase (PARP). As consequence of the inhibition of GAPDH by ROS and possibly PARP, glycolytic substrates accumulate within cells and feed the pathways upregulated during diabetes complications (32, 33). Although very intriguing, this hypothesis might be dependent on the metabolic state and demand of the cells involved.

An alternative previous theory suggested that changes in pyridine nucleotide balance (especially a reduction in NAD^+/NADH ratio), due to the intracellular accumulation of glucose in permissive cells, is the cause of development and progression of diabetic complications. Williamson and colleagues called this imbalance “pseudohypoxia” because of the similar metabolic characteristics found in response to hypoxia but in presence of normal oxygen tension (34). Excess of glucose entrance into the pentose phosphate and sorbitol pathways, as well as enhanced glycolysis, can increase the NADH and/or NADPH levels in the cells (35). The possibility of re-oxidation might be inhibited in the mitochondria when an excess of substrates or high ATP levels are present and the NADH has to be oxidized *via* production of lactate. In fact, an increase of NADH/NAD^+ is reflected by an increase of the lactate/pyruvate ratio. A small imbalance of pyridine nucleotides can affect several enzymes and pathways such as increase of diacylglycerol synthesis, inhibition of fatty acid oxidation

and prostaglandin production. Further measurements of the redox state of pyridine nucleotides in cytosol and mitochondria of different cell types and tissues using innovative methods would further clarify this mechanism of action described by the authors (36-38).

Although these two theories have gathered much attention as potential explanation for the complications of diabetes, the mechanism behind these complications may be different in different tissues and is still a matter of debate and intense research. The challenge is to develop tools and characterize metabolic changes *in vivo* in the affected tissue, for example monitoring substrate oxidation, ROS production, pyridine nucleotide balance and ATP to understand which the primary impairment is and how to intervene.

1.1.6 Therapies

The introduction of recombinant insulin, improved methods to monitor glucose and pump systems to infuse insulin, strongly reduced the risk of hypoglycemia and extended the life expectancy of patients with T1DM, which is now comparable to that of the non-diabetic population without metabolic syndrome. However, even if a tight intensive glucose control considerably reduced the diabetic complications, the study at 30 years of Nathan and colleagues showed that retinopathy (21%), nephropathy (9%) and cardiovascular (9%) complications are still present (39).

A complete cure for diabetic patients might be the only effective treatment that can abolish these complications. Islets transplantation is limited to the number of islets available (at least until methods for generating functional islets will be available) and the necessity for immunosuppressive therapies. Stem cells, also derived from adult cell progenitors, could become a source of β-cells that can replace the human pancreas (40). However, another limitation in islets transplantation is the poor survival due to hypoxic necrosis. For this reason, research is conducted to find and develop several putative tools, such as for instance islets scaffold, to promote rapid neovascularization (41).

Systemic approaches to decrease β-cell death in T1DM are immunosuppressive drugs, which cannot be used as a long-term treatment. Developing therapies are aiming to partly eliminate the immune cells specifically reacting against β-cell, acquire tolerance to the target β-cell antigens, or quenching inflammation. An intriguing possibility might be the modification of β-cells antigens to allow them to escape their destruction (41).

T2DM patients are initially treated with lifestyle modification to reduce weight and increase muscle mass, with the goal to normalize blood glucose. Treatment failure leads to

pharmacological approach aiming at reducing insulin resistance in the liver and muscle, stimulate endogenous insulin release, reduce glucagon production, appetite and glucose uptake in the proximal tubules in the kidney. Along the traditional agents such as metformin, sulfonylureas, glinides, α-glucosidase inhibitors and glitazones, new treatments are emerging such as glucagon-like peptide-1 (GLP-1) and glucose dependent insulinotropic polypeptide (GIP) receptor agonists, and amylin agonists. If these drugs do not improve the metabolic control, the patients will start insulin treatment, which side effects are weight gain and risk of hypoglycemia.

Several other approaches than improved glucose control have been tested to treat or prevent diabetic complications, but until now without clear success. Therapies aimed at lowering advanced glycosylated end products (AGEs) have been tried but stopped due to their toxicity, even though some testing is still on going. Inhibitors of aldose reductase targeting the polyol pathway were tested in clinical trials during the 80s and 90s but showed no beneficial or collateral effects. At the moment the only inhibitor of the above mentioned enzyme available in the market (Epalrestat) is approved only in Japan to treat symptoms of diabetic neuropathy with some beneficial effects on nerve conduction velocity (42). Protein kinase C (PKC) inhibitors exist but they also affect other ATP-binding kinases exerting toxic effects *in vivo*. Recently, a specific PKC-b inhibitor has shown a potential in reducing endothelial dysfunction and other complications (43). Although animal studies showed beneficial effects of antioxidant supplementation to delay the progression of diabetic complications (44, 45), antioxidant supplementation is still far from being successful as a therapeutic strategy in humans (46).

1.2 THE MITOCHONDRION

1.2.1 Structure and Organization

The mitochondria are organelles composed of a double-membrane structure. The external membrane is permeable to small molecules and ions, which are able to move through proteins called porins, and to bigger molecules, which are actively transported by the translocase of the outer membrane (TOM). The inner membrane contains the components of the electron transport chain (ETC) and the ATPase complex and it is impermeable to molecules that do not possess a specific transporter. Inside the inner membrane the aqueous space called matrix contains all the oxidative pathways (beside the cytosolic glycolysis) that ultimately produce energy.

1.2.2 The Respiratory Chain

1.2.2.1 Complex I or NADH:CoQ Oxidoreductase

Also known as NADH dehydrogenase, it is composed of 45 polypeptide chains with one flavoprotein, FMN and at least 6 iron-sulfur clusters. The iron-sulfur proteins participate in redox reactions in which one electron at a time is transferred, using changes in the oxidation state of the iron atom. Complex I catalyze the exergonic transfer to CoQ of 2 electrons and one hydride ion (H^-) from NADH and one proton from the matrix. In the reaction, 4 protons from the matrix are pumped into the intermembrane space. The CoQ is a small hydrophobic molecule that can diffuse freely in the lipid raft reaching the Complex III where it is oxidized. It acts as an electron bridge between less mobile electron carriers and can accept either one electron (semiquinone QH°) or two (ubiquinol QH_2). Because this molecule transports both protons and electrons, it is very important in the process of coupling between proton movement and electron flux.

1.2.2.2 Complex II or Succinate Dehydrogenase

It is the only enzyme from the Krebs's cycle associated with the inner membrane. It is formed by 5 prosthetic groups and 4 protein subunits: A and B contain 3 iron-sulfur clusters, a FAD and a binding site for the succinate, C and D are integral in the membrane and contain a heme *b* group and a binding site for the CoQ. The heme *b* group seems to be involved in the electron transfer but can decrease the frequency of the electron slip from the system. Other substrates can donate electrons without passing through CI e.g. Acyl-CoA dehydrogenase (to flavoprotein ETF and then to the ETF:CoQ oxidoreductase) and the glycerol-3-phosphate dehydrogenase that reduces the CoQ in a similar way as the succinate dehydrogenase.

1.2.2.3 Complex III or bc1 Complex

Complex III, known also as CoQ:cytochrome *c* oxidoreductase, couples the electron transfer from the CoQ to cytochrome *c* with the translocation of 4 protons for each electron couple. When the heme group of the cytochrome *c* accepts one electron from CIII, the cytochrome moves towards CIV to donate it to the binuclear copper center of this enzyme. The cytochromes are heme-containing proteins divided into 3 classes depending on their absorbance spectra (*a*, *b*, *c*). As for flavoproteins, the standard potential of reduction of the iron atom in the heme depends on its interaction with the side chains of the protein. The cytochromes *a*, *b* and *c1* are proteins that integrate in the inner mitochondrial membrane, while the cytochrome *c* is a soluble protein that binds at the external membrane surface due to electrostatic interactions.

1.2.2.4 Complex IV or Cytochrome Oxidase

This complex transports electrons from the reduced cytochrome *c* to reduce molecular oxygen to water. For every 4 electrons that flow through this complex, 4 protons are moved from the matrix to convert the oxygen into 2 molecules of water. The complex uses the energy from this redox reaction to pump a proton in the intermembrane space for each electron.

1.2.2.5 Complex V or ATP Synthase

ATP synthase is a large enzymatic complex in the inner membrane composed of two distinct subunits, one is integral in the membrane (Fo) and the other is peripheral (F1). F1Fo complex forms a protein channel that couples the transfer of protons from the positive side (intermembrane space) to the negative side (matrix). The F1 subunit alone catalyzes the hydrolysis of ATP while the two together catalyze the phosphorylation of ADP to ATP. The equilibrium of the enzymatic reaction ADP + Pi to ATP is close to zero. However, due to the proton flow directed to the matrix, the ATP molecule is allowed to leave the enzyme after its synthesis.

1.2.3 The Oxidative Phosphorylation (OXPHOS)

The ultimate reaction of the ETC is the flow of electrons from NADH, succinate or other primary electron donors, through flavoproteins, ubiquinone (CoQ), iron-sulfur clusters and cytochromes to reduce the molecular oxygen. These transporters are in order of redox potential and the electrons tend to flow spontaneously along the ETC.

The total amount of protons pumped from the matrix to the intermembrane space is 4 from CI, 4 from CIII and 2 from CIV for each couple of electrons transferred to the molecular oxygen. The resulting energy is called the proton motive force and can be divided into two components. The first component is the chemical gradient due to the different concentration of protons at each side of the inner mitochondrial membrane. The second one is an electrical gradient generated from the charge separation between the two sides. The resulting proton motive force allows the protons to flow back into the matrix through the ATPase at the same time using this energy to convert ADP to ATP.

1.2.4 Replication of Mitochondria

One to three copies of mitochondrial genome per mitochondrion and a total of 1000-10000 per cell are compacted in structures called nucleoids (47, 48), which include mtDNA, mitochondrial transcription factor A (TFAM), mitochondrial single strand binding protein

(mtSSBP) and helicase Twinkle (49). Although much progress in understanding the regulation of mitochondrial genome has been made, the processes of mtDNA expression and replication remains largely unknown.

TFAM is a nuclear encoded transcription factor imported in the mitochondria where it coordinates mtDNA packaging, transcription and replication. TFAM binds to specific mtDNA promoter sites with different affinity and to mtDNA at different ratios depending on the cell types (50). Its binding is very abundant in yeasts (every 15bp) where the TFAM concentration is predicted to be inhibitory, while in human epidermal carcinoma cells it is estimated to bind at every 1000bp (predicted to be stimulatory) (48). It has been shown that the transcription efficiency is similar between 1000bp to 20bp distance between TFAM molecules. At shorter distance (less than 20bp) there is a decline in mitochondrial transcripts, probably due to the packaging of mtDNA that becomes less accessible to the mitochondrial polymerase (51). Not only does the copy number of mtDNA depend on the amount of TFAM, but also TFAM amount depends on the mtDNA copy number (48). The degree to which human TFAM and polymerase are in excess for transcription *in vivo* is unknown.

Recently, another mitochondrial transcription factor that stimulates transcription from the L-strand promoter called mitochondrial transcription factor B (TFBM) has been discovered (52). Following research detected two different proteins in mammals (TFB1M and TFB2M) that interact directly with the mitochondrial RNA polymerase stabilizing the heterodimer complexes and activating the mtDNA transcription in the presence of TFAM (53). Further studies suggested that the two forms are not redundant. In fact, TFB2M has been related to the transcription of mitochondrial genes and mtDNA abundance while TFB1M seems to modulate mitochondrial translation (54, 55).

The mtDNA encodes 37 genes necessary for mitochondrial replication machinery and maintenance. Only 13 of these genes encode for proteins involved in the ETC. Complex II is the sole complex completely transcribed from nuclear DNA. The transcription of mtDNA and other nuclear proteins necessary for mitochondrial functions involve a complex intracellular crosstalk. The nuclear master regulator of mitochondrial transcription is the peroxisome proliferator-activated receptor gamma co-activator 1-alpha (PGC1α). It can integrate cell stimuli and activates key transcription factors such as nuclear transcription factors 1-2 (NRFs), estrogen-related receptor α (ERRα) and peroxisome-proliferator activated receptors (PPARs) (56).

1.2.5 Mitochondria in Diabetes

Over the years, evidence that describes alterations in mitochondrial number, morphology or functions in diabetes has been accumulating. However, whether these mitochondrial changes are cause or consequence of the diabetic condition is under debate. Below are described *in vivo* evidence that link extra pancreatic mitochondrial alterations to diabetes and its complications.

1.2.5.1 Mitochondrial Alterations in Diabetic Subjects

Most of the work in humans, trying to elucidate mitochondrial impairments in diabetes, has been performed in blood cells, muscle and kidney tissues due to ethical reasons and accessibility to the samples.

To consider the spectrum of mitochondrial impairments during diabetes, it is necessary to separate T1DM from T2DM. In the latter, the high comorbidity with obesity and dyslipidemia, as well as insulin resistance, is a confounding factor that may lead to mitochondrial alterations. In fact, it is still not clear whether mitochondrial dysfunctions are cause of, or a consequence of insulin resistance. However, few works have pointed out that, at least in muscle, mitochondrial defects might be a consequence; for example, mice with progressive respiratory defects in muscle are not insulin resistant and mitochondrial impairments due to insulin deprivation in streptozotocin treated mice was partially reversed by insulin treatment (57, 58). Moreover, patients with severe insulin resistance due to genetic mutation of the insulin receptor gene display decreased phosphocreatine recovery, which is dependent of muscle mitochondrial metabolism (59). This is in line with another work in which 9 hours discontinuation of insulin in T1DM patients decreased rapidly mitochondrial ATP production and mitochondrial gene expression in muscle tissue (60).

Ritov and colleagues showed that respiration, distribution and amount of mitochondria was reduced in muscle of T2DM subjects and correlated with insulin resistance (61). The same group also found altered mitochondrial morphology in T2DM muscle biopsies similar to obese subject (62). In another work, Patti and colleagues found a reduced expression of PGC1α and NFR in muscle of T2DM and again in insulin resistant prediabetic subjects (63). Moreover, in muscle biopsies, mitochondrial density and gene expression were decreased in offspring of diabetic patients. AKT and IRS-1 phosphorylation levels were suggested to be responsible, since no decrease in mtDNA, PGC1α or TFAM was detected (64). Taken together, these findings indicate a reduced number of mitochondria in muscle of T2DM patients, even though the impact of obesity is still not well understood. The effect of obesity

is important especially considering that a significant proportion of T2DM patients in Eastern countries are not obese. In a recent work studying mitochondrial dysfunction in subcutaneous adipose tissue of T2DM subjects, it was found that non-obese T2DM patients displayed a different pattern compared to obese T2DM patients. The authors found decreased activities of mitochondrial complexes, decreased $\Delta\psi_m$ and phosphorylation capacity in obese subjects and even more pronounced in obese diabetics compared to non diabetic and T2DM non obese patients (65).

In insulin dependent diabetic patients, oxygen consumption supported by palmitoyl-L-carnitine and glutamate in permeabilized atrial fibers showed reduction in V_{max}, which correlates with the amount of HbA1c, without changes in mitochondrial number (66). Metabolomics in urine of T1DM and T2DM showed decreased mitochondria-derived metabolites in diabetic nephropathy along with decreased complex IV amount in kidney biopsies (67) and decreased mRNA transcripts of mitochondrial proteins (68).

Leukocytes of prediabetic patients displayed a decrease in mtDNA copy number, which correlated with glucose during fasting (69). In contrast, Reiling and colleagues using blood or mouth samples from diabetic patients found that mtDNA was not associated with T2DM and/or blood glucose levels (70). This finding was confirmed in monocytes and lymphocytes of T2DM, in which an equal mitochondrial mass but altered morphology, $\Delta\psi_m$ and ROS production have been showed (71). In platelets from TD2M subjects decreased basal respiration, ATP production and an increase in antioxidant enzymes linked to high carbonyl levels have been found (72).

Although results in different tissues, diabetes types and stages may lead to unclear conclusions on the role and features of mitochondria during diabetes in human, animal studies have helped to corroborate some results in humans.

1.2.5.2 Mitochondrial Evidence in Animal Models of Diabetes

Whereas mitochondria have been studied in T2DM patients, little is known about mitochondria in T1DM human tissues and most of the data derive from animal models of the disease. In OVE26 mice 100 days after the exacerbation of diabetes, heart isolated mitochondria displayed decreased respiratory control ratio, ultrastructural changes and modification of mitochondrial proteins (73). Streptozotocin treated rats displayed also abnormal heart mitochondrial morphology, decreased state 3 and maximal respiration. Insulin treatment was able to reverse the defects when it was introduced early after diabetes onset (74). Isolated mitochondria from liver of pancreatectomized rats displayed also decrease in

state 3 respiration in relation to the severity of diabetes (75). In streptozotocin induced diabetic rats a decline in complexes I-III has been shown during nephropathy (76-78). However, 12 weeks old Akita mice did not display changes in gene expression, protein expression or mitochondrial respiratory capacity in kidney tissue (79). The conflicting results could be explained by the different severity and characteristics of nephropathy in Akita mice depending on their genetic background and age (80). Moreover, in streptozotocin rodent models, decreased ATP output from mitochondria has been reported in kidney cortex during nephropathy (81), whereas the total kidney ATP was unchanged albeit 8 days after diabetic onset (82). In summary, mitochondria isolated from heart, liver and kidney of T1DM animal models mostly display dysfunctions in mitochondrial morphology, decrease in maximal respiration and ATP production.

Regarding T2DM models, the most studied are the hyperleptinemic mice db/db. In kidney from 5 month old db/db mice, which develop diabetic nephropathy, an upregulation of complex I protein levels only has been found, along with decreased activity of complex III (83). Persson and colleagues found that in 4 months old db/db mice mitochondrial fragmentation and size was increased along with mitochondrial uncoupling in kidney cortex (84). The accumulation of triglycerides in the heart of 9 weeks old db/db mice increases mitochondrial biogenesis and mitochondrial volume in the heart. Using permeabilized fibers, it was shown a decreased state 3 respiration as well as decreased ATP synthesis and ATPase protein levels. In the same work, a fatty acid mitochondrial uncoupling mediated by UCP and partially ANT was also showed (85). In 16 weeks old db/db animals, reduced amount of mtDNA and OXPHOS activity has been found in muscle oxidative fibers and it was associated with increased intramyofibrillar lipids. However, in the same study the respiratory rates were higher in glycolytic muscle fibers with unaltered fat content (86). Choo and colleagues found that in white adipose tissue but not in liver or muscle, mitochondrial number and function was decreased, and morphology was altered in 12 weeks old db/db mice (87). Another study in 8 weeks old db/db and mice fed on high fat diet showed that the PPARγ agonist rosiglitazone reversed the decrease of mitochondrial gene transcription in adipose tissue (88).

In muscle of high fat fed mice, mitochondrial decrease in number, transcripts, complex I linked respiration and β-oxidation as well as changes in morphology appeared only together with an insulin resistance state. In fact, when the mice were glucose intolerant but sensitive to insulin, no changes in mitochondria were found (89).

The inconsistent results reported above regarding mitochondria in humans and animal models of diabetes, in different types of cells and tissues show how important it is to rule out confounding effects. The most important are the comorbidity of diabetes with other conditions such as obesity, dyslipidemia and hypertension, and the different response between tissues. This is pivotal to understand the mitochondrial metabolic impact as cause of diabetes and its complications.

1.2.6 Mitochondrial and Cellular Oxidative Stress in Diabetes

1.2.6.1 Radical Species and Generations Sites

Radical species are molecules, atoms or ions containing one or more orbital with unpaired electrons. They can be very small molecules or be part of macromolecules such as proteins, lipids, carbohydrates and nucleic acids. Some radical species are highly reactive while others are relatively harmless.

The oxidative stress, and more recently nitrosative stress, can be defined as a perturbation of balance between pro-oxidant and antioxidant systems (90). ROS such as superoxide anion, hydroxyl radical and peroxyradicals, non-radical ROS such as hydrogen peroxide, oxygen singlet, as well as carbon, sulfur and nitrogen radicals are the variety of molecules that can induce cellular oxidative stress (91, 92). Every process that induce a reduction of one electron on the oxygen, produce a radical called superoxide anion. The subsequent or other partial reductions form oxygen singlet, a reactive form with paired electrons. The superoxide anion is continuously generated from some cellular processes, including ETC and microsome. In addition to that, xanthine dehydrogenase/oxidase and other intracellular oxidases can be important sources of this molecule. The ubiquitous presence of superoxide dismutase in cytosol and mitochondria ensure a fast clearance of the majority of this radical, converting it to hydrogen peroxide. Hydrogen peroxides are less reactive and can diffuse far from the site where they are generated. Main targets of this radical are the sulfhydryl group (thiols) part of the glutathione and several proteins. This reaction generates thiol-radicals (93). Hydrogen peroxide can also react with nitric oxide (NO) producing peroxynitrous acid that attacks cysteine, methionine and tyrosine in the protein (94). Transition metals such as iron and copper can react with superoxide anion generating the more reactive hydroxyl radical (95). This radical is considered to be the main toxic agent among the ROS because of its high reactivity with all biological macromolecules. This radical acts close to where it is generated, thus in most of the cases the damage is site specific.

Mitochondria are one of the main ROS generators. Although it was though that 1-2% of their electrons were diverted to generate oxygen radicals, this value has been revised and a lower estimated value has been proposed depending on the mitochondrial metabolic state (96). Eleven different sites with different properties are able to generate superoxide or/and hydrogen peroxide from catabolism and ETC. Complexes I and III are considered the main producer of ROS depending on the ETC state. Moreover, CI is known to produce ROS in the matrix while CIII produces ROS in both matrix and/or intermembrane space, depending on the generation site (90, 96, 97).

1.2.6.2 ROS in Diabetes

Patients with newly diagnosed T1DM followed for 3 years showed increased levels of nitrosative stress in plasma that correlates with the glycemic control (98). Moreover, T1DM patients with short duration of the disease (5-6 years) and no dyslipidemia, displayed decreased total plasma antioxidant levels, increased conjugate dienes and lipid hydroperoxides (99). Lymphocytes extracted from insulin-dependent diabetic patients with variable disease duration, are characterized by increased DNA damage that correlates with serum glucose levels (100). Measuring 8-Oxo-2'-deoxyguanosine (8-OHdG) as marker for oxidative stress in mononuclear cells, Dandona and colleagues found a 6 and 4 fold increase in T1DM and T2DM patients respectively (101). Strong evidence supports the notion of an excess of ROS during diabetic nephropathy (102). However, the site of production is still under debate and late results are challenging the common thought that mitochondrial superoxide is the primary source (103). The actual methods and the difficulty to demonstrate the ROS generation site limit the understanding of the mitochondrial involvement in ROS production (104).

The importance of ROS in the progression of diabetic complications (nephropathy and neuropathy) is further demonstrated by works in which antioxidant treatments were able to delay these complications in db/db mice (45, 84, 105). Cameron and colleagues showed that treatment with the antioxidant β-hydroxitoluene prevents the nerve dysfunction in streptozotocin rats after 2 months of diabetes (106). Mitochondria isolated from retina of streptozotocin mice have increase ROS production and impairment of CIII that was alleviated by overexpression of SOD in transgenic mouse model (107).

1.3 PRIMARY CILIUM

Over the last two decades, primary cilia have emerged as important hubs of cellular signaling. Whereas in invertebrates such as *Drosophila melanogaster* and *Caenorhabditis elegans*,

primary cilia are primarily found in sensory neurons, roughly 80% of the cells in the vertebrate body are ciliated. The primary cilium is a protrusion from the cellular membrane which functions in sensing the extracellular environment (i.e. photoreceptor, olfactory neurons, kidney epithelial cells) and is also involved in several signaling pathways during development and tissue homeostasis (108). Mutation in genes encoding for ciliary proteins cause developmental defects (neural tube closure) for example by altered Hedgehog signaling due to the attenuated signal transduction at the cilium (109, 110). Moreover, disrupting primary cilia or knocking down several genes associated with the ciliopathy Bardet-Biedl Syndrome (BBS) result in an over activation of the Wnt pathway suggesting that the cilium is necessary to restrain this signaling pathway (111, 112). Whereas the importance of ciliary signaling is well recognized during development, the impact of cilia in adult tissue homeostasis is still largely unexplored. Recently, ciliary function has been recognized as important for the mTOR signaling (113-115) and autophagy (116, 117).

1.3.1 Structure

Cilia are assembled and reabsorbed from their distal part or tip. Because there is no protein synthesis in the ciliary compartment, transport mechanisms are essential for cilia formation and maintenance carrying ciliary proteins to and from the basal body (Fig.1). Cargos, which carry the proteins, are actively transported along the axoneme by intraflagellar transport proteins (IFTs). The IFT machinery was discovered first in *Chlamydomonas reinhardtii* and its impairment leads to absence or defects of the cilium or flagellum itself (119). IFT particle B is a multimeric protein complex that mediates anterograde transport to the flagellar/ciliary tip by attaching cargo to cilia-specific kinesin-II motor proteins. Retrograde transport, from the tip to the basal body, is dependent on IFT particle A and cytoplasmic dynein I. At the basal body, several BBS proteins have been implicated in the modulation of ciliary trafficking together with other ciliopathy proteins (120). Two mechanisms are responsible for protein entry into the ciliary compartment: movement of membrane proteins (or receptors) and cytosolic proteins. Some

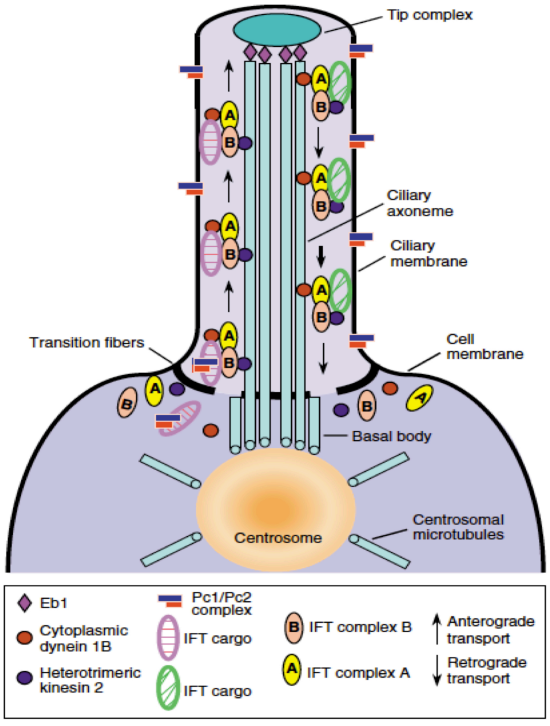

Figure 1. Structure and transport in primary cilia (118).

membrane components can reach the ciliary membrane by moving in the lipid bilayer at the side of the cilium, while cytoplasmic proteins pass through a region called transition zone which is where the basal body transitions to the ciliary axoneme. Here, the structure of the basal body formed by nine microtubular triplets change to the ciliary structure formed by nine microtubular doublets. Recent works have identified different classes of proteins involved in gating cytoplasmic proteins such as ciliopathy gene products, nucleoporins and septins (121, 122). Moreover, entry of proteins above the ciliary size barrier can occur in a similar manner to the one used in the nucleus that involves small G protein Ran (123).

Cilia assembly and disassembly is linked to the cell cycle. They are assembled in G_0-G_1 phase and disassembled before the starting of mitosis. Cilia length and morphology is specific for cell type and tightly regulated. However, cilia length can be modified by several mechanisms including tubulin post-translational modification, IFT proteins, intracellular calcium, guanylate and adenylate cyclase and several signaling pathways such as protein kinase A, MAP kinase and mTOR (124).

As mentioned before, cilia formation, maintenance and function are dependent on molecular trafficking to and along the ciliary axoneme. Kinesin (anterograde) and dynein (retrograde) motors hydrolyze ATP to produce the energy necessary for their movement, while protein sorting and trafficking at the basal body involves GTP/GDP equilibrium (Ras GTPase superfamily) (125, 126). Cellular energy depletion can directly affect motor proteins that use ATP such as kinesin and dynein and GTPases involved in transport and import of ciliary protein such as Rheb and Ras (125-127).

1.3.2 Ciliopathies and the Link to Diabetes

More than 1000 proteins were identified and classified in the ciliary proteome. Current knowledge evidence that mutation in one of the 40 specific ciliary genes give raise to a spectrum of disorder called ciliopathies. The ciliopathies are a heterogeneous class of disorders that displays different or similar phenotypes depending on the original mutation (Table 1). The most common manifestations of the disease are retinal degeneration, renal cysts and cerebral abnormalities. However, two ciliopathies such as BBS and Alström disease present obesity and high comorbidity with diabetes.

BBS is an autosomal recessive disease with prevalence between 1:13.500 and 1:175.000. Up to now, 16 different loci that account for 80% of the syndrome have been identified (128). The clinical manifestations are commonly visible in the first decades of life. Polydactyly affects more than half of the patients and is detected at birth, while the rode-cone dystrophy

presenting as retinitis pigmentosa is present in almost all patients and causes blindness (129, 130). Developmental delay, cognitive defects, speech deficits, ataxia, renal cysts are among the most common signs together with obesity. Truncal obesity is visible in the first year of life on one third of the subjects and present in the majority of the patients later on. It has been suggested that as secondary effect of metabolic syndrome and insulin resistance, these patients develop T2DM (128, 129). An early study described that almost half of BBS patients were affected by diabetes, whereas another work reported diabetic prevalence of 6% (129, 130). However, the authors themselves speculated that an underestimation was possible due to the low number of patients tested. Moreover, the age of the patients can be a discriminant and the diabetic phenotype can be developed at later age.

Phenotype	LCA	SLS	NPHP	MKS	BBS	JBTS
Cerebellar hypoplasia			√		√	√
Encephalocele				√		
Hepatic disease		√	√	√	√	√
Renal disease		√	√	√	√	√
Mental retardation	√		√		√	√
Obesity					√	√
Polydactyly				√	√	√
Retinopathy	√	√	√		√	√
Situs inversus		√	√	√	√	√
Skeletal dysplasia				√		
Cleft palate				√		

LCA, Leber's congenital amaurosis; NPHP, nephronophthisis; BBS, Bardet–Biedl syndrome; SLS, Senior–Løken syndrome; JBS, Joubert syndrome; MKS, Meckel–Gruber syndrome

Table 1. Phenotype spectra of ciliopathies (131).

Alström syndrome is a rare disease (around 300 known cases) caused by a mutation of a gene encoding for a protein (ALMS1) that localizes in the centrioles and basal body and might be involved in calcium signaling (132). The mutation causes developmental retardation without cognitive defects, kidney failure before adulthood and cardiac failure. Moreover, patients can develop T2DM as early as the age of 5 and 82% of the patients over 16 are diabetic (133).

Autosomal polycystic kidney disease has been linked to primary cilium impairment and signaling even though the causal relationship is still not clear (134). The disease has prevalence <5:10000 and is characterized by renal cysts and extra-renal manifestations (135). Dialysis or kidney transplantation is required in these patients. In subjects with normal renal function, it has been reported that OGTT as well as fasting glucose were significantly higher, suggesting lower insulin secretion (136). However, other studies found insulin resistance and a normal plasma fasting glucose (137).

2 GENERAL AIMS

This thesis aimed to study the role of the mitochondrion and primary cilium in the pathophysiological mechanisms of diabetes and its complications. Further, we aimed to clarify the mitochondrial and cellular metabolism in response to different oxygen tension regarding islets function, in the context of therapeutic approaches to improve islets survival during transplantation.

2.1 SPECIFIC AIMS

1. Clarify the mitochondrial and metabolic response to acute and/or chronic hyperglycemia and hyperosmosis in primary human cells. (Study I)

2. Study the effects *in vitro* of hypoxia and hyperoxia on mitochondria, energy metabolism and insulin secretion in pancreatic islets and exploring islets pre-transplantation treatments using diazoxide and high oxygen tension to reduce the negative impact of hypoxia. (Study II and III)

3. Provide a possible link between insulin signaling, diabetes development and primary cilia and elucidate the role of mitochondrial function and cellular energy balance on ciliary maintenance. (Study IV and study V/preliminary results)

4. Understand the impact of mtDNA depletion linked to diabetes on mitochondrial bioenergetics. (Study VI/preliminary results)

3 MATERIALS AND METHODS

3.1 CELL CULTURE AND TREATMENTS

All chemicals were purchased from Sigma-Aldrich (St. Louis, U.S.). Primary Human Dermal Fibroblasts (HDF) and Human Dermal Microvascular Endothelial cells (HDMEC) isolated form healthy donors were purchased from Promocell GmbH (Heidelberg, Germany). To avoid donor specific phenotype, three different donors for HDF and two for HDMEC were used. HDF were cultured in Dulbecco's Modified Eagle's Medium (DMEM) 1g/L glucose, L-glutammine and pyruvate supplemented with 10% heat inactivated FBS (Gibco, Waltham, U.S.), penicillin 100UI/ml and streptomycin 100µg/ml. HDMEC were cultured in endothelial cell growth medium MV supplemented with growth factor (Promocell), penicillin 100UI/ml and streptomycin 100µg/ml. Cells between passages 4-9 or earlier than 20 population doublings were used and media was changed every other day. For experiments performed after one week of treatments (called long-term experiments), cells were incubated with different concentration of glucose or mannitol as follows: control C (5,5 mM glucose), hyperglycemia HG (27,5mM glucose) or hyperosmotic control M (5,5 mM glucose + 22mM mannitol). New batches of media were prepared every other week to avoid sugars concentration errors. Mouse cardiomyoblast cell line (H9c2) were cultured in DMEM 4.5g/L glucose, L-glutammine and pyruvate supplemented with 10% heat inactivated FBS, penicillin 100UI/ml and streptomycin 100µg/ml. Mouse insulinoma cell line (min6m9) were donated from Seino´s lab (Kobe University, Kobe, Japan) and cultured in DMEM 1g/L glucose, supplemented with 10% FBS, penicillin 100UI/ml, streptomycin 100µg/ml and 50µM β-mercaptoethanol (Gibco). Mouse inner medullary collecting duct cell lines (IMCD3) were donated from Berggren´s group (Karolinska Institute, Solna, Sweden) and Lickert´s lab (Helmholtz Center Münich, Neuherberg, Germany). IMCD3 were grown in DMEM F:12 (Gibco) supplemented with 10% FBS, penicillin 100UI/ml and streptomycin 100µg/ml. Human telomerase reverse transcriptase immortalized retinal pigmented epithelial 1 cell line (RPE1) was purchased from ATCC (Manassas, U.S.). RPE1 were grown in DMEM F:12 (Gibco) supplemented with 10% FBS and 0.01 mg/ml Hygromycin B. For all the experiment during confluence, 20000 cells/cm^2 were plated at day 0 and allow reaching confluence until day 4. The same day the cells were starved using 0.5% FBS until day 7. The cells were than treated according to the experiment using the medium supplemented with 0.5% FBS. Human Embrionic Kidney (HEK) 293A and 293FT were used for viral production. 293A were grown in DMEM 4.5g/L glucose, 10% FBS, penicillin 100UI/ml and streptomycin 100µg/ml while 293FT in DMEM 4.5g/L glucose, 10% FBS, 0.1mM MEM (NEAA), 6mM glutamine, 1mM

sodium pyruvate, P/S, geneticidin 500µg/ml.. HeLa cells were grown using the same medium and were used for testing the non-replication of viruses. All cells were incubated at 37° and 5% CO_2 and passaged before confluence.

3.2 MOLECULAR BIOLOGY

3.2.1 Short Hairpin RNA

To silence the expression of genes of interest we designed short hairpin mRNA (shRNA) (Dharmacon siDESIGN centre, GE Healthcare, Munich, Germany). We used the accession number of the genes of interest (NCBI Reference Sequence: *Tfam* NM_009360.4, *Ift88* NM_009376.2) and selected 3 possible candidates (open reading frame ORF and two untranslated region after the stop codon 3´UTR) with high score value after blasting the sequence for *mus musculus*. The oligonucleotides were purchased from Eurofins Operon (Huntsville, U.S.) after some necessary modifications to successfully integrate the double-stranded oligonucleotides into the chosen vector. We changed uridin with thymidine bases and removed the last two uridin bases to avoid degradation of the shRNA. We added to the oligonucleotide sense strand a short sequence (CACC) at the 5´ and an additional guanidine as starting nucleotide. To form the shRNA loop we added a sequence at the 3´ (GAGA). To form the double strand oligonucleotide we designed a complementary oligonucleotide with addition of AAAA at 5´ and the rest complementary to the top strand but the CACC sequence. The shRNA used for the experiments were generated with the oligonucleotides listed in Table 2.

Oligonucleotides	Sequence 5´-….-3´	Strand
Ift88	CACCGTGTTAAACCTGGATCAAATGAGAATTTGATCCAGGTTTAACA	Sense
	AAAATGTTAAACCTGGATCAAATTCTCATTTGATCCAGGTTTAACAC	Antisense
Tfam	CACC GTGTCAAACTAGAACGGATA GAGA TATCCGTTCTAGTTTGACAC	Sense
	AAAA GTGTCAAACTAGAACGGATA TCTC TATCCGTTCTAGTTTGACAC	Antisense
LacZ	CACCGCTACACAAATCAGCGATTTCGAAAAATCGCTGATTTGTGTAG	Sense
	AAAACTACACAAATCAGCGATTTTTCGAAATCGCTGATTTGTGTAGC	Antisense

Table 2. Oligonucleotides used to generate shRNA.

After plasmid delivery into the cells, cellular dicer complex cleaves the transcribed sequence and the 5´ part will bind the mRNA of interest (*Tfam* or *Ift88*). The RNA-induced silencing complex (RISC) will then binds the mRNA complexes and will destroy it, thus silencing the information.

The entry vector kit BLOCK.iT U6 RNAi (Invitrogen, Waltham, U.S.) was used to generate the plasmid for shRNA delivering. The annealing of the oligonucleotides (Table 2) was performed at room temperature (rT) adding: 5µl top and 5µl bottom strands (200µM final

concentration), 2µl 10x oligonucleotides annealing buffer and 8µl DNAse/RNAse free water. The microfuge tubes were incubated 4 min 95° and then at rT 10 min. After brief centrifugation and gently mixing we diluted the oligonucleotides solution 100 times in H_2O (resulting in 500nM concentration) and then again including 10% annealing buffer 10x (final concentration 5nM). The annealed double strand (ds) oligonucleotides were stored at -20°.

Each ds oligonucleotide was inserted into the pENTR/U6 vector. The ligation at rT was performed adding in the following order: 4µl 5x ligation buffer, 2µl pENTR/U6 (0.5ng/µl), 1µl ds oligonucleotides 5nM, 12µl H_2O and 1µl T4DNA ligase. The reaction was incubated 2h and the ligation product stored at -20°. Subsequently, 2µl for each ligation were added to a tube of competent TOP10 E.coli (Invitrogen). The tubes were incubated 30 min on ice and heat shocked 30 sec at 42°, returned on ice for 2 min and 250µl of SOC medium (0.5% yeast extract, 2% triptone, 10mM NaCl, 2.5mM KCl, 10mM $MgCl_2$, sterile glucose 20mM) at rT was added. The tubes were shaken at 200rpm 37° 1h and 100µl of bacteria were spread in pre-warmed agar plates (15g liquid broth (LB) in 600ml H_2O) with kanamycin (0.1mg/ml) as resistance for selection. After overnight incubation at 37°, 3 single colonies for each plate were picked for plasmid expansion and characterization. Each single colony was transferred into a tube containing 5ml LB with 0.1mg/ml kanamycin and left in the shaking rotating incubator at 37° overnight. The day after, 300µl of bacterial suspension and 500µl sterile 80% glycerol in deionized H_20 were used as stock (stored at -80°) and the rest of bacterial suspension for plasmid purification carried out with geneJET plasmid miniprep commercial kit (Invitrogen). The plasmids were sequenced using the primer M13rev (Table 3) to ensure that the ligated sequence was correct.

3.2.2 Virus Generation

3.2.2.1 Recombination

We recombined the shRNA sequence using the entry clone pEntr/U6, in both pAd/BLOCK-iT for adenoviral and pLent/Block-iT destination vector for lentiviral production. The recombination was possible due to the enzyme mix LR clonase that cut two sites flanking the shRNA inserted in pEntr/U6 and recombines it into the destination vector. The reaction was performed at rT by adding and mixing: entry clone 1-7µl (50-150 ng), destination vector 1µl (150ng/µl), sterile Tris-EDTA (TE) buffer, pH 8 up to 8µl (1L: 10ml 1M Tris and 2ml 0.5M Na_2EDTA). The LR clonase was thawed and mixed 2 min on ice, vortexed twice 2 sec and 2µl to each reaction were added. After overnight incubation at 25° the reaction was blocked using 1µl of proteinase K 10 min at 37°. The plasmid was then transferred in competent

E.coli. True expression clones were ampicillin resistant (100µg/ml) and chloramphenicol sensitive (30µg/ml). Preparations from single clones were sequenced using the primers Adenorev and Lentirev listed in Table 3.

Primers for sequencing	Sequence 5´-….-3´
pENTR/U6 (sequencing)	GGACTATCATATGCTTACCG
pAd/BLOCK-iT (sequencing)	CCTTAAGCCACGCCCACACATTTC
pLent/Block-iT (sequencing)	ACCGAGGAGAGGGTTAGGGAT
ORF Mito-PAGFP Forward	NNNGCGGCCGCGCCACCATGTCCGTCCTGACGCCGCTGCTGC
ORF Mito-PAGFP Reverse	NNNGGCGCGCCCTTGTACAGCTCGTCCATGCCGAGAGTG

Table 3. Primers used for sequencing the plasmids to verify the correct insertion of shRNA and to amplify Mito-PAGFP ORF.

3.2.2.2 Adenovirus

The purified pAd/BLOCK-iT destination vector was digested overnight to expose the left and right inverted terminal repeats (ITRs) to allow proper viral replication and packaging (10µg with 3µl of PacI enzyme (Thermo Scientific, Waltham, U.S.).

After purification the cut vector was shuttled into HEK293A (HEKA) cells. We seeded $1.3x10^6$ cells at day 0 in 6 well plates in growth medium with antibiotics. At day 1, we changed the medium adding 1.5ml of the one without antibiotics and transfected the cells adding 1µg of digested plasmid. At day 2, the medium was replaced with complete growth medium and at day 3, cells from each well were transferred into a 10cm dish. The medium was changed every 2-3 days until cytopathic effects (CPE) were observed (between day 10 and 13). In this moment the cells and the medium were collected. To purify the virus, tubes containing the cells and adenoviral suspension were placed at -80° for 30 min and then at 37° for 15 min. This procedure was repeated twice to cause cell lysis allowing the release of all virus particles. The tubes were centrifuged 3000 rpm 15 min and the supernatant aliquot and stored at -80°.

To generate a viral higher titer (10^{7-8} to 10^{8-9}), it was necessary to amplify the crude lysate. HEKA cells were plated 24h before the transduction in 10cm dishes at concentration of $3x10^6$ cells. After addition of 100µl of crude lysate, cells were incubated until the infection reached 80-90%, which was recognizable when the cells have rounded up and were floating or lightly attached to the dish (typically 2-3 days after infection). The virus was harvest as before.

To measure the virus titer, $1x10^6$ HEKA cells were plated at day 0 into 6 well plates. At day 1, virus serial dilutions from 10^{-4} to 10^{-9} were prepared and added to the wells. After overnight incubation the medium was removed and 2ml agarose solution (12ml of prewarmed 37° medium and 1.2ml of 65° 4% agarose) was gently overlaid to the cells. The

plate was returned back into the incubator after 15 min. At day 6-7 another 1ml of agarose medium per well was added. When the plaques were visible (around day 10-14) we applied for each well 300µl of 5mg/ml thiazolyl blue tetrazolium (MTT), waited 3h and counted the plaques. The titer was determined counting the number of plaques using a specific dilution of the virus. The titer was approximately $2\text{-}3x10^8$. Knowing the titer we calculated the multiplicity of infection (MOI), which is the amount of viral particles that will enter one cell (viral particles/cells infected). We seeded IMCD3 cells in a 48 well plates and added different volumes of crude virus. We aimed to have a lowest MOI that give us the best gene knock down (KD), to minimize the possibility of phenotype changes. We used MOI of 0.5-1-2-5-10-20-50 to determinate the optimal degree. We transduced the cells of interest and measure the mRNA KD at the desired time point. We identify in MOI 15 the amount of virus that gives us maximum KD with the minimum amount of virus.

To ensure the replication deficiency of the adenovirus outside their competent cells (HEKA) we seeded $1x10^6$ IMCD3 in 10cm dishes. The day after we added the crude lysate on the cells and the following day we used one new plate of HEKA in which we added again crude lysate and one in which we added the third PBS wash of the IMCD3 cells. After three days HEKA cells treated with crude lysate were not attached while the one treated with the supernatant (third wash) were unaffected. This experiment proved the absence of virus after the wash. Moreover, the fact that the IMCD3 cells after virus treatment did not lyse implied an absence of viral replication.

3.2.2.3 Lentivirus

To produce the virus we used HEK293-FT that stably expresses a hexamer protein allowing optimal virus production, namely dominant-acting oncoprotein derived from the polyomavirus SV40 (SV40 large T antigen) under the control of cytomegalovirus (CMV) promoter. The pLenti6/Block-iT destination vector contains elements required to allow packaging of the expression construct into virions and a blasticidin resistance sequence to allow generation of stable cell line. Moreover, it has a deletion in LTR viral promoter that results in a self-inactivation of the lentivirus after transduction. ViraPower Packaging Mix contains mixture of three packaging plasmids (pLP1,2, VSVG) for structure and replications of the virus.

At day 0 we diluted 3.3µg of ViraPower Packaging Mix and 1.1µg of pLenti-DEST in 550µl Optimem. In a separate tube we diluted 13.2µl Lipofectamine 2000 (Invitrogen) in 550µl Optimem and incubated 5 min. We then combined the solutions and waited 20 min. Next, we

added DNA Lipofectamine complex to the plate containing 2ml of media without antibiotics and pyruvate, and $2.2x10^6$ cells. At day 1, the medium was replaced with 3ml of complete culture medium. At day 4, the supernatant containing the virus was harvested and centrifuged 3000rpm 5 min, aliquot and stored at -80°.

To verify the absence of viruses after the wash we plated $2x10^5$ min6m9 and transduced them. After the overnight incubation, the medium was removed and 1ml of the first and the third wash were added to HeLa cells plated the day before into a 6 well plate ($1x10^6$ in 1ml medium). After two days of incubation the cells were treated with 5µl/ml of blasticidin. After 5 days the cells treated with the third wash were dead while the one treated with the first wash displayed some colonies, showing that after the third wash the medium was free from viruses.

To calculate the rate limiting dilution of the virus (RLD) we used a method similar to the one used for measuring the adenovirus titer. At day 0, we seeded $2x10^5$ HEKA. The day after we diluted 100µl of crude viral stock in 900µl medium adding polybrene, which facilitates the binding between viral envelope and cellular membrane (final concentration 4-8µg/ml). We treated the cells with 600µl (in 12 well plates to increase viral concentration in proximity of the cells) of crude virus diluted between 10^{-3} and 10^{-7}. At day 2, cells were washed 2 times in PBS and the medium was changed. At day 3, cells were split in 6 well plates and the following day the medium was supplemented with blasticidin. Cells were then passaged at low density and after 5 days the formed colonies were stained with MTT or Cristal violet. The RLD is the number of colonies multiplied by the dilution factor (e.g. 10 colonies in 10^{-5} virus dilution = RLD 10^6).

3.2.3 Cloning

Mito-PAGFP (Addgene #23348 (138)) plasmid was used to amplify its ORF with primers listed in Table 3, designed using clone manager (Sci-ED software, Morrisville, U.S.). At the 5′ end of the forward primer we added a sequence compatible with the enzyme cutter NotI followed by a Kosak sequence. In the reverse primer we added at the 5′ end a sequence compatible with the enzyme cutter AscI. We then used 100pg of plasmid Mito-PAGFP and amplified the ORF with Phusion hot start II DNA polymerase (Invitrogen). The product was stored at -20° and 5µl were used to verify the correct amplification of the sequence (agarose gel 1%).

We cut the amplification product at the NotI and AscI sites and purify it (QiaQuick, Hombrechticon, Switzerland). As vector to insert the Mito-PAGFP sequence we used the plasmid pCAG-2A-Arl13b-TagRFP kindly donated from Dr. Ingo Burtscher (Helmholtz

Center Munich). This plasmid contains two cutting sites (NotI and MluI) compatible with the ones we generated outside the sequence of Mito-PAGFP (NotI and AscI). Thus, the plasmid (6-8 µg of vector) was cut using NotI and MluI adding 10µl buffer and 1.5µl each enzymes to 100µl total reaction. The reaction was left at 37° overnight. After DNA purification we loaded 100ng of the cut vector in agarose gel 0.7% to check that the plasmid was singularly cut. To ligate the amplified fragment with the open vector we used in a total volume of 10µl: 200ng vector and 2.5 times of the fragment (calculated in molecules) as follows: Mito-PaGFP (839bp) and pCAG vector (8508bp); amount of insert: 839/8508 x 200 x 2.5 = 49.3 ng. The ligation was carried out overnight at 14° followed by 2h at rT using 1µl T4 ligase (Invitrogen), 1µl T4 buffer and 8µl of the combined vector, insert and water. We then transformed competent E.Coli using 2µl ligation in carbonicillin-enriched plates. The day after, we picked at least 30 colonies, let them grow overnight and made preparation to identify the colonies expressing the plasmid of interest. To do that we cut (2h 37°) the plasmid several times inside and outside the Mito-PAGFP ORF sequence with BSerI restriction enzyme. The predicted band size of the correct ligation pCAG-MitoPAGFP-2A-Arl13b-TagRFP separated in 1.5% agarose gel were 1114, 1316, 1503, 1885, 3529bp while the bands of the plasmid in which the insert did not ligate were 1316, 1503, 3529, 2167bp.

We selected 3 candidates to verify the point mutations of our insert by sequencing. We linearized the plasmids before using them for transfecting the cells of interest, digesting overnight 10µg of the three ligations using the single cutter enzyme ScaI. After purification, 1,6µg of each plasmid were bound to lipofectamine and the solution transferred into the culture dish. $2x10^5$ IMCD3 or min6m9 cells were seeded in 12 well plates the day before the transfection. The transfection medium was changed after 7h with normal growth medium and after 48h 1µg/ml puromycin was added to induce selection.

3.3 METABOLIC ANALYSIS

3.3.1 Seahorse Metabolic Flux Analysis

Metabolic flux analysis was performed using Seahorse XF24 or XF96 Extracellular Flux Analyzer (Seahorse Biosciences, Billerica, U.S.). The cells were incubated at 37°C without CO_2 1h prior all the experiments. Running template for all cellular experiment was: 2 min mix, 1 min wait and 2 min measures.

In Paper I, $1.5x10^3$ HDF or HDMEC/well were seeded and allowed to reach confluence. The day of the experiment the growing medium was replaced with XF medium (as specified by Seahorse bioscience) containing 2mM GlutaMax (Gibco), 1mM sodium pyruvate, glucose or

mannitol (see 2.1), 2% FBS (HDF) or 1.8 ml of MV growth factors (HDMEC). In the acute treatment experiments, we measured the respiration at basal level and after injection of glucose or mannitol. In the long-term treatment experiments, we measured the respiration at basal level in their respective media, and following injection of oligomycin (final concentration 1 μM), carbonylcyanide 4-trifluoromethoxy-phenylhydrazone (FCCP 4-6 μM), and antimycin A (8 μM). Careful titration was conducted to know the concentration of chemicals to use. The high concentration of FCCP and antimycin were due to the presence of serum in the assays, which partially quenches these chemicals. For long-term experiments the data were normalized on the number of cells per well, while for acute treatment data are presented as comparison against basal oxygen consumption rate (OCR) and extracellular acidification rate (ECAR). Normalization was carried out staining the nuclei at the end of the experiment with Hoechst 33342 (Molecular Probes) for 10 min and imaged using BD pathway 855 (BD Biosciences, Franklin Lakes, U.S.) (10x objective, montage 5x4, λex/em 405/425-475). The number of cells per well was quantified using cell profiler software (Broad Institutes, Cambridge, U.S.).

In Paper IV and preliminary data, $3x10^4$ min6m9 cells/well were seeded two days after viral transduction. The day after, the growing medium was replaced with XF medium containing 2mM GlutaMax, and 2% FBS. The respiration was measured before (baseline) and after addition of glucose (11mM final concentration).

In experiments on IMCD3 and RPE1 (preliminary data), 5000 cells/well were seeded and treated (see 2.1). The day of the experiment the growing medium was replaced with XF medium containing 2mM GlutaMax, 1mM sodium pyruvate, 16mM glucose and 0.5% FBS. We measured the basal OCR and ECAR and after injection of different concentrations of oligomycin, rotenone and rotenone + antimycin (4μM final each). Data are presented as comparison against basal OCR and ECAR.

In Paper II and III, 70 size-matched rat islets were washed in XF containing 3,3mM glucose, 2mM GlutaMax, and 1% FBS and plated in a specific 24 well plate for islet measurement (Seahorse Bioscience) with 500μl medium. The total time between preparation and first measurement was between 2 and 3 hours. The running template for the measurement was: 2 min mix, 1 min wait and 4 min measures. We measured the basal OCR and after injection of glucose (final concentration 16,7mM), oligomycin (8 μM), FCCP (1μM) and antimycin A (10μM).

3.3.2 Polarographic Assay

HDF and H9c2 cell lines were allowed to reach confluence, detached, harvested, suspended in their respective media (see 2.1) and assayed for oxygen consumption at 30°C in DMEM 1g/L glucose, 1mM pyruvate, 2mM Glutamax and 2% FBS using a thermostatically controlled 1,6 ml chamber (Instech, Plymouth Meeting, U.S.). After recording basal respiration for approximately 4 min, 35µl of either medium or 1M glucose or mannitol were injected and the respiration was monitored for the following 5 min. Approximately 1.5-2x10^6 HDF and H9c2 were used and counted with hemocytometer.

3.3.3 Glucose Uptake

Two days after viral transduction, 2x10^5 min6m9 cells/well were seeded in growing medium and starved overnight in Optimem. The following day the medium was replaced with Optimem containing 11mM glucose and 5µl/ml deoxy-D-glucose, 2-[1,2-^{3}H(N)] (Perkin-Elmer, Waltham, U.S.) for 1h. The cells were washed 3 times with PBS and 400µl of lysis buffer (1%SDS in 0.1M NaOH) were added. The lysate was shaken for 1h and recollected. The radioactive count was performed using a Wallac 1409 liquid scintillation counter (Perkin-Elmer). Glucose levels were normalized to Accublue DNA determination (Biotium, Freemont, U.S.).

3.3.4 Adenosine and Pyridine Nucleotides Content

Adenosine and pyridine nucleotides were extracted and separated using a modified version of the previously described method (139). For the acid extraction, cells were washed once in PBS and 700µl ice-cold perchloric acid 1M every 10cm dish was added. The plates were immediately frozen on dry ice and store at -80°. Cells were scraped on ice and the suspension collected in microfuge tubes. After centrifugation at 14000xg at 4° 10 min the supernatant was neutralized using KOH 20M and phosphate buffer (50ml 12g KH_2PO_4 and 2.1g K_2HPO_4 pH 7) and returned back at -80° for 30 min. The solution was thawed on ice and centrifuged as before. The supernatant was collected and 50µl were injected in the HPLC. Basic extractions was carried out detaching the cells with trypsin and suspending the cellular pellet in 200µl of H_2O and 20µl of cold solution 0,5M KOH, 50% vol/vol ethanol and 35% wt/vol CeCl. The tube was kept on ice for 5 min and centrifuged at 14000xg 15 min at 4°. 100µl of supernatant was then directly injected in the HPLC.

In Paper I we used a reverse phase Kinetex C18 column 250x4.6mm/5µm (Phenomenex, CA, U.S.) in a HPLC Waters 510 system. Absorbance at 260nm was monitored using a photodiode detector (Waters 996, Milford, U.S.). For measurement on IMCD3 and RPE1

(preliminary results), the separation module used was a Waters 2795 (Waters) equipped with Supelcosil LC-18 15cmx4,6mm/3µm column, guard column and Waters 2996 photodiode array detector 294 (Waters).

The mobile phase used for separation consisted of sonicated and filtered (45µm) Buffer A (23,3mM KH_2PO_4, 1,7mM K_2HPO_4, 10mM tetrabuthylammonium sulfate, pH 5.7) and B (Methanol HPLC grade Promochem, Germany). The gradient used for the separation at 0.7ml/min was linear from A 91.7% B 8.3% to B 27.7% at 24 min and then immediately B 8.3% until 32 min. The day of the experiment the column was equilibrated with 50 column volumes of buffer A and at the end of the day the column was flushed with 10 volumes of water and 10 volumes of water:methanol 70:30.

The peaks were analyzed using Mass Lynx spectrometry software (Waters). The amount of adenosine and pyridine nucleotides were calculated based on standard curve performed using adenosine nucleotides standard at concentration of 100mM.

3.4 MITOCHONDRIAL INTERMEMBRANE POTENTIAL ($\Delta\Psi_M$)

Mitochondrial intermembrane potential was measured in HDF and HDMEC using imaging plates and the same protocol as for the flux analysis. The media was replaced 1h before the measurement with XF media (see 2.3.1) and supplemented with 25nM TMRE (Molecular Probes). The measurements were performed with a LEICA SP5 II confocal microscope (Leica, Munich, Germany), equipped with heating plate station. Microscope settings: objective 40x, zoom x2, 4% laser power to avoid photobleaching and photodamage, 512x512 pixel/image, λex/em 514-565/600, optimized Z stacks, and pinhole 1 Airy. Images were processed with image j software (rsb.info.nih.gov/ij). After identification of the mitochondria ("objects" with intensity >30), the total intensity from objects above 300 voxels was calculated and divided for the total objects area. Three fields for each sample were measured. The data represent three replicates of three individual experiments.

For $\Delta\psi_m$ of mitochondrial network in proximity of primary cilia in IMCD3 (preliminary results), cells were seeded in Ibid 8 well chamber with glass bottom for live recording (Ibid, Martinsried, Germany), allowed to reach confluence and starved (see 2.1). The IMCD3 Arl13b-TagRFP stable cell line was loaded with the potentiometric probe JC-1 (Molecular Probes) at final concentration of 8µM for 20 min. The medium was washed twice before the addition of new medium. Both JC-1 monomer (green) and aggregate (red) can be viewed using λ excitation at 488nm and emission at 505-535nm (green monomers) and 565-650nm (red aggregates). The IMCD3 Arl13b-Venus stable cell line was loaded with 25nM TMRE in

the medium for 30 min prior the assays. Measurements were performed with a LEICA SP5 confocal microscope, equipped with hybrid detectors. Microscope settings: objective 63x, 512x512 and pinhole 1 Airy. Mitochondria as surface objects were localized using the surface tool of Imaris software (Bitplane, Zurich, Switzerland). Using the mean fluorescence per object and the volume of the object we calculated the mean fluorescence/voxel of all cellular mitochondrial network and the mitochondria within 2µM distance from each primary cilium. For JC-1 staining the calculation were done considering the red/green ratios for each object. Every image included at least 5-10 cells.

3.5 CILIARY STAINING

On 12mm diameter glass coverslips in 24 well plates, $2x10^4$ IMCD3 or RPE1 cells were seeded and treated (see 2.1). The day of the experiment the cells were washed once in PBS and fixed using 3% paraformaldehyde (PFA) in PBS at 37° for 10 min. The PFA was removed and the cells washed 3 times in PBS. Fixed cells were permeabilized and the specific protein binding sites blocked using 5% FBS in PBS and 0,1% Triton for 30 min. After washing once, the cells were incubated overnight with primary antibodies against ciliary localized protein acetylated tubulin and ARL13b. The day after, cells were washed 3 times in PBS and incubated with fluorescent secondary antibodies 1h in the dark at rT. After 10 min incubation with PBS containing 1µg/ml DAPI the cells were washed twice and mounted on slides for imaging.

LEICA SP5 II confocal microscope equipped with Hybrid detectors was used for imaging. Microscope settings: objective 63x, 512x512, sequential scan to avoid bleed through (DAPI λex/em 405 425-475, Green λex/em 488 505-535, Red λex/em 555 565-650), pinhole 1 Airy. Zoom, gain and laser power were dependent on the assays. For measurement of ciliary morphology in RPE1 cells Z stack were optimized. Cilia number was counted by visual recognition of both cilia and nuclei. Cilia morphology was measured using Imaris software as follows. After setting the threshold using the red channel (ARL13b), the objects recognized as cilia were analyzed singularly using the CC Bounding box tool, which identifies the maximum length for the long axis of the object.

For ciliary staining in animal kidney slices see section 2.11.4.

3.6 MITOCHONDRIAL CONTENT

3.6.1 Citrate Synthase

HDF and HDMEC were harvested, washed once in PBS and suspended in 400µl (each 10cm plate) of buffer (Tris-HCl 10 mM, KCl 100 mM, KH_2PO_4 5mM, EGTA 1mM, EDTA 3mM, $MgCl_2$ 2mM, pH 7.4). Cells were counted with TC10 Automated Cell Counter (Bio-Rad, Hercules, U.S.) and stored in microfuge tubes at -20°C prior assay. Approximately 1-2x10^4 cells were used for each measurement that was repeated in double for each sample. Three samples were measured at each experiment. 100µl of cell suspension was incubated in a quartz cuvette together with 740µl of Tris-HCl 125mM pH 8, 50µl Triton X-100, 3µl Acetyl-CoA 30mM in water, and 50µl of 5,5'-dithiobis-(2-nitrobenzoic acid) (DTNB) 2mM, under continuous stirring in SAFAS UVmc2 spectrophotometer (SAFAS S.A., Monaco) at 30°C for 3 min. The increase of absorbance at 412nM was measured for 2 min after addition of 50µl freshly made 10mM oxaloacetate solution. Absorbance was then normalized for the cell count.

3.6.2 mtDNA Copy Number and *Tfam* Gene Expression

In HDF and HDMEC cells (Paper I), we measured the ratio between the mitochondrial genes *CYTB* and *16SrRNA* and human nuclear genes *GAPDH* and *RPL32* using qPCR (Applied Biosystems 7300 unit and ViA 7 Life Technologies). For min6m9 and IMCD3 cells (preliminary results) we measured the ratio between the mitochondrial genes *Cox2* and *16SrRNA* and mouse nuclear genes *Hbb* and *18SrRNA*. Briefly, cells were detached, washed in PBS, and suspended in 200µl PBS. Total DNA was extracted using QIamp DNA Blood Mini kit (QiAgen, Venlo, Netherlands) according to the manufacturer's instructions and measured by NanoDrop 2000-C spectrophotometer (Thermo Scientific). PCR reactions consisted of 40 cycles using 4ng of total DNA template in a 20µL volume, containing SYBRGreen Supermix (Invitrogen) and 10pmol of each primer.

Gene expression of Tfam was detected in IMCD3 and min6m9 cells (preliminary results) after mRNA extraction using TRIzol (Invitrogen). Briefly, 1 ml of reagent was added to every well of 12 well plate-containing cells. After 5 min the cells were detached and the suspension added in a microfuge tube containing 200µl of chloroform. The tubes were shaken for 15 sec and centrifuged 12000xg 10 min at 4°. The supernatant containing mRNA was pipetted in another tube containing 500µl isopropanol and left for 10 min at rT. The tubes were centrifuged again as before, the supernatant was discarded and 2 washes with 75% ethanol were performed. The pellet was suspended in 30µl deionized H_2O and the quality and

quantity of mRNA was measured using NanoDrop. For each sample, 1 µg of mRNA was used to generate cDNA using Maxima First Strand cDNA synthesis kit (Invitrogen). qPCR reactions consisted of 40 cycles using 1µl of cDNA template in a 10µL volume, containing SYBRGreen Supermix (Invitrogen) and 10pmol of each primer. qPCR cycles were performed as follow: 15 sec of denaturation at 95°C and 30 sec of hybridization and extension step at 60°C.

The primers were synthesized by Eurofins MWG Operon and are listed in Table 4.

Primers	Forward (5´-…-3´)	Reverse (5´-…-3´)
RPL32	TTAAGCGTAACTGGCGGAAAC	GAGCGATCTCGGCAGAGTAA
GAPDH	ATGGGGAAGGTGAAGGTCG	GGGGTCATTGATGGCAACATTA
mtCYTB	ACATCGGCATTATCCTCCTG	GTGTGAGGGTGGGACTGTCT
mt16sRNA	GGCAGGTCAATTTCACTGGT	AAATCTTACCCCGCCTGTTT
Hbb	AGGCAGAGGCAGGCAGAT	GGCGGGAGGTTTGAGACA
18s rRNA	CGCGGT TCTATTTTGTTGGT	AGTCGGCATCGTTTATGGTC
mt12sRNA	ACCGCG GTCATACGATTAAC	CCCAGTTTGGGTCTTAGCTG
mtCox2	AATTGCTCTCCCCTCTCTACG	GTAGCTTCAGTATCATTGGTGC
Tfam	CAGGAGGCAAAGGATGATTC	CCAAGACTTCATTTCATTGTCG
Hmbs	CGGAGTCATGTCCGGTAAC	GGTGCCCACTCGAATCAC
Tbp	TGCTGTTGGTGATTGTTGGT	CTGGCTTGTGTGGGAAAGAT

Table 4. Primers used for gene expression and mtDNA measurements.

3.7 CELL GROWTH

3.7.1 Count

HDF and HDMEC growth was primarily evaluated by cellular count using TC10 Cell Counter (Bio-Rad). Briefly, HDF (1,5-2,5x10^4) and HDMEC (6-8x10^4) were plated in 10cm Petri dish in triplicate, allow them to attach, and treated (see 2.1). After 3, 5 and 7 days the cells were harvested and counted.

3.7.2 (6-^{3}H)-Thymidine Incorporation

HDF and HDMEC were plated (2x10^3 per well) in a 12 multiwell plate, allowed to adhere and treated. The third day, 3µCi of (6-^{3}H)-thymidine (Perkin-Elmer) per well were added and the cells were incubated 4h. After washing twice with NaCl 0.9%, 750µl of 5% vol/vol trichloroacetic acid was added and the cells incubated 15 min at rT. The solution was then removed, 500µl of 0.1M NaOH were added and the plate slowly shaken for 2h. The solution was then transferred in scintillation tubes, and 4ml of Emulsifier-Scintillation Plus liquid (CiAB, Stockholm, Sweden) was added. The radioactive count was performed using Wallac 1409 liquid scintillation counter (Perkin-Elmer).

3.7.3 Cell Cycle Analysis

IMCD3 and RPE1 cells were trypsinized, washed in PBS and fixed in a microfuge tube by slowly vortexing the cells in 500µl precooled (-20°) ethanol 70%. After storage on ice for 1h, tubes were centrifuged 2 min at 4000 rpm. The pellet was suspended in 500µl PBS and returned 30 min on ice, followed by another centrifugation step. The pellet was suspended in 300µl PBS containing 10µg/ml RNase A, 0,25% Triton X and 20µg/ml propidium iodide. The solutions were transferred in tubes and incubated in the dark for 15 min and then on ice prior measurements. The histograms analyzed using FLOWJO software (Ashland, U.S.) represent the fluorescence collected using PE-Texas Red filter from minimum $2x10^4$ cells . The cell population used for analysis was identified using forward and side scatter and subsequent doublet discrimination (scatter width versus area). Plotting the forward scatter versus the PE-Texas signal we analyzed the typical cell cycle distribution represented by two peaks (G_1 and G_2/M phases) and a valley (S phase). The analyzed peaks were reported as phase's percentage of the total cells analyzed.

3.8 MITOCHONDRIAL AND CYTOSOLIC REACTIVE OXYGEN SPECIES

HDF and HDMEC were seeded in multiwell plates, allowed to reach confluence and treated. After 7 days, cells were washed once with PBS and loaded 1h in DMEM serum-free with 10µM carboxy-methyl-2'-7'-dichlorofluorescin-diacetate (DCFDA, Molecular Probes). Cells were harvested, washed twice with PBS and fluorescence was detected by flow cytometry (Cyan, Beckman Coulter, Munich, Germany). Negative control was performed with unstained cells, whereas positive control was treated 30 min with tert-butyl hydroperoxide at final concentration of 100µM.

In experiment using RPE1 and IMCD3 cells, DCFDA was loaded at final concentration of 10µM for IMCD3 and 2,5µM for RPE1 in their corresponding culture medium. The cells were returned back into the incubator for 30 min than harvested, washed and suspended in 500µl PBS. The measurement has been performed using BD FACSaria III (BD Biosciences).

For all cell types mitochondrial ROS were measured using 2,5µM MitoSOX Red (Molecular Probes) loaded for 1h, followed by the same procedure described for DCFDA staining.

3.9 APOPTOSIS

To measure apoptosis in living cells we used Annexin V-FITC Apoptosis Detection Kit (Abcam, Cambridge, U.K.). IMCD3 cells were trypsinized, washed in medium and suspended in 500µl 1x binding buffer containing 5µl Annexin V FITC and 5µl PI (stock 50µg/ml). The tubes were incubated 5 min in the dark and stored on ice prior the

measurements performed with BD FACSaria III. The population was identified as described above (see 2.7.3). Negative control was performed with unstained cells or either with Annexin V FITC or PI to set the gating. Positive control was performed using pro-apoptotic chemical staurosporin at final concentration of 6μM for 2h. In the resulting graph plotted with FITC versus PE-Texas red, we could identify a double negative population (living non-apoptotic cells), a positive for Annexin V or PI (apoptotic and necrotic cells, respectively) and double positive population (apoptotic dead cells). The results in percentage were normalized on the total cells.

3.10 WESTERN BLOT

Cells were washed in PBS and for every 6cm dish 500μl of ice-cold RIPA modified lysis buffer (150mM NaCl, 50mM Tris-HCl, pH 7.4, 1% NP-40, 1mM EDTA and 0.1% DOC) supplemented with one unit of both Pierce phosphatase and protease inhibitor (Thermo Scientific) every 10 ml. For actin determination the lysis buffer used was 2% SDS in PBS to prevent repolymerization of actin filaments. The plates were scraped and left 15 min on ice. The suspension was transferred in a microfuge tube on ice and vortexed sometimes for 30 min. The tubes were centrifuged at 4° 15 min 18000xg and the supernatant stored at -80° until usage. Protein measurement was performed using Lowry determination (140).

After dilution with loading buffer and reducing agent the samples were boiled for 10 min to allow complete denaturation of the proteins. The samples were allowed to cool down before the loading in 10% polyacrylamide gel. All proteins were transferred in nitrocellulose membrane except WB involving actin (PVDF, GE Healthcare, UK). In gels used to determine actin and mTOR, the proteins were transferred using Bio-Rad wet transfer apparatus, while for the others we used semidry Trans-Blot Turbo apparatus (Bio-Rad).

For actin determination the membranes were blocked 1h in PBS-Tween supplemented with 5% milk powder and blotted using anti-β-actin and anti-γ-tubulin. The membranes were washed 4 times 10 min in PBST and incubated 1h with anti-mouse IgG horseradish peroxidase conjugate (GE Healthcare). After 3 washes the membranes were incubated 1 min with Supersignal West Femto chemiluminescent reagent (GE Healthcare). The membranes were scanned using LAS-1000 EMCCD camera (Fuji-film, Tokyo, Japan).

For all other proteins, the membranes were blocked for 1h at rT using Odyssey blocking buffer (Li-Cor biosciences, Lincoln, U.S.). The membranes were washed 3 times 10 min in TBST and incubated overnight with the appropriate antibodies in Odyssey blocking buffer. The membranes were washed again and incubated 1h in the dark using fluorescent secondary

antibodies (Li-Cor). The membranes were washed again and developed using Odyssey imaging system (Li-Cor). The list of antibodies used is reported in Table 5.

ANTIBODIES							
	SPECIES	DILUTION	COMPANY		SPECIES	DILUTION	COMPANY
β-actin	Mouse	1:5000	Millipore	**Arl13b**	Rabbit	1:1000	Proteintech
γ-tubulin	Mouse	1:5000	Sigma	**Tfam**	Rabbit	1:2000	Abcam
PDH-E1α (p293)	Rabbit	1:1000	Millipore	**AMPKα**	Mouse	1:1000	Cell Signalling
PDH-E1α (p300)	Rabbit	1:1000	Millipore	**AMPKα pThr172**	Rabbit	1:1000	Cell Signalling
PDHX	Mouse	1:1000	Sigma	**AKT (pan)**	Mouse	1:1000	Cell Signalling
Acetylated Tubulin	Mouse	1:1000	Sigma	**AKT pSer 473**	Rabbit	1:2000	Cell Signalling
Aquaporin2	Mouse	1:500	Abcam	**Na^+K^+ ATPAse**	Mouse	1:500	Abcam
IFT-88	Rabbit	1:1000	Proteintech	**mTOR**	Mouse	1:1000	Cell Signalling
PRAS40	Rabbit	1:1000	Cell Signalling	**mTOR pSer 2448**	Rabbit	1:1000	Cell Signalling
PRAS40 (Thr246)	Mouse	1:1000	R&D Systems				
IRDye 680LT anti-mouse	Donkey	1:10000	Li-Cor	IRDye 680LT anti-rabbit	Donkey	1:10000	Li-Cor
Alexa 488 anti-mouse	Donkey	1:1000	Invitrogen	Alexa 555 anti-rabbit	Donkey	1:1000	Invitrogen

Table 5. Antibodies list. Primary antibodies are reported in bold.

3.11 ANIMAL EXPERIMENTS

3.11.1 Animal Model

Animal experiments were conducted in female BKS.Cg-*Dock7*$^{m+/+}$*Leprdb*/J (db/db) mice and their corresponding age-matched wild-type (wt) littermates (Charles River Laboratories, Wilmington, U.S.) at the age of 8 and 24 weeks. The manufacturer carried out the genotyping and body weight was determined immediately before sacrifice. Animal care and experiments were in accordance to the Animal Experiment Ethics Committee at Karolinska Institutet.

3.11.2 Blood Measurements

Non-fasting glucose, triglycerides and cholesterol were measured prior to euthanasia, using a drop of blood obtained from the vein tail. Blood glucose was determined using a FreeStyle Glucometer (Abbot Diabetes Care, Alameda, U.S.). Blood triglycerides and cholesterol levels were determined by using a multi-parameter diagnostic device for triglycerides and cholesterol (multiCare-in, Biochemical Systems International S.r.l., Arezzo, Italy).

3.11.3 Serum Biochemistry

Biochemical studies were carried out in plasma samples in duplicate from five individual age-matched animals. Before euthanasia, blood samples were collected from the vein tail in capillary tubes (Sarsted, Nümbrecht, Germany). Immediately after collection, blood samples were centrifuged at 4°C 5000xg for 30 min. After centrifugation, plasma was collected from the supernatant and transferred into two sets of tubes: one for creatinine determination and the others for hormonal characterization. Creatinine levels were measured in deproteinized plasma samples (10kDa spin columns to avoid interferences with the assay) by using a commercial colorimetric kit (Abcam). Plasma insulin, c-peptide, glucagon, adiponectin and leptin levels were measured in all animals using commercial ELISA kits (CrystalChem, Downers Grove, U.S. for insulin, glucagon, c-peptide and adiponectin; and Phoenix Pharmaceuticals Inc., Burlingame, U.S. for leptin).

3.11.4 Histology and Immunohistochemistry

For histological and immunohistochemical analysis, mice were anesthetized with isoflurane and transcardially perfused with PBS followed by freshly prepared 4% (wt/vol) PFA in PBS. Kidneys were dissected out and post-fixed for 2h in the fixative. Prior to cryopreservation kidneys were processed with a sucrose gradient (10-30% (wt/vol) sucrose solution in PBS containing 0.01% (wt/vol) sodium azide and 0.02% (wt/vol) bacitracin), frozen in dry ice and preserved at -80°C until use. 20µm sections were counterstained with hematoxylin-eosin for morphological studies.

For immunohistochemistry, 20µm thick longitudinal kidney cryosections were collected on Superfrost Plus slides (Thermo Scientific). After sectioning, the slides were equilibrated at rT for 2h and then hydrated once for 5 min in PBS. Tissue permeabilization was performed for 15 min using 0.5% (vol/vol) Triton X-100 in PBS. Thereafter, blocking solution containing 5% (wt/vol) BSA and 0.5% (vol/vol) Triton X-100 in PBS was applied for 1h at rT before overnight incubation at 4°C with primary antibodies. Afterwards, sections were washed three times 5 min with 0.05% (vol/vol) Tween-20 in Tris/NaCl solution (0.1M Tris-Base; 0.15M NaCl). For double labeling appropriate secondary antibodies were applied 1h at rT. After incubation, sections were washed again three times 5 min and mounted using a mounting medium containing DAPI (ProLong® Gold Antifade, Thermo Scientific) for nuclear counterstaining. Images were captured using a Leica SP5 II confocal microscopy. Cilia number and length were measured per nuclei in the collecting duct and proximal tubule cells of kidney sections using two non-consecutive kidney sections separated by 200µm. For each

section, 3 fields were collected in five individual animals per experimental group and controls at both ages. Cilia number and length were analyzed in double blind using ImageJ software.

3.12 STATISTICAL ANALYSIS

Statistical analyses were performed with Sigma Stat software (San Jose, U.S.) using t-test, Mann-Whitney or ANOVA and Tukey or Dunn post-hoc test after outliers identification and removal using Grubbs' test (http://www.graphpad.com/quickcalcs/Grubbs1.cfm). Data are presented as mean ± s.e.m, median + IQr or mean + CI dependently of the data distribution and analyses applied, unless otherwise specified. Statistical significance was considered for $p < 0.05$. Data were represented graphically using Graph Pad Prism software (La Jolla, U.S.).

4 RESULTS AND DISCUSSION

4.1 PAPER I. SHORT AND PROLONGED EXPOSURE TO HYPERGLYCEMIA IN HUMAN FIBROBLASTS AND ENDOTHELIAL CELLS: METABOLIC AND OSMOTIC EFFECTS

Mitochondrial impairments during diabetes have been described in humans and animal models (see 1.2.5). However, the mechanisms linking mitochondrial impairments to diabetes complications still remain unclear. Mitochondrial metabolism and overproduction of ROS following hyperglycemia *in vitro* have been suggested to be the trigger for the activation of deleterious pathways involved in diabetes complications (31, 141-147). However, different mechanisms of cell damage in the absence of radicals have been found (148-150). In this paper, we aimed to clarify the metabolic response to acute and/or chronic hyperglycemia in human cells such as human primary dermal fibroblasts (HDF) and microvascular dermal endothelial cells (HDMEC), which are not insulin dependent for their glucose uptake and are involved in wound healing during diabetes.

4.1.1 Mitochondrial and Metabolic Adaptations to Acute Hyperglycemia in Human Healthy Cells

It has been suggested that raising extracellular glucose increases its uptake and utilization within cells expressing GLUT1 as main glucose transporter (31). Thus, we studied metabolic changes in HDF and HDMEC during acute hyperglycemia, using mannitol, which cannot penetrate the cell membrane, as osmotic control. In HDF, we measured the OCR using Seahorse Flux Analyzer (Fig.2A), where the cells were still adherent to the plate surface, as well as the oxygraph chamber (Paper I Fig.1E-H), in which the cells were floating after detachment. In good agreement with each other, both methods showed an acute decrease in

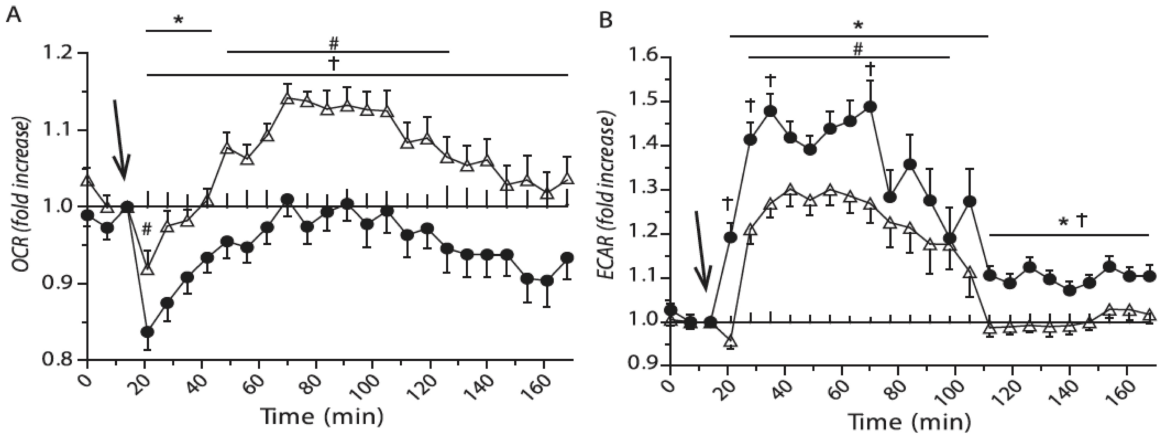

Figure 2. Oxygen consumption rate (A) and extracellular acidification rate (B) normalized on the control (medium) in HDF after acute glucose (HG) or mannitol (M) treatments (black arrow). Black circle = glucose; open triangle = mannitol. Data are expressed by mean ± s.e.m. Significance was determined by ANOVA and Tukey post-test between [HG] vs [C] (*), [HG] vs [M] (†), and [C] vs [M] (#).

OCR compared to baseline respiration immediately after glucose addition. Moreover, we found a higher OCR in response to mannitol compared to glucose both in HDF (Fig.2A) and HDMEC (Paper I Fig.1C), although significantly reduced compared to the control. Along with decreased respiration after glucose addition, we found an increased ECAR indicating a metabolic switch towards aerobic glycolysis. These results were consistent in both HDF (Fig.2B) and HDMEC (Paper I Fig.1D) suggesting a common response to the acute hyperglycemic stress.

To better clarify the cells response to hyperglycemia, we divided it into two components: osmotic stress (approximately from glucose addition to 120 min) and metabolic adaptation (from glucose addition onwards). The osmotic factor was proven by the fact that, after acute glucose or mannitol addition, the cells responded altering their metabolism until they resumed a new equilibrium. A previously described redistribution of molecules and ions during hyperosmosis might be the cause of these results (151, 152). Moreover, we suggest that the osmotic pressure could act mechanically on the mitochondria leading to a fast drop in oxidative phosphorylation. The metabolic component accounts for the difference in OCR and ECAR between glucose and mannitol treatments, which was still present when the new equilibrium after osmotic insult was established. The metabolic component of high glucose treatment was completely abolished by using an inhibitor of glucose uptake (cytochalasin B) (Paper I Fig.1I,L). In summary, the raise of extracellular glucose levels led to its intracellular utilization as fuel, reducing the OXPHOS and favoring the lactate production.

In contrast with previous hypothesis (31) we found a reduced $\Delta\psi_m$ after acute exposure to glucose in HDF and HDMEC (Paper I Fig.3E,F). This event can be explained either by an increase in cellular respiration, a higher proton leak from the ETC, or due to alteration in the cell membrane potential ($\Delta\psi_p$). Since our data demonstrated that glucose treatment induced a rapid decrease in respiration, and an acute boost of proton leak is unlikely in this short period of time, we suggest that the osmotic stress induced a re-equilibration of water content and ion charges into the cell pushing the probe outside the mitochondria thus decreasing the measured $\Delta\psi_m$. In fact, it has been previously suggested that the osmotic insult could reversibly decrease the intracellular water content and increase in intracellular Ca^{2+} levels thus promoting mitochondrial depolarization (151, 152). The utilization at the same time of plasma membrane and Ca^{2+}probes could serve as ultimate proof to clarify this result.

4.1.2 Hyperosmosis Reduces Cell Growth and Causes Cytoskeletal Rearrangement

During acute hyperglycemia the body experiences short period of hyperosmosis before the kidneys establish a new osmotic equilibrium (152). Thus, metabolic changes associated to hyperosmosis during diabetes might be present as we observed in the metabolism of HDF and HDMEC. Together with metabolic alterations during hyperosmosis, we also found a reduced cell proliferation in both HDF (Fig.3A,C and Paper I Sup.Fig.1H) and HDMEC (Fig.3B and Paper I Sup.Fig.1H). We found that cell growth during hyperglycemia was

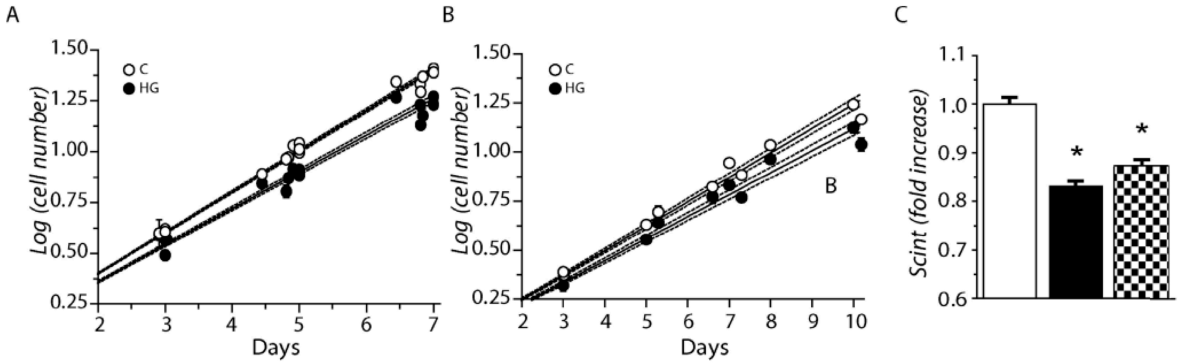

Figure 3. A-B) Cellular growth of HDF (A) and HDMEC (B). Regression curve mean + CI. C = control HG = high glucose. C) Thymidine incorporation at day 3 in HDF treated with glucose (black bar), mannitol (squared bar), and control cells (white bar). Data are expressed by mean ± s.e.m. Significance was determined by ANOVA and Tukey post-test between [HG] and [M] vs [C].

comparable to the one using mannitol and was dependent on their concentration in the medium (Paper I Sup.Fig.2A). Moreover, cells exposed to hyperglycemia as well as mannitol, displayed an increase in protein content (Paper I Fig.5D and Sup.Fig.2B), which was, at least in part, due to the raise in β-actin protein levels (Paper I Fig.5E,F).

In our view, the re-organization of the cytoskeleton to counteract the osmotic pressure was the main reason for the reduced cell proliferation. The decreased cell growth due to hyperosmosis as component of high glucose, can partly provide an *in vitro* explanation for some *in vivo* complications of diabetes involving fibroblasts and endothelial cells, such as the reduced wound healing ability in diabetic patients (153).

4.1.3 Prolonged High Glucose Exposure Reset Metabolism with Changes in Cellular Energy Levels

Prolonged exposure to high glucose has been demonstrated to activate deleterious pathways leading to diabetes complications. Under condition of chronic hyperglycemia, diabetic tissues seem to exhibit decreased energy levels and higher oxidative stress (see 1.2.5 and 1.2.6). Therefore, we aimed to better understand the impact of chronic hyperglycemia on mitochondrial function and energy metabolism. Thus, we mimicked *in vitro* a condition of

long-term exposure to high glucose levels culturing confluent HDF and HDMEC and measured mitochondrial and cellular bioenergetic parameters. Also here, we used mannitol as osmotic control. After 7 days of treatments, we found that high glucose culture shifted the fuel utilization from mitochondrial OXPHOS to aerobic glycolysis (Paper I Fig.2E). This result is in line with the one described above during the acute hyperglycemic treatment (Fig.1). In fact, the basal OCR was decreased in both HDF and HDMEC (Fig.4), while the ECAR and thus lactate production increased (Paper I Fig.2D). Moreover, the uncoupled mitochondrial respiration was slightly but significantly reduced after one week of high glucose exposure (Fig.4). The reason of this metabolic switch remains elusive. It might be speculated that a less effective ATP production to clear the intracellular glucose favors lactate production to be able to re-oxidize the coenzyme NADH necessary to avoid the slowdown of glycolytic flux.

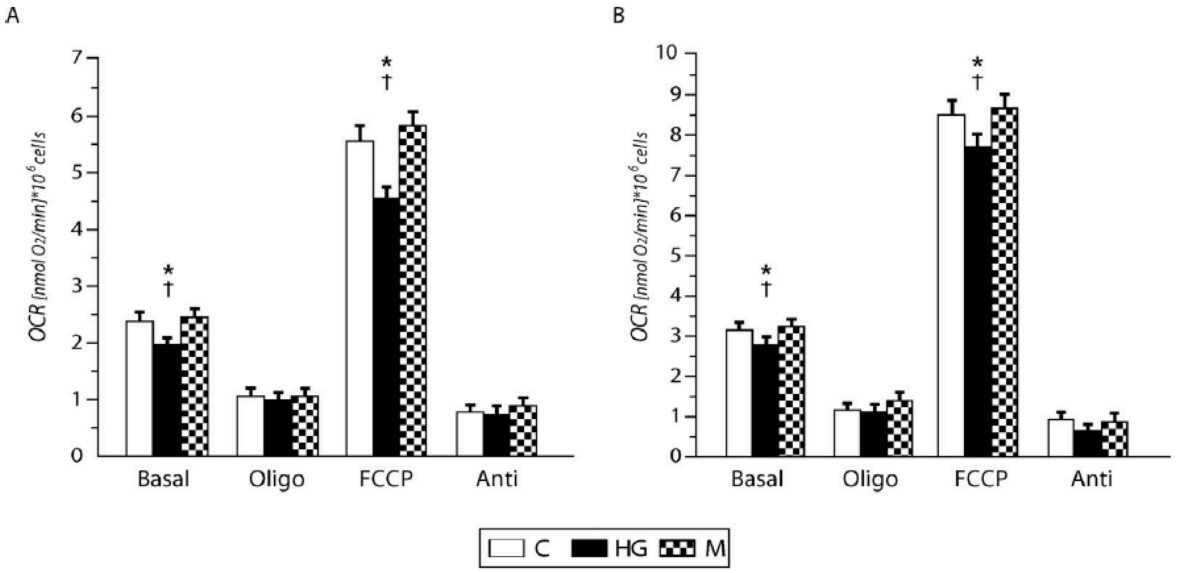

Figure 4. A-B) OCR after one week of high glucose or mannitol exposure in HDF (A) and HDMEC (B). Data are expressed by mean + CI. Significance was determined by ANOVA and Tukey analysis between high glucose [HG] vs control [C] (*), and [HG] vs mannitol [M] (†).

Cells exposed to chronic hyperglycemia were able to maintain high ATP levels even though the aerobic glycolysis is less efficient. However, the raise in ADP in cells treated with high glucose changed the ATP/ADP ratio (Paper I Fig.4A,B). The cause of this imbalance could be attributable, as mentioned above, to an increase in energy expenditure for protein synthesis during high glucose treatment. An alternative explanation could be the usage of ATP to maintain the $\Delta\psi_m$ using the ATPase in a reverse mode. However, adenosine nucleotides ratio is different between cytosol and mitochondria and, with the techniques in our knowledge, we could not discern in which compartment the ATP/ADP ratio was changed.

The decrease in respiration and the preference of aerobic glycolysis we observed after prolonged exposure to hyperglycemia was not due to ROS overproduction, which could affect the ETC functions (Paper I Fig.3I,L). The absence of ROS during hyperglycemia was corroborated by the absence of changes in cellular redox state by means of NAD^+/NADH ratio (Paper I Fig.4A,B). However, as for the ATP/ADP ratio, the total NAD^+/NADH ratio does not consider the compartmentalization between cytosol and mitochondria.

The decrease in OCR we found after long-term exposure to hyperglycemia was not due to an impairment of ETC activity (Paper I Fig.3M) suggesting a metabolic regulation of fuel channeling from pyruvate to lactate bypassing the mitochondrial respiration. One possible candidate diverting the pyruvate away from mitochondrial utilization is the enzyme pyruvate dehydrogenase (PDH). Even though we did not detect difference in its phosphorylation state (Paper I Fig.2C and Sup.Fig.1D,E), a decrease in Ca^{2+} levels as adaptive mechanism to counteract hyperglycemia could be a factor inactivating the enzyme without changes in phosphorylation state (154).

4.2 PAPER II. PRECONDITIONING WITH ASSOCIATED BLOCKING OF CA^{2+} INFLOW ALLEVIATES HYPOXIA-INDUCED DAMAGE TO PANCREATIC BETA-CELLS

PAPER III. HYPEROXIA INHIBITS GLUCOSE-INDUCED INSULIN SECRETION AND MITOCHONDRIAL METABOLISM IN RAT PANCREATIC ISLETS

Transplantation of pancreatic islets is used as rescue treatment for insulin-dependent diabetic patients. During islets engraftment, the hypoxic environment preceding islets neovascularization leads to the loss up to more than half of the transplanted islets (155). To improve the yield and function of the transplanted islets, several approaches are currently being developed (see 1.1.6). In papers II and III, we explored possible pre-hypoxia and/or pre-transplantation treatments of pancreatic islets using either the K^{+}_{ATP} channel opener diazoxide or high oxygen tension (hyperoxia) to reduce the negative impact of hypoxia during engraftment. Moreover, we studied how hypoxia as well as hyperoxia affect mitochondria, metabolism and secretion of pancreatic islets *in vitro*.

4.2.1 Hypoxia and Hyperoxia Impair Insulin Secretion and Mitochondria of Pancreatic Islets

In paper II, we used islets of Langerhans isolated from rats and cultured them for 5.5 hours at 0.8% oxygen tension (hypoxia). We found that hypoxia induced a significant reduction in the biosynthesis of insulin and proinsulin (Paper II Fig.4A and Sup.Fig.1A), together with a lower rate of insulin secretion upon glucose stimulation and total insulin content (Paper II Fig.3A,B). Insulin biosynthesis and release are ATP dependent and rely on mitochondrial energy production, since lactate production is negligible in β-cells (8). Therefore, we investigated the effect of hypoxia on islets mitochondria and found that the decrease in insulin secretion and production was accompanied by a reduction in number of mitochondria and ETC complexes I, II and III (Paper II Table 1 and Fig.5).

Same parameters were measured again after re-oxygenation of the islets to mimic the recovery phase after the hypoxic insult during islets engraftment *in vivo*. Here, we found that after 22 hours of re-oxygenation, the cells within the islets were not able to completely restore their previous metabolic functions (Paper II Fig.6D,E). However, we found some improvements in several metabolic and mitochondrial parameters such as insulin and proinsulin content, insulin secretion, mtDNA, ETC complexes and ATP levels.

The decrease in mtDNA and ETC complexes after hypoxia re-oxygenation was in line with the marked decrease in basal and glucose-stimulated islets OCR (Fig.7). However, the absolute respiratory response to glucose stimulation was maintained, confirming that the

defective insulin secretion observed in pancreatic islets subjected to hypoxia was due to a decrease in mitochondrial number or ETC complexes rather than an impairment of the ETC itself. In line with our finding, previous works showed that mitochondrial mass and gene expression were reduced during hypoxia, which could be due to cellular energy depletion (156, 157). This effect can be more relevant in β-cells, where the glycolysis alone cannot compensate for the cellular ATP needs. Other possible explanation for the decreased respiration in pancreatic islets after hypoxia re-oxygenation treatment could be the reduction in β-cells mass due to necrosis (Paper II Fig.4D). The mechanisms causing mitochondrial dysfunction during hypoxia are still not clear. The reasons could be the high ATP levels necessary for the function of mtRNA polymerase (156), mechanisms to save cellular energy such as proteolysis, or ROS overproduction (158). In contrast, other works found an upregulation of mitochondria biogenesis in response to hypoxia (159, 160). However, the level of oxygen required for cells to be hypoxic depends on the metabolism of the specific tissue since the respiratory gradient (which depends on the mitochondrial respiration) determines the access of oxygen into the cells (158). Moreover, the time of hypoxic exposure and the accountability for ATP production by OXPHOS for each cell and tissue is a determinant of cell fate during hypoxia.

Whereas hypoxia is deleterious after transplantation, hyperbaric management was found to improve functionality and yield of transplanted islets due to a decrease in apoptosis (155). An intriguing perspective would be to culture isolated islets in a hyperoxic environment for a limited period of time to possibly upregulate mechanisms to endure the initial hypoxia after transplantation. Thus, in paper III we investigated this possibility culturing the islets for 18 hours at 95% oxygen tension. We found that hyperoxia decreased glucose-induced insulin secretion (Paper III Fig.2A) without reducing insulin content (Paper III Fig.2B). Necrosis or apoptosis after the hyperoxic period was not detected (see Paper III section 3.5). These results led us to investigate whether the defective insulin secretion observed under hyperoxic conditions could be related to a disrupted mitochondrial metabolism. Indeed, we found a decrease in mitochondrial respiration both at basal level and after glucose stimulation (Fig.5 and Paper III Fig.2E), together with a reduction in the protein levels of mitochondrial complexes I and II (Paper III Fig.2F).

Although hyperoxia was found previously to induce oxidative stress, we detected a decrease in cytoplasmic ROS and an significant increase only after further 22h normoxic culture (see Paper III section 3.4) (158). This result might be due to the difference in tissues metabolism or time of treatments we used compared to previous works. Finally, we cultured the islets 5.5 hours in hypoxia after hyperoxia and did not find a protection induced by hyperoxic treatment (Paper III Fig.4).

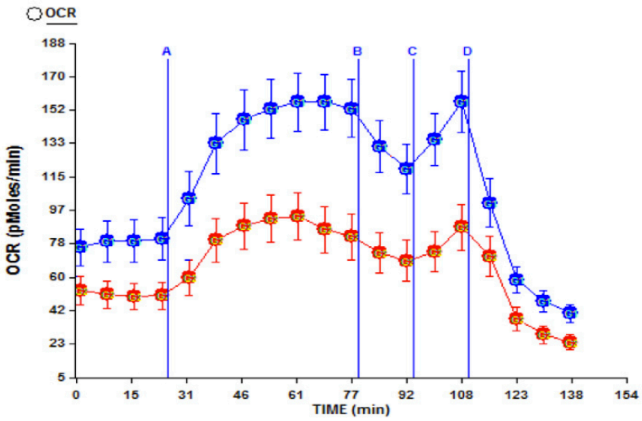

Figure 5. OCR of rat islets cultured at 95% oxygen tension (red circles) and normoxia (blue circles). Injections: A glucose; B Oligomycin; C FCCP; D antimycin. Data are expressed as mean ± s.e.m..

4.2.2 Diazoxide Protects Islets from Hypoxia and Increase Yield after Transplantation

In paper II, we aimed to test pharmacological approaches to ameliorate the negative effects of hypoxia. Here we used the K^+_{ATP} channel opener diazoxide to pretreat pancreatic islets for 22 hours prior to hypoxic culture or transplantation. This chemical was chosen due to its protective effect against hypoxia in excitable cells such as nerve and myocardium (161). Rat pancreatic islets pretreated with diazoxide improved insulin secretion and insulin content (Fig.6 and Paper II Fig.4A). Using the same protocol, we could reproduce the increase in insulin content in human islets (Paper II Pag.8). The positive effect of diazoxide on insulin content and secretion had been recently corroborated using a model of cold ischemic pancreatic tissue perfused with this compound. Isolated islets from ischemic and diazoxide treated mice, displayed preserved mitochondrial morphology and network (162, 163). Moreover, cell necrosis in rat islets observed during the re-oxygenation phase was partially decreased by diazoxide pretreatment (Paper II Fig.4D). Whereas hypoxia

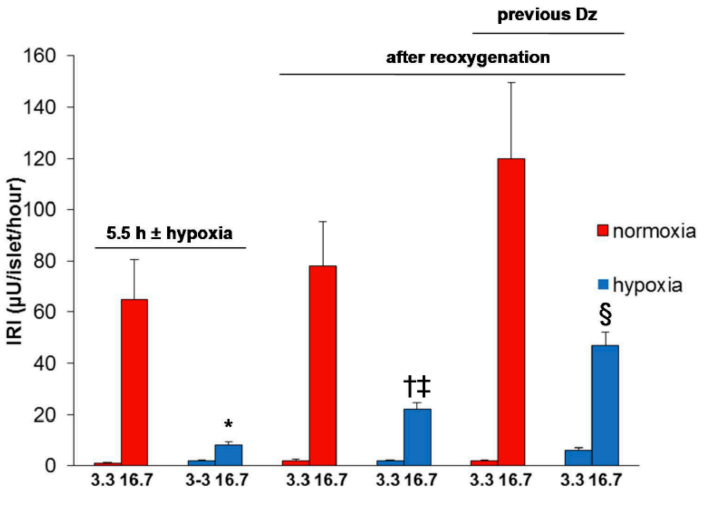

Figure 6. Insulin secretion at basal level (3.3mM glucose) and following glucose stimulation (16.7mM glucose) after different treatments. Data are expressed as mean ± s.e.m. Significance was calculated using t-test or Anova and Student-Newman-Keuls. Before re-oxygenation: * hypoxia vs normoxia. P<0.02. After re-oxygenation: † hypoxia vs no re-oxygenation P<0.01, ++hypoxia re-oxygenation vs normoxia re-oxygenation P<0.02 § diazoxide pretreatment vs no diazoxide P=0.027.

decreased significantly mitochondrial complexes I, II and III, in diazoxide preconditioned islets the levels were comparable to control (Paper II Fig.5). After re-oxygenation, islets cultured in hypoxia (diazoxide pretreated or not) displayed similar amount of mitochondrial complexes compared to control, with the exception of complex I in hypoxia treated islets (Paper II Fig.5).

In contrast, we found a reduction of the amount of mtDNA after hypoxia/re-oxygenation compared to normoxic culture (Paper II Table 1). The decreased mtDNA content after hypoxic culture, and thus probably the number of mitochondria, was in line with the decrease of both basal and glucose-stimulated respiratory levels (Fig.7). Moreover, ATP levels, protein content and glucose oxidation were markedly decreased after hypoxia (Paper II Table 1).

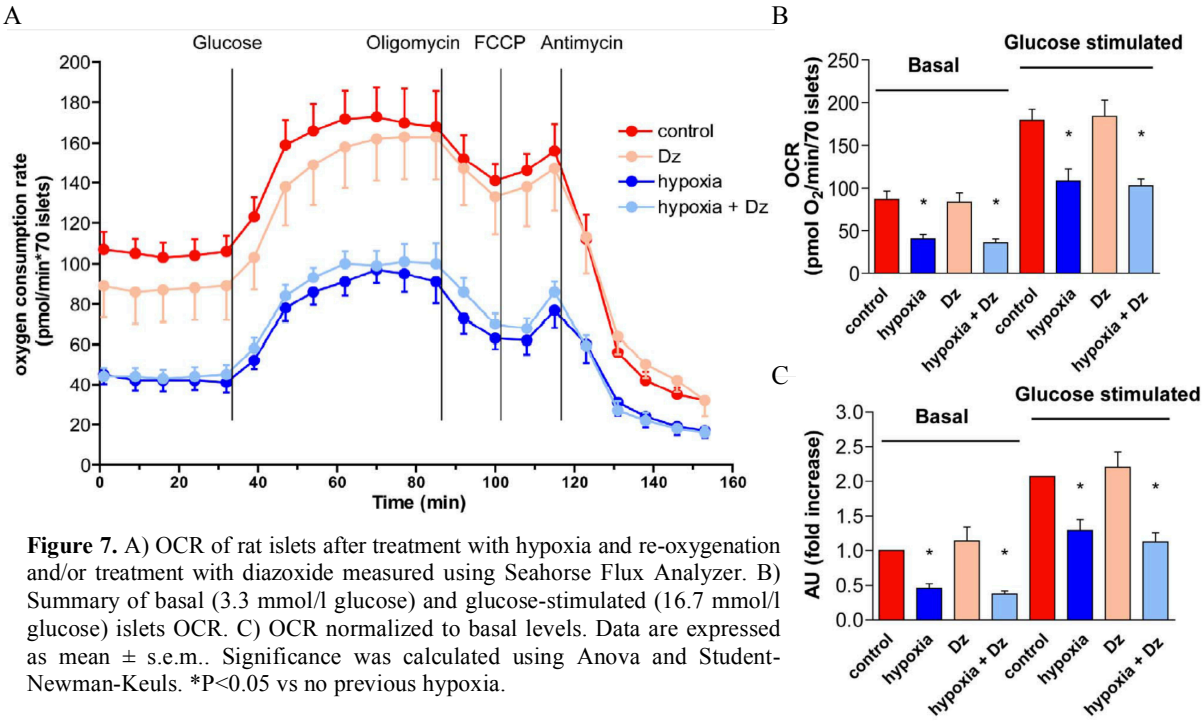

Figure 7. A) OCR of rat islets after treatment with hypoxia and re-oxygenation and/or treatment with diazoxide measured using Seahorse Flux Analyzer. B) Summary of basal (3.3 mmol/l glucose) and glucose-stimulated (16.7 mmol/l glucose) islets OCR. C) OCR normalized to basal levels. Data are expressed as mean ± s.e.m.. Significance was calculated using Anova and Student-Newman-Keuls. *P<0.05 vs no previous hypoxia.

We suggested that the opening of K^+_{ATP} channels and the consequent blockade of Ca^{2+} inflow into the β-cells were able to keep the islets in a "resting state" protecting them from hypoxia. This concept was introduced before by Ritzel and colleagues, using a selective K^+_{ATP} channel opener in β-cells (164).

Thus, we used the Ca^{2+} channel blocker nifedipine or a co-treatment with the K^+_{ATP} channel closer tolbutamide and diazoxide. Here, the positive effect of diazoxide was blocked by tolbutamide, while nifedipine had similar effect compared to diazoxide, strongly suggesting that blockade of Ca^{2+} inflow in β-cells was protective from hypoxia (Paper II Fig.7A,B). Corroborating our hypothesis, diazoxide as well as nifedipine preconditioning decreased glucose oxidation even in presence of normal oxygen tension (Fig.8).

An alternative mechanism of decreased necrosis after re-oxygenation could be a reduction in ROS, which can be mediated by the uncoupling effect of diazoxide. Further, it has been suggested that diazoxide effect could be due to the transient opening of the mitochondrial transition pore during preconditioning, which might protect the cells from ischemia-reperfusion (165).

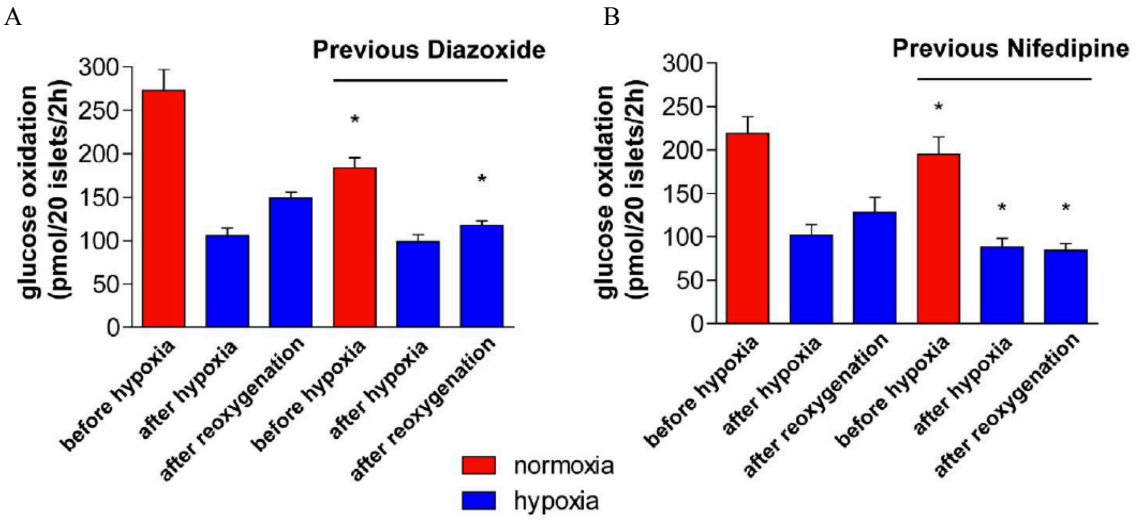

Figure 8. Diazoxide (A) or Nifedipine (B) effect on glucose oxidation in pancreatic islets. Data are expressed as mean ± s.e.m.. Significance was calculated using t-test. * $P<0.05$ vs. no preconditioning.

After we found a protective effect of diazoxide from hypoxia re-oxygenation *in vitro*, we sought to demonstrate its efficacy after transplantation. Thus, we measured the insulin content in engrafted islets 5 days after transplantation in non-diabetic rats. In preconditioned islets we found increased insulin content as well as cell survival compared to the absence of treatment (Paper II Fig.8). Moreover, preconditioned rat or human islets were more effective to lower blood glucose levels when transplanted in streptozotocin treated mice (Paper II Fig.8B-D). These results provide new therapeutic values for K^+_{ATP} channel openers to improve the efficacy and the efficiency of the islet transplantation.

4.3 PAPER IV. CILIARY/ BASAL BODY DYSFUNCTION IMPAIRS INSULIN SECRETION SIMILAR TO THAT IN TYPE 2 DIABETES SUSCEPTIBILITY

The primary cilium is an organelle involved in multiple cellular signaling pathways and tissue homeostasis (108). Although the importance of ciliary signaling is well recognized during development, the impact of cilia in tissue homeostasis is still largely unexplored. Recently, ciliary function has been involved in mTOR signaling (113-115) and autophagy (116, 117). Features of two different ciliopathies, namely BBS and Alström disease, are obesity and high comorbidity with diabetes, providing a possible link between insulin signaling and primary cilia. In this work we investigated this link and its possible mechanism of action.

4.3.1 Ciliary Dysfunctions Impair Insulin Secretion and Promote Development of Type 2 Diabetes in Rodents

To study the link between primary cilia and diabetes we first used a ciliopathy mouse model of BBS ($Bbs4^{-/-}$ mouse), which develops obesity and diabetes. Although the islets and pancreas developed normally without differences in insulin content, at 7-9 weeks of age the mutants displayed impaired glucose tolerance compared to wild type mice (Fig.9A).

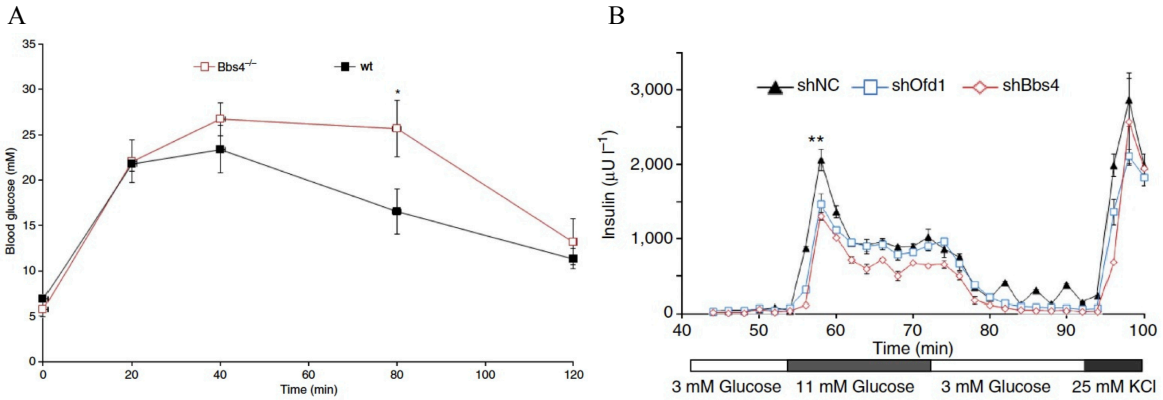

Figure 9. A) Glucose tolerance of $Bbs4^{-/-}$ mice compared to wild type littermate. Data are expressed as mean ± s.e.m.. Significance was calculated using t-test. P=0.0496. B) Glucose-stimulated insulin secretion of whole islets depleted of *Ofd1* or *Bbs4* mRNA. Data are expressed as mean ± s.e.m.. Significance was calculated using ANOVA. *P=0.001.

We cannot exclude that at this stage a different distribution of lean and fat mass could play a role in this phenotype. In fact, pair-weight mice and human subjects affected by BBS display increased abdominal adiposity (166, 167). To test whether defects in ciliary/basal body can impair insulin secretion, we used shRNA targeting two basal body proteins in isolated islets and min6m9 cells, namely Oral-facial-digital syndrome I (OFD1) and Bardet-Biedl-Syndrome 4 (BBS4). We found a reduced first-phase insulin secretion in treated islets (Fig.9B), which was rescued by overexpression of human BBS4 in *Bbs4* shRNA knock down islets (Paper IV Fig.2B). We excluded a metabolic defect in min6m9 cells due to the cilium impairment by measuring glucose-stimulated mitochondrial respiration and glucose uptake

(Fig.10A,B respectively). Moreover, we excluded defective microtubular organization defects in *Bbs4* and *Ofd1* depleted cells (Paper IV Fig.3B-E), which has been previously suggested regarding BBS protein (168).

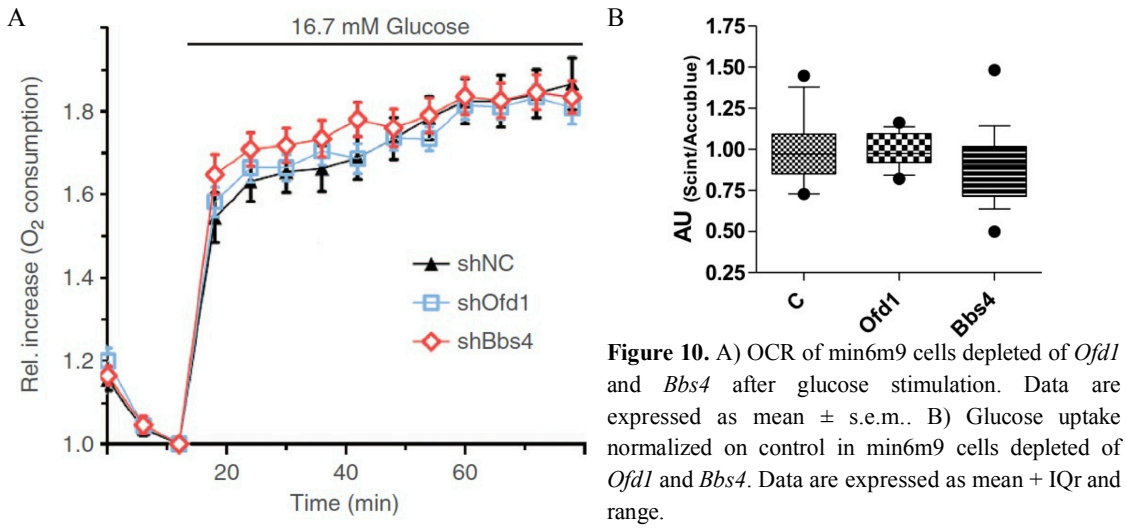

Figure 10. A) OCR of min6m9 cells depleted of *Ofd1* and *Bbs4* after glucose stimulation. Data are expressed as mean ± s.e.m.. B) Glucose uptake normalized on control in min6m9 cells depleted of *Ofd1* and *Bbs4*. Data are expressed as mean + IQr and range.

Due to the similar phenotype between Bbs4$^{-/-}$ and βIRKO mice (insulin receptor knockout in β-cells (169)), we investigated the possible interaction between insulin receptor and primary cilium. Interestingly, we found that only activated insulin receptor A (IR-A) isoform, but not IR-B, was recruited to the cilium in min6m9 cells and human β-cells upon insulin stimulation (Paper IV Fig.4). In *Bbs4* and *Ofd1* depleted cells we found reduced insulin content after glucose challenge (Paper IV Fig.5J), which could be due to the reported activity of IR-A to activate transcription of insulin (*ins*) (170)). The necessary recruitment of IR to the cilium for insulin signal transduction was showed by the reduced phosphorylation of protein kinase B (AKT) and regulatory subunits of phosphatidylinositol-3-kinase (PI3K) (Paper IV Fig.5A-F) in both min6m9 cells and islets depleted of *Bbs4* and *Ofd1*. AKT is upstream activator of Forkhead Box Protein O1 (FOXO1), which in turn regulates Syntaxin1a protein (STX1a). STX1a is in turn implicated in the soluble N-ethylmaleimide attachment receptor (SNARE) complex necessary for insulin exocytosis. We found a reduction in mRNA and protein levels of STX1a and SNAP25 components of the SNARE complex in islets treated with *Bbs4* and *Ofd1* shRNA as well as in islets from Bbs4$^{-/-}$ mice (Paper IV Fig.5G,H). Furthermore, overexpression of STX1a in min6m9 cells increased the insulin disposition index similar to control (Paper IV Fig.5I). These results confirmed that the disrupted insulin signaling we described above in *Bbs4* and *Ofd1* knock down islets as well as in isolated islets from Bbs4$^{-/-}$ mice, could be the cause of impaired exocytosis machinery.

Finally, we established a link between primary cilium and diabetes. Here, we found a strong reduction of ciliated cell per area in the lean model of diabetes Goto-Kakizaki rats (GK),

when β-cells density and islet volume are still conserved (2-3 months of age) but hyperglycemia is present (Paper IV Fig.6A-G). In the same rats, we found a dysregulation of ciliary genes (*Ift88*, *Bbs4*, *Pmc1*), increased protein levels of PMC1 and KIF3a and decreased levels of STX1a (Paper IV Fig.6H,I).

4.4 PRELIMINARY RESULTS I: ENERGY BALANCE AND REACTIVE OXYGEN SPECIES AFFECT PRIMARY CILIUM MORPHOLOGY

In addition to other signaling pathways previously linked to the primary cilium (see 1.3), we found that this organelle is also involved in the insulin signaling in β-cells (see 4.3). Cilia formation, maintenance and function are energetically costly and highly dependent on ATP, which is mainly (80-90% depending on cell type) produced by mitochondrial OXPHOS (171, 172). In this work, we aimed to elucidate how mitochondrial function and thus cellular energy balance influence ciliary maintenance. Here, we report cilia morphology changes in response to energy depletion as well as mitochondrial ROS production. Moreover, we translated our *in vitro* results into *in vivo* evidence of defective ciliogenesis in kidney of a diabetic mice model.

4.4.1 Blocking Complex I or ATPase Decrease Energy Levels and Ciliation in IMCD3

To investigate the link between mitochondrial function and ciliary homeostasis we treated mouse inner medullary collecting duct cells (IMCD3) with increasing concentrations of rotenone, an inhibitor of mitochondrial complex I (Fig.11A,B). After 48h, blockade of complex I decreased the number of ciliated cells in a dose-dependent manner (Fig.11B)

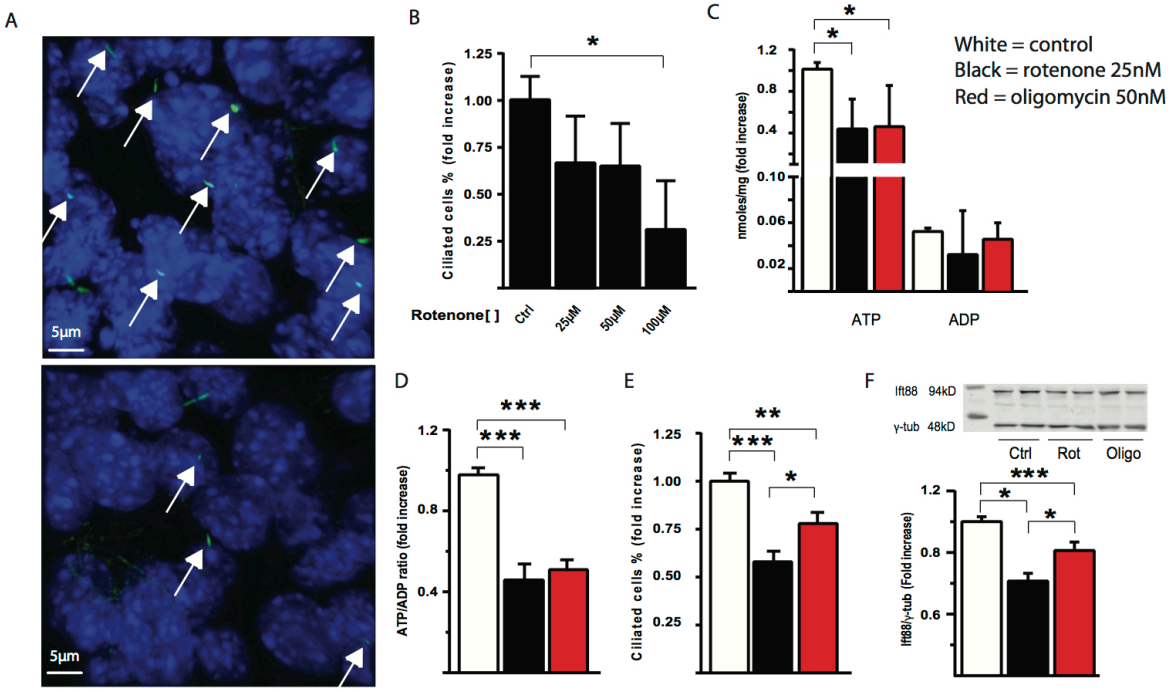

Figure 11. A) Representative image of IMCD3 cell line control (top panel) and treated with 100nM of rotenone (bottom panel) for 48h. Cilia stained with anti-acetylated tubulin are indicated with white arrows. B) Quantification of dose-dependent effect of rotenone on number of ciliated IMCD3 cells. Data represent 3 experiments (n=16 with approximately 20 cells each). Median + IQr, Kruskal-Wallis + Dunn´s P=0.001. C) ATP and ADP cell content normalized on the control in IMCD3 treated 48h with 25nM rotenone or 50nM oligomycin. Data represent 3 experiments (n>5). Median + IQr, Kruskal-Wallis + Dunn´s. P=0.001. D) ATP/ADP ratio in IMCD3 treated as above. Data represent 3 experiments (n>5). Mean + s.e.m ANOVA + Tukey. P<0.001. E) Quantification of IMCD3 ciliated cells treated as above. Data represent 4 experiments in duplicate (n>15 with approximately 60 cells/field). Mean + s.e.m ANOVA + Tukey. P<0.001. F) Representative WB and quantification of IFT88 protein in IMCD3 treated as above. Data represent 4 experiments (n>7). Mean + s.e.m ANOVA + Tukey. P<0.001.

(ciliated cells % normalized to the control; median + IQr: control 1.00 (0.84, 1.19); rotenone 25nM 0.71 (0.36, 0.97); 50nM 0.68 (0.31, 0.92); 100nM 0.32 (0.18, 0.60)). Using a second batch of cells we further tested whether the decrease of ciliation was related to the cell energy status or to a rotenone specific effect. Thus, we used oligomycin to decrease the mitochondrial ATP output and, at the same time, measured cilia number and cell energy status by means of nucleotides content. Here, we found that 48h treatments with either 25nM rotenone or 50nM oligomycin were able to decrease the total energy status (Fig.11C) and the ATP/ADP ratio (Fig.11D) in a similar extent *(nmoles ATP/mg protein normalized on the control; median + IQr: control 1.00 (0.98, 1.08); rotenone 0.43 (0.14, 0.72); oligomycin 0.45 (0.18, 0.85)) (ATP/ADP ratio normalized on control; mean ± s.e.m. control 1.00 ± 0.03; rotenone 0.46 ± 0.08; oligomycin 0.51 ± 0.05)*. Interestingly, not only rotenone, but also oligomycin treatment was able to reduce the amount of ciliated cells compared to the control (Fig.11E) *(ciliated cells normalized to the control; mean ± s.e.m.: control 1.00 ± 0.03; rotenone 0.58 ± 0.05; oligomycin 0.78 ± 0.05)*. To corroborate the finding of impaired ciliogenesis, we measured the intraflagellar transport protein 88 (IFT88) as part of ciliary transport mechanism and found reduced protein levels comparable with the decrease in ciliation after treatment with rotenone and oligomycin (Fig.11F) *(Ift88/γtub normalized on control; mean ± s.e.m.: control 1.00 ± 0.03; rotenone 0.61 ± 0.05; oligomycin 0.81 ± 0.05)*.

Our results suggest that reducing the ATP content in IMCD3 cells impairs ciliogenesis. The effect of reduction in cellular energy could decrease the activities of ATP-dependent motor proteins such as kinesin and dynein and Rheb and Ras GTPases involved in transport and import of ciliary proteins (125-127). However, rotenone had a stronger effect on reducing ciliated cells compared to oligomycin treatment suggesting an additive mechanism to impair ciliogenesis other than decrease in cellular energy status.

4.4.2 Reactive Oxygen Species, but not Cell Cycle and Apoptosis, are in part Responsible for Decreased Ciliation in IMCD3

As well known, rotenone binding to the complex I causes overproduction of superoxide anion thus increasing intramitochondrial ROS (96). However, depending on the metabolic state of the cell, also oligomycin can induce ROS formation by blocking the respiratory chain in a similar state 4 (90, 109). We therefore investigated rotenone and oligomycin induced ROS production as a possible effector of the decreased ciliogenesis.

Rotenone, but not oligomycin, increased the intramitochondrial ROS (Fig.12A and Sup.Fig.1A) *(MitoSOX Red intensity normalized to the control; median + IQr: control 1.00 (0.94, 1.06); rotenone 1.95 (1.62, 3.00); oligomycin 1.02 (0.86, 1.34))*. ROS production by

rotenone resulted also in an increase of cytosolic radicals (Fig.12B and Sup.Fig.1B). Moreover, oligomycin treatment was also responsible for an increase in cytosolic ROS similar to the one in presence of rotenone (Fig.12B) *(DCFDA intensity normalized on control; median + IQr: control 1.00 (0.93, 1.07); rotenone 4.28 (3.07, 6.22); oligomycin 3.20 (2.60, 7.64))*.

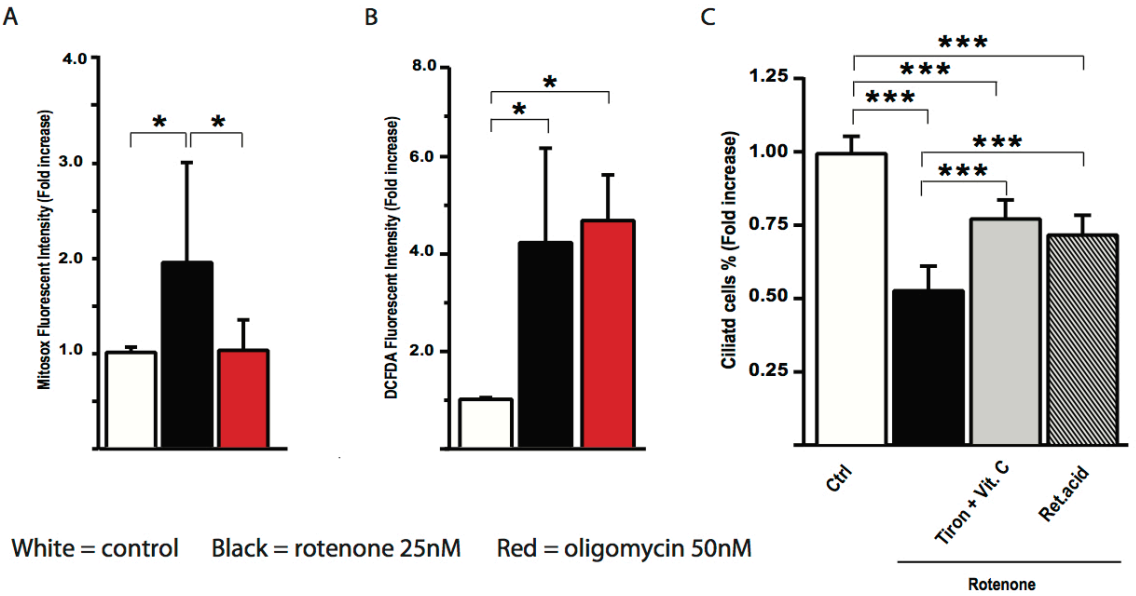

Figure 12. A) Quantification of MitoSOX intensity in IMCD3 cells treated 48h with 25nM rotenone or 50nM oligomycin. Data represent 6 experiments (n>11 of 50000 events). Median + IQr, Kruskal-Wallis + Dunn´s. P<0.001. B) Quantification of DCFDA intensity in IMCD3 cells treated as above. Data represent 5 experiments (n=10 of 50000 events). Median + IQr, Kruskal-Wallis + Tukey. P<0.001. C) Quantification of cilia number in IMCD3 cells treated 48h with 25nM of rotenone in the presence of antioxidants (Tiron + Vit.C 1mM, retinoic acid 1uM). Data represent 4 experiments (n>16) Mean + s.e.m ANOVA + Tukey. P<0.001.

To reproduce the cytosolic redox imbalance using another approach and investigate cilia morphology, we treated the cells with the oxidative stress inducing agent tert-butyl hydroperoxide (TBOOH) for 48h. In this case the number of ciliated cells was unaffected using concentrations up to the point in which the compound induced cell death (100µM) (Sup.Fig.1C). However, at all concentrations TBOOH did not reproduce the redox imbalance we found using mitochondrial inhibitors (Sup.Fig.1D). Using a different radical inducer such as paraquat, we replicated the same results (Sup.Fig.1E). As evidence that ROS are involved in decreased cell ciliation, we then adopted the opposite approach by quenching the radicals induced by rotenone with a combination of hydrosoluble (ascorbic acid and Tiron) or a liposoluble (retinoic acid) antioxidants. By administration of these compounds in combination with rotenone for 48h (Fig.12C), we found a significant maintenance of ciliated cells compared to rotenone alone *(ciliated cells % normalized on the control; mean ± s.e.m.: control 1.00 ± 0.03; rotenone 25nM 0.53 ± 0.04; rotenone + tiron and ascorbic acid 0.77±0.03; rotenone + retinoic acid 0.72 ± 0.03)*. However, this approach was not able to completely restore the cilia at the level of the control cells. These results showed that ROS

have an impact on cilia loss in IMCD3, which was at least partially restored by using antioxidants. The different reduction of ciliated cells after rotenone and oligomycin treatments, in the presence of an equally reduced energy status, could be simply due to the timing of the radical production and exposure to the chemicals. However, we cannot exclude that ROS generated at specific sites could act through a different signaling pathway compared to the ones generated outside mitochondrial matrix.

We next investigated whether impairments in the cell cycle could be a possible cause of decreased ciliation in IMCD3 (Fig.13A). Here, we found a significant increase in the S phase

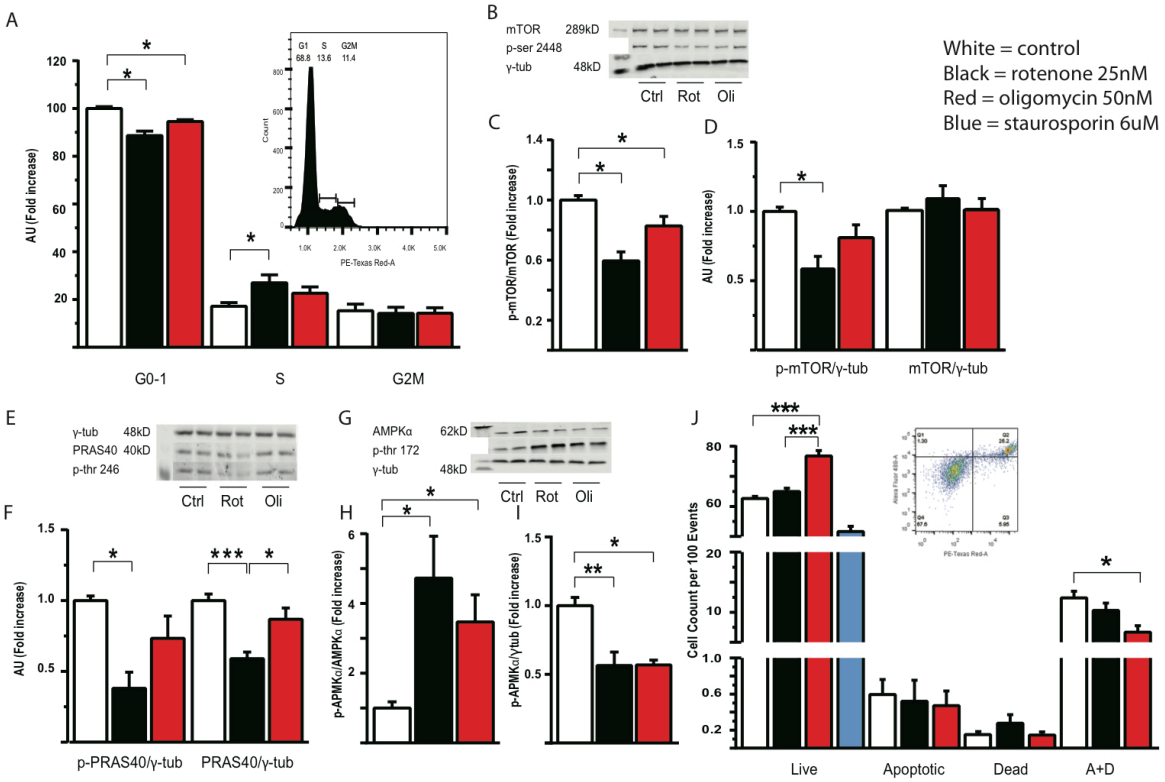

Figure 13. A) Cell cycle analysis with PI staining in IMCD3 treated for 48h with 25nM rotenone or 50nM oligomycin. Representative image of cell cycle plot in control cells. Data represent 4 experiments (n>8 with 50000 events each). $G_{0\text{-}1}$ phase: median + IQr, Kruskal-Wallis + Tukey. P<0.001. S phase: mean + s.e.m, ANOVA + Tukey. P=0.043. G_2M phase: mean + s.e.m, ANOVA. P=0.94 B) Representative image of WB of phosphorylated and total mTOR in IMCD3 treated as above. C) Quantification of B) p-mTOR/mTOR. Data represent 4 experiments (n>7). Median + IQr, Kruskal-Wallis + Dunn´s. P<0.001 D) Quantification of B) p-mTOR and mTOR normalized on loading control. Data represent 4 experiments (n>7). pmTOR/γtub: mean + s.e.m, ANOVA + Tukey. P=0.003. mTor/γtub: median + IQr, Kruskal-Wallis. P=0.37. E) Representative image of WB of phosphorylated and total PRAS40 in IMCD3 treated as above. F) Quantification of E) p-PRAS40 and PRAS40 normalized on the loading control. Data represent 3 experiments (n>6). Mean + s.e.m ANOVA + Tukey. pPRAS40/γtub P=0.006. Pras40/γtub P<0.001 G) Representative image of WB of phosphorylated and total AMPKα in IMCD3 treated as above. H) Quantification of G) p-AMPKα versus AMPKα. Data represent 3 experiments (minimum n=6). Median + IQr, Kruskal-Wallis + Tukey. P=0.003. I) Quantification of G) AMPKα vs loading control. Data represent 3 experiments (n>6). Mean + s.e.m ANOVA + Tukey. P=0.002 J) Analysis of apoptotic and necrotic IMCD3 treated as above normalized per 100 events. Representative image of control cells plot. Staurosporin 6μM has been added 2h prior the trypsinization as positive control. Data represent 4 experiments (n=9 with 20000 events each). Live: Mean + s.e.m, ANOVA + Tukey P<0.001. Apoptotic: median + IQr, Kruskal-Wallis P=0.59. Dead: median + IQr, Kruskal-Wallis P=0.88. Apoptotic + Dead: median + IQr, Kruskal-Wallis + Tukey P=0.012.

after rotenone treatment and a decreased G_1 phase in cells treated with rotenone and oligomycin *(S phase; mean ± s.e.m.: control 17.2 ± 1.5; rotenone 27.0 ± 3.3; oligomycin 22.6*

± 2.6) ($G_{0\text{-}1}$ phase; median + IQr: control 100.0 (98.7, 101.2); rotenone 89.1 (82.9, 93.9); oligomycin 94.1 (92.6, 96.7)). None of the treatments significantly affects the G_2M phase. One of the main regulators of cell cycle is the mTOR pathway, which has also been linked to primary cilium. On one hand a reduced ciliation using knock down approaches resulted in mTOR hyperactivation (114, 117, 173). On the other hand, inhibition of mTORC1 has been shown capable to regulate ciliary length via decreased protein synthesis (174, 175). Here, we found a decreased mTOR phosphorylation in cells treated with rotenone and oligomycin, which was in accordance with cell cycle analysis (Fig.13B,C). Decrease in absolute mTOR phosphorylation was significant after rotenone treatment (Fig.13B,D), without changes in the total mTOR protein levels *(phospho-mTOR/γtub normalized on control; mean ± s.e.m.: control 1.00 ± 0.03; rotenone 0.58 ± 0.09; oligomycin 0.81 ± 0.09; phospho-mTOR vs total mTOR median + IQr: control 1.00 (0.97, 1.03); rotenone 0.59 (0.56, 0.65); oligomycin 0.83 (0.68, 0.89))*. To further understand the possible involvement of mTORC1 in cell cycle changes, we measured PRAS40 as part of mTORC1 complex. We found that, after rotenone treatment, both phosphorylated and total PRAS40 protein levels were significantly reduced in IMCD3 cells (Fig.13E,F) *(phospho-PRAS40/γtub normalized on control; mean ± s.e.m.: control 1.00 ± 0.03; rotenone 0.38 ± 0.11; oligomycin 0.73 ± 0.16; total PRAS40/γtub: control 1.00 ± 0.05; rotenone 0.59 ± 0.05; oligomycin 0.87 ± 0.08)*. mTORC1 is negatively regulated by AMPK, which responds to a decrease in cellular energy status. As consequence of ATP decrease after rotenone and oligomycin treatments, we found an increase in AMPK activation by phosphorylation (Fig.13H), but also a decreased in the total AMPK protein levels (Fig.13I) *(phospho-AMPKα/total AMPKα normalized on control; median + IQr: control 1.0 (0.8, 1.2); rotenone 4.72 (2.6, 5.9); oligomycin 3.47 (2.8, 4.2)) (AMPKα/γtub normalized on control: mean ± s.e.m.: control 1.00 ± 0.07; rotenone 0.51 ± 0.12; oligomycin 0.58 ± 0.05)*. Moreover, absolute AMPK phosphorylation tended to be increased (Sup.Fig.1G). To exclude that ciliary impairment was directly repressing mTOR pathway we generated stable *Ift88* knock down IMCD3 cells. With our integrated shRNA we achieved a knock down similar to the one we observed after chemical treatments *(mean ± s.e.m. IFT88/γtub protein LacZ 1.00 ± 0.02; Ift88KD 0.62 ± 0.02)* (Sup.Fig.1H). However, we did not find any changes in mTOR phosphorylation state, indicating that the impairment of primary cilium was not the cause of decreased mTOR activation (Sup.Fig.1I).

In conclusion, we found that mTORC1 repression decreased cell cycle progression and possibly protein synthesis in IMCD3. In fact, in IMCD3 the decreased total protein levels of PRAS40, AKT and AMPK indicate that protein synthesis was partly responsible for cilia impairment after rotenone and oligomycin treatments.

A decreased number of ciliated cells could also indicate the increase of apoptotic events that could trigger reabsorption of the cilium. Therefore, we investigated the amount of apoptotic and necrotic cells (Fig.13J). Rotenone treatment did not alter vitality and apoptosis compared to the control at the concentration we used *(living cell %, mean ± s.e.m.: control 62.7 ± 0.7%; rotenone 65.0 ± 1.1%; dead apoptotic cells, median + IQr: control 10.8% (10.0,15.2); rotenone 8.8% (7.7,12.7))*. Surprisingly, we found a significant protection against cell death using oligomycin (Fig.13J) *(living cell %, mean ± s.e.m.: 76.8 ± 1.8%; dead apoptotic cells, median + IQr: 5.2% (4.3, 10.2))*.

In summary, we found fewer IMCD3 cells out of the cell cycle after rotenone treatment and, in a lower extent, using oligomycin. This result was in agreement with the mTOR activation status. The increase of cells in the S+G_2M phases was not enough to justify the decrease in ciliated cells observed with rotenone or oligomycin treatments. Moreover, we demonstrated that early apoptotic events were not the trigger for cilium reabsorption.

4.4.3 Rotenone Treatment Elongates Cilia in Human Retinal Epithelial Cells

To what extent increase in ROS and/or energy depletion affect IMCD3 cell ciliation was not possible to discern, since both mitochondria inhibitors were responsible for ROS overproduction. Trying to uncover the cause of ciliary defect and to test if the effect of rotenone was cell-type specific, we used a different cell line used in ciliary studies namely human telomerase reverse transcriptase immortalized retinal pigmented epithelial 1 (h-TERT RPE1). Here, we found a dose-dependent increase in maximum and median ciliary length using rotenone (Fig.14A,B and Sup.Fig.2A, respectively) *(maximum ciliary length normalized on control; median + IQr: control 1.00 (0.86, 1.12); rotenone 100nM 0.99 (0.82, 1.25); 200nM 1.34 (1.04, 1.46); 400nM 1.68 (1.39, 1.96)); (median cilia length normalized on control; median + IQr: control 1.00 (0.92, 1.09); rotenone 100nM 0.96 (0.86, 1.02); 200nM 0.96 (0.87, 1.1); 400nM 1.11 (1.02, 1.21))*. It is worth to note that the minimum length was not altered (Fig.14B).

To understand the link between the cilia elongation and a dose-dependent blockade of complex I and to find the correct dose of oligomycin that maximally inhibits the ATP linked respiration, we measured the OCR in response to acute treatments in RPE1 cells (Fig.14C and Sup.Fig.2B). We found that the OCR after acute rotenone treatment was decreased in a dose-dependent manner up to 800nM, while oligomycin inhibition of ATPase was maximal already at 200nM *(spare OCR%; mean ± s.e.m: rotenone 200nM 31.8 ± 0.7; 400nM 29.4 ± 1.1; 800nM 25.5 ± 0.7; median + IQr oligomycin 200nM 37.8 (29.0, 42.6); 400nM 34.0*

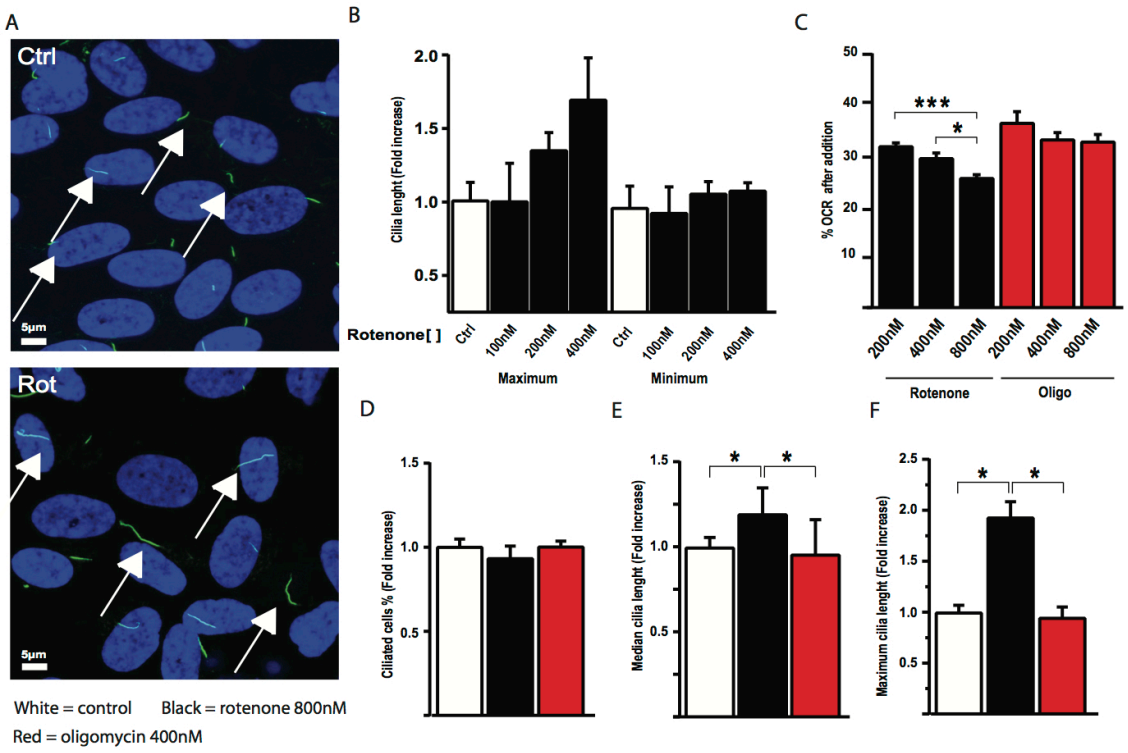

Figure 14. A) Representative images of RPE1 control (top panel) and treated with 400nM of rotenone (bottom panel) for 48h. Cilia stained with anti-acetylated tubulin are indicated with white arrows. B) Quantification of dose-dependent effect of rotenone maximum (P<0.001) and minimum (P=0.12) cilia length in RPE1 cells. Data represent 3 experiments (n>12 with minimum 20 cells each). Median + IQr, Kruskal-Wallis + Dunn´s. C) Oxygen consumption rate normalized to the baseline after addition of different doses of rotenone and oligomycin in RPE1. Data represent 3 experiments (n=18). Mean + s.e.m ANOVA + Tukey P<0.001. D) Quantification of RPE1 ciliated cells treated 48h with 800nM rotenone (black) or 400nM oligomycin (red). Data represent 3 experiments (n>15 with approximately 40 cells each). Median + IQr, Kruskal-Wallis P=0.87. E) Quantification of the median ciliary length in RPE1 treated as above. Rotenone (black) Oligomycin (red). Data represent 3 experiments (n>15 with approximately 40 cells each). Median + IQr, Kruskal-Wallis + Dunn´s P<0.001. F) Quantification of the maximum ciliary length in RPE1 treated as above. Rotenone (black) Oligomycin (red). Data represent 3 experiments (n>15 with approximately 40 cells each). Median + IQr, Kruskal-Wallis + Dunn´s P<0.001.

(27.8, 38.7); 800nM 33.8 (31.2, 35.7)). Thus, we chose concentration of 800nM rotenone and 400nM oligomycin, treated the cells for 48h and measured again cilia length and number (Fig.14D-F and Sup.Fig.2C). Under these treatments the number of ciliated cells was unaltered (Fig.14D). Moreover, we again found an increase of median (Fig.14E) and maximum ciliary length (Fig.14F) using rotenone *(median cilia length normalized on control; median + IQr: control 1.00 (0.97, 1.06); rotenone 1.20 (1.10, 1.36); oligomycin 0.96 (0.89, 1.17)) (maximum cilia length normalized on control; median + IQr: control 1.00 (0.94, 1.08); rotenone 1.94 (1.35, 2.11); oligomycin 0.95 (0.92, 1.07))*.

To understand whether the elongation of primary cilia due to rotenone treatment was accompanied by upregulation of anterograde transport along the axoneme, we measured the amount of IFT88 protein. Here, we did not find any significant changes in IFT88 protein levels (Sup.Fig.2D).

Taken together, our results in RPE1 cells show that rotenone induced an elongation of cilia in a dose-dependent manner, without altering cilia number per cells. This effect was not accompanied by increase of proteins involved in ciliary transport.

4.4.4 Increased Mitochondrial ROS are Responsible for Ciliary Morphology Alteration in RPE1 cells

To investigate whether or not cellular energy status was responsible for the morphological ciliary changes we observed in RPE1 cells, we measured adenosine nucleotides after treatments with rotenone and oligomycin. Here, we found that neither rotenone nor oligomycin reduced cellular ATP (Fig.15A) but oligomycin treatment increased the ADP levels (Fig.15A) resulting in a significantly decreased ATP/ADP ratio (Fig.15B) *(ATP/ADP ratio normalized on control; mean ± s.e.m.: control 1.00 ± 0.02; rotenone 0.88 ± 0.04; oligomycin 0.66 ± 0.04) (nmoles ADP/mg protein normalized on the ATP levels; median + IQr: control 0.032 (0.030, 0.035); 0.037 (0.033, 0.044); 0.046 (0.040, 0.070))*. We cannot exclude that using other methods to decrease ATP in RPE1 could result in reabsorption or failure of ciliary maintenance as seen in IMCD3. The reduced ATP/ADP ratio using oligomycin in RPE1, pointed out that ATP levels rather than ATP/ADP ratio affect ciliary maintenance in the two cell lines we studied.

Further, we measured the activation of AMPK in response to the energy balance shift after the treatments (Fig.15C,E and Sup.Fig.2E). Both rotenone and oligomycin activated AMPK by means of phosphorylated levels (Fig.15E and Sup.Fig.2E) without affecting the total AMPKα *(p-AMPKα/AMPKα normalized on the control; median + IQr: control 1.00 (0.96, 1.37); rotenone 1.86 (1.13, 2.28); oligomycin 2.14 (1.49, 2.26)) (p-AMPKα/γtub normalized on the control; median + IQr: control 1.00 (0.96, 1.04); rotenone 1.98 (1.17, 2.31); oligomycin 2.09 (1.34, 2.55))*. AMPK activation is a negative regulator of mTOR signaling (173, 176). In fact, we found that after 48h of treatments, the phosphorylated form of mTOR was decreased (Fig.15D,F and Sup.Fig.2F) *(phospho-mTOR/mTOR normalized on control; median + IQr: control 1.00 (0.96, 1.04); rotenone 0.74 (0.62, 0.89); oligomycin 0.78 (0.64, 0.89)) (phospho-mTOR/γtub normalized on control; mean ± s.e.m.: control 1.00 ± 0.09; rotenone 0.70 ± 0.7; oligomycin 0.73 ± 0.07).* The total amount of mTOR protein was not affected (Sup.Fig.2F).

Taking together, the results of the two cell lines showed that mTOR repression alone without a decrease of protein synthesis did not act as signaling for cilium reabsorption. In fact, in RPE1, AMPK phosphorylation in response to rotenone and oligomycin treatments led to a repression of mTOR, showing that in our experimental settings ciliary impairment could be consequence and not cause of reduced mTOR signaling.

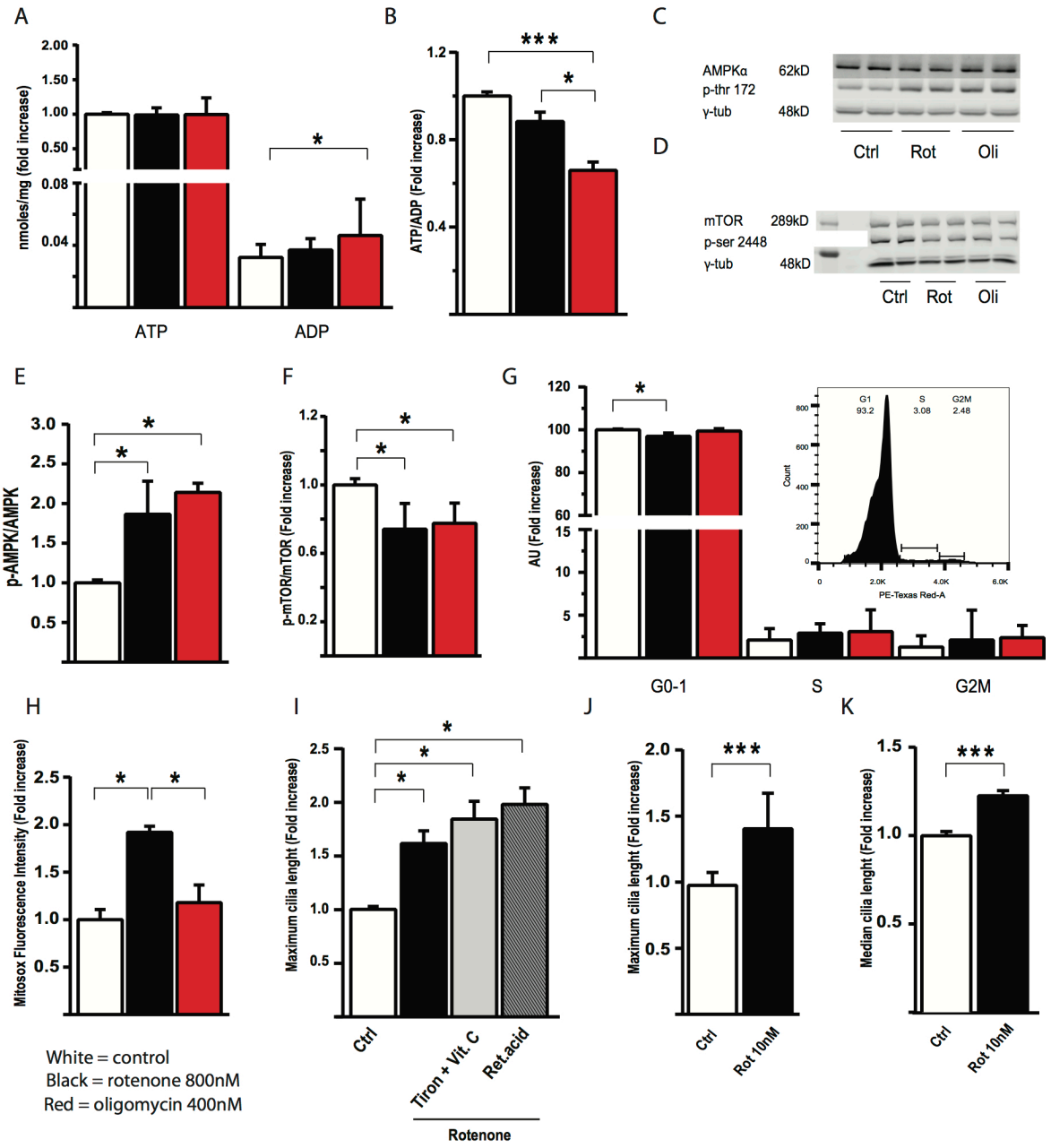

Figure 15. A) ATP and ADP (nmol/mg protein) normalized on the control in RPE1 cells treated 48h with 800nM rotenone (black) or 400nM oligomycin (red). Data represent 3 experiments (n>5). Median + IQr, Kruskal-Wallis + Dunn´s ATP P=0.89; ADP P=0.02. B) ATP/ADP ratio in RPE1 treated 48h as above. Data represent 3 experiments (n>5). Mean + s.e.m ANOVA + Tukey P<0.001. C) Representative image of WB of phosphorylated and total AMPKα in RPE1 cells treated as above. D) Representative image of WB of phosphorylated and total mTOR in RPE1 cells treated as above. E) Quantification of C) p-AMPKα versus AMPKα. Data represent 4 experiments (n=7). Median + IQr, Kruskal-Wallis + Tukey P=0.001. F) Quantification of D) p-mTOR versus mTOR. Data represent 4 experiments (n=7). Median + IQr, Kruskal-Wallis + Tukey P=0.007. G) Cell cycle analysis with PI staining in RPE1 treated as above. Representative image of plot of cell cycle in control cells. Data represent 4 experiments (n>8 with 50000 events each). Median + IQr, Kruskal-Wallis + Tukey. $G_{0\text{-}1}$ P=0.004; S P=0.50; G_2M P=0.42. H) Quantification of Mitosox intensity in RPE1 cells treated as above. Data represent 5 experiments (n>10 of 50000 events). Median + IQr, Kruskal-Wallis + Dunn´s. P=0.001 I) Quantification of maximum ciliary length in RPE1 cells treated with 800nM of rotenone 48h in the presence of antioxidants (Tiron + Vit.C 1mM, retinoic acid 1uM). Data represent minimum 3 experiments (n>14). Median + IQr, Kruskal-Wallis + Dunn´s. P<0.001 J) Quantification of maximum ciliary length in RPE1 cells treated with 10nM rotenone in glucose-free galactose media. Data represent minimum 3 experiments (n=15). Median + IQr, Mann-Whitney. P<0.001. K) Quantification of median ciliary length in RPE1 cells treated as above. Data represent minimum 3 experiments (n=15). Mean + s.e.m., t-test. P<0.001.

As mentioned before, cilia reabsorption and elongation is dependent of the cell cycle phase. Therefore, to explain the phenotype observed, we investigated the cell cycle as possible regulator of cilia length. After 5 days of starvation most of the RPE1 cells are in $G_{0\text{-}1}$ phase (Fig.15G). We found a slight but significant decrease in $G_{0\text{-}1}$ after rotenone treatment *(median + IQr arbitrary units: control 100.0 (99.6, 100.4); rotenone 97.0 (95.9, 98.5); oligomycin 99.5 (98.9, 100.6))*. We did not detect differences in the S and G_2M phase.

In contrast to IMCD3 cells, in RPE1 cells rotenone treatment was able to elongate the cilia. The effect was not dependent on the cellular energy status. Moreover, most of the RPE1 cells were found in $G_{0\text{-}1}$ phase allowing us to exclude also the cell cycle as reason for the ciliary morphology change.

We therefore shifted our attention to ROS as trigger for impaired cilia morphology. We found an increased mtROS generation after rotenone treatment (Fig.15H and Sup.Fig.2G) that was not reflecting an increase in cytosolic ROS (Sup.Fig.2H,I) *(MitoSOX fluorescence intensity normalized on the control; median + IQr: control 1.00 (0.89, 1.11); rotenone 1.92 (1.42, 1.98); oligomycin 1.18 (1.00, 1.36))*. To be able to rescue the phenotype, we used the same antioxidant approach as for IMCD3 cells. In RPE1 cells we could not rescue the phenotype by means of maximum ciliary length (Fig.15I) and median ciliary length (Sup.Fig.2J). This can be due to the antioxidant mechanism of action and radical site in which the ROS are produced and eventually quenched. A previous study using RPE1 cells showed how the ROS production can be blocked or not depending on the compartment where they are generated (117, 177).

To prove that the effect of rotenone on cilia morphology changes in RPE1 was due to mitochondrial ROS production and not unspecific effect of the drug, we decreased its concentration and used a glucose-free galactose culture media. Using galactose media the aerobic glycolysis is unfavorable and the cells use almost exclusively mitochondria as energy source. Here, using 10nM of rotenone for 48h we reproduced the increase in maximum ciliary length (Fig.15J) and median ciliary length (Fig.15K) that we found at higher rotenone concentrations using glucose media *(maximum ciliary length normalized on control; median + IQr: control 1.00 (0.91, 1.10); rotenone 1.44 (1.23, 1.71)) (median ciliary length normalized on control; mean ± s.e.m: control 1.00 ± 0.02; rotenone 1.22 ± 0.03).* The similar phenotype observed using galactose culture in RPE1 treated with 80 fold less concentration of rotenone suggest that the elongation of cilia was due to redox signaling from mitochondria.

4.4.5 Mitochondria are in Close Relationship with Basal Body

More than 1000 proteins are identified and classified in the ciliary proteome. Searching a database of predicted or *bona fide* ciliary proteins (CiliaDB (178)) that combines results from high throughput proteomics, differential expression and comparative genomics studies, we found listed several mitochondrial proteins (Table 6). These proteins included, but were not limited to, subunits of mitochondrial complexes as well as transporters involved in ATP generation and ETC from a variety of organisms including humans.

Name	Ciliary evidence	Organisms with ciliary evidence	Non Flagellary evidence	Proteomic studies	Evidence in Hsapiens
Ubiquinol-cytochrome c reductase core protein II	6	4	3	3	0
NADH dehydrogenase (ubiquinone) Fe-S protein 1, 75kDa (NADH-coenzyme Q reductase)	5	5	2	1	1
ATP synthase, H+ transporting, mitochondrial F1 complex, beta polypeptide	5	5	1	1	1
Creatine kinase, mitochondrial 1B	5	3	2	2	1
Isocitrate dehydrogenase 2 (NADP+), mitochondrial	5	5	3	3	1
Inner membrane protein, mitochondrial	5	4	3	3	1
Acyl-CoA dehydrogenase, short/branched chain	5	2	3	0	1
Voltage-dependent anion channel 2	5	4	4	3	0
Solute carrier family 25 (mitochondrial carrier; phosphate carrier), member 3	4	4	4	2	1
Solute carrier family 25 (mitochondrial carrier; dicarboxylate transporter), member 10	4	3	3	3	0

Table 6. List of the 10 most represented mitochondrial proteins found in the ciliary database ordered by ciliary evidence.

To investigate the spatial relationship and the possible properties of mitochondrial subsets in the proximity of the cilium, we generated stable IMCD3 cell lines overexpressing a cilia-specific protein, ADP-ribosylation factor-like protein 13b tagged with Venus (ARL13b-Venus) or RFP together with a photoactivatable GFP targeted to the mitochondrial matrix (subunit VIII of cytochrome c oxidase) (Mito-PAGFP) (Fig.16A-D). In IMCD3 ARL13b-Venus cells stained with Mitotracker Deep Red (Fig.16A) and IMCD3 ARL13b-RFP-Mito-PAGFP (Fig.16B,C), we observed a subset of mitochondria in proximity to the cilium both during growth (Fig.16B) and at confluence after starvation (Fig.16A,C).

To test if the subsets of mitochondria close to the basal body displayed different bioenergetics properties, we measured their $\Delta\psi_m$ and compared it to the cellular average of all mitochondria using the potentiometric dyes TMRE (Fig.16D,E) and JC-1 (Sup.Fig.2L,M).

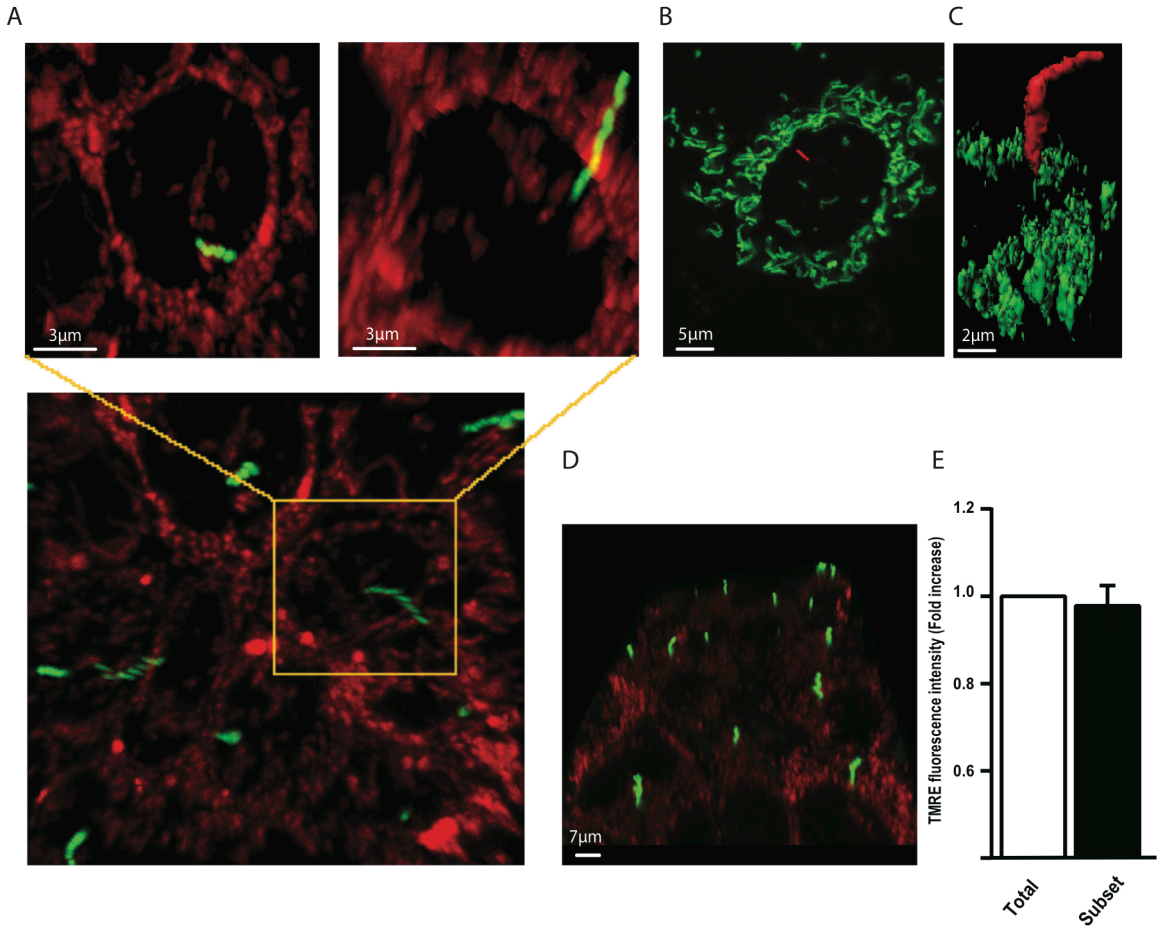

Figure 16. A) Representative image of live recording of stable cell line IMCD3 Arl13b-GFP loaded with 25nM Mitotracker Deep Red FM. In the zoomed box the plane was rotated using Imaris software to show the mitochondrial subset close to the cilium. B) Representative image of stable IMCD3 cell line Arl13b-RFP-Mito-PAGFP during growth. C) Imaris 3D rendering of a singular cilium in IMCD3 Arl13b-RFP-Mito-PAGFP and mitochondrial network at confluence. D) Representative cropped image of IMCD3 Arl13b-venus stained 1h with 25nM TMRE. E) Mitochondrial membrane potential of mitochondria within <2µm from the cilium compared to the overall cell mitochondrial network measured with TMRE in IMCD3 Arl13b-Venus stable cell line. Data represent 3 experiments (n=15 with approximately 20 cells each). Mitochondria close to the cilium Mean + CI 0.85-1.17.

We selected as ciliary mitochondrial subset the mitochondria within 2µm distance around the cilium (Sup.Fig.2K). Comparing $\Delta\psi_m$ of these subsets in proximity of the cilium with the average $\Delta\psi_m$ of the whole mitochondrial network, we did not detect any significant difference in IMCD3 at confluence in basal medium culture condition with both fluorescent dyes (Fig.16E and Sup.Fig.2M). These results suggest that mitochondria in proximity of the primary cilia have a similar metabolism and are in equilibrium with the intracellular mitochondrial network, under the chosen conditions.

4.4.6 Ciliation is Impaired in Kidney of a Diabetic Nephropathy Mouse Model

To the best of our knowledge, the results showed above are the first demonstrating an effect of internal radical production on cell ciliation. Previously, high doses of the radical inducer hydrogen peroxide have been proven to decrease ciliation in MDCK cells. The same effect was achieved after ischemic injury in kidney (179).

It has been previously described that during diabetic nephropathy, kidneys are subjected to increased oxidative stress, mitochondrial dysfunction and probably hypoxia (67, 84, 102, 105, 180). We used the db/db mouse model to translate our finding of decreased ciliation in IMCD3 cells, to diabetic nephropathy *in vivo* (Fig.17). The db/db mice have been widely used as a model of human diabetic nephropathy because of their common features (181). Whereas at 8 weeks of age kidneys from db/db mice were functionally and morphologically normal, at week 24 the blood creatinine levels were significantly higher and kidney morphology was altered, indicating the progression of nephropathy (Fig.17A-C) *(non-fasting plasma creatinine (µmol/L) mean ± s.e.m. 8 weeks: wt 71.9 ± 9.9; db/db 68.5 ± 8.6; 24 weeks wt 123.1 ± 12.6; db/db 284.6 ± 30.0).* At 8 weeks of age db/db mice were already hyperglycemic, obese and hyperinsulinemic compared to control littermates (Fig.17D and Sup.Fig.3A,C) *(non-fasting blood glucose (mmol/L) mean ± s.e.m. 8 weeks: wt 5.67 ± 0.02; db/db 20.58 ± 2.49; 24 weeks: wt 5.27 ± 0.31; db/db 21.00 ± 3.00)*. Moreover, hyperleptinemia was observed in both 8 weeks and 24 weeks old db/db mice to a similar extent (Fig.17E) *(non-fasting plasma leptin (ng/ml) mean ± s.e.m. 8 weeks: wt 0.89 ± 0.09; db/db 41.98 ± 5.74; 24 weeks: wt 2.45 ± 0.38; db/db 46.74 ± 3.20).* Using kidney sections we investigated the number and morphology of cilia in two different medullary cell types such as collecting duct and distal tubules cells. In the medullary collecting duct cells (Fig.17F), which correspond to IMCD3 cells *in vitro*, we found a robust and consistent significant decrease in cilia number (Fig.17G) and cilia length (Fig.17H) in db/db mice at 24 weeks of age *(ciliated collecting duct cells (%); median + range 8 weeks: wt 57.6 (54.5, 60.2); db/db 57.4 (53.2, 58.8); 24 weeks: wt 52.6 (49.0, 57.0); db/db 27.0 (13.4, 30.5) (ciliary median length (µm); median + range 8 weeks: wt 3.04 (2.79, 3.14); db/db 3.34 (3.02, 3.54); 24 weeks: wt 3.30 (3.26, 3.32); db/db 2.41 (2.22, 2.79)).*

To understand whether the phenotype was extended to other parts of the kidney we analyzed in the identical manner cilia of distal tubules cells (Fig.17I-K). Here we found a decrease in number of ciliated cells (Fig.17J) in 24 weeks old db/db mice without alteration of length in the remaining cilia (Fig.17K) *(ciliated distal tubules cells (%); median + range 8 weeks: wt 60.5 (56.7, 63.4); db/db 48.6 (35.7, 62.5); 24 weeks: wt 46.8 (30.4, 58.4); db/db 14.6 (11.9,*

27.9) (ciliary median length (µm); median + range 8 weeks: wt 2.48 (2.29, 2.69); db/db 2.40 (2.12, 2.42); 24 weeks: wt 2.67 (2.42, 2.82); db/db 2.59 (2.03, 2.80)).

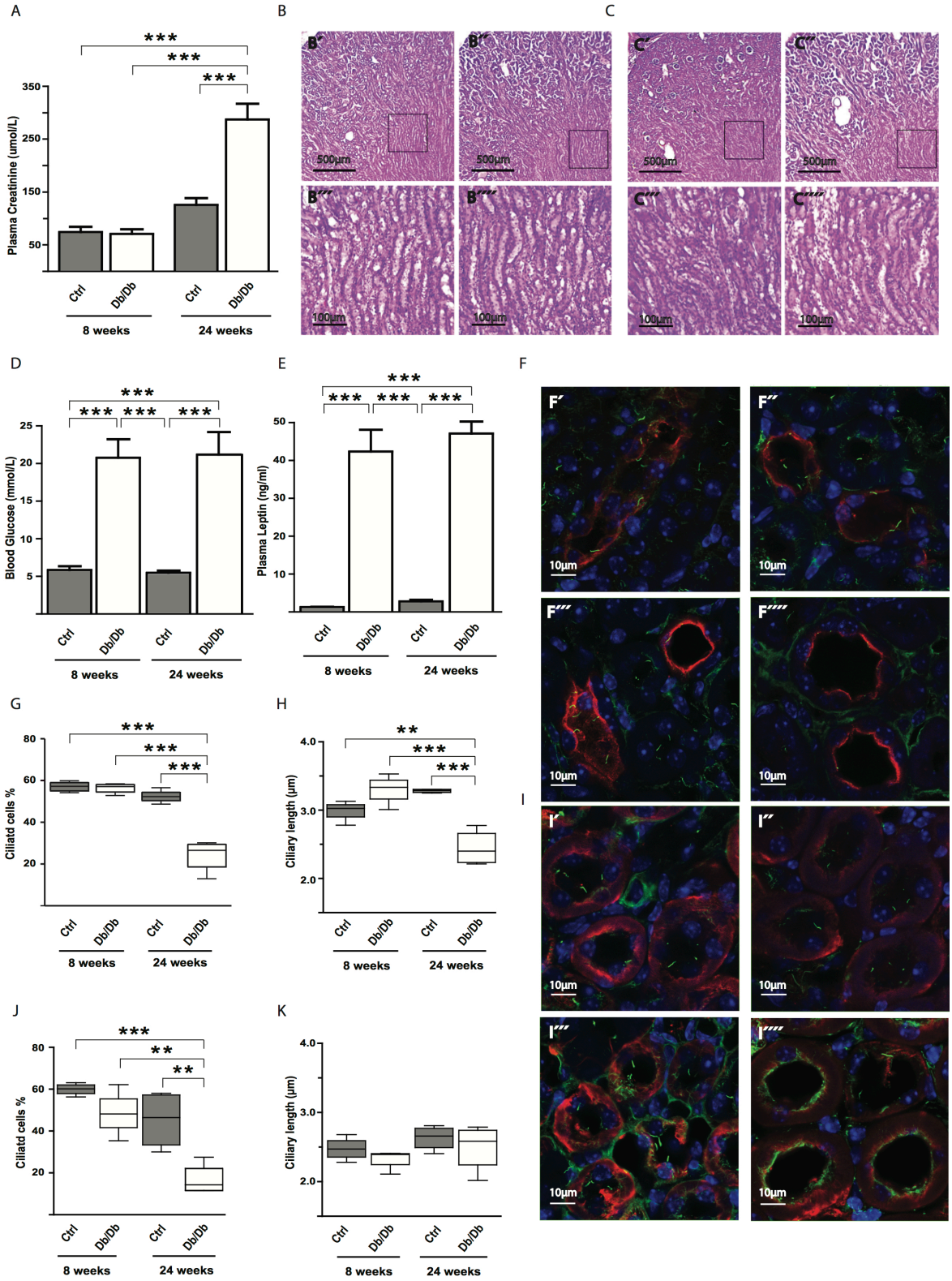

Figure 17. A) Non-fasting plasma creatinine in wt and db/db mice at 8 (n=4) and 24 (n=3) weeks of age. Mean ± s.e.m ANOVA+Tukey P<0.0001. B) Representative morphological kidney sections (20µm) counterstained with hematoxylin-eosin of 8 weeks wt (B´ and B´´) and db/db mouse (B´´and B´´´´). B´´´and B´´´´represent the magnification of the squares in B´ and B´´. C) Representative morphological kidney sections (20µm) counterstained with hematoxylin-eosin of 24 weeks wt (C´ and C``) and db/db mouse (C´´and C´´´´). C´´´and C´´´´represent the magnification of the squares in C´ and C´´. D) Non-fasting blood glucose in wt and db/db mice at 8 and 24 weeks of age (n=4 each group). Mean ± s.e.m ANOVA+Tukey P<0.0001. E) Non-fasting plasma leptin in wt and db/db mice at 8 (n=4) and 24 (n=3) weeks of age. Mean ± s.e.m ANOVA+Tukey

P<0.0001. F) Representative images of kidney sections (one stack) double stained with acetylated tubulin (green) for cilia measurement and aquaporin-2 (red) to identify collecting duct cells. Nuclei (blue) were counterstained with DAPI. F´ wt 8 weeks; F´´db/db 8 weeks; F´´´wt 24 weeks; F´´´´ db/db 24 weeks. G) Percentage of ciliated collecting duct cells in wt and db/db mice at 8 and 24 weeks of age. Data represents 3 medullary images (upper, middle and lower kidney) in duplicates for each mouse (n=4). Minimum 10 collecting duct cells have been counted for each image. Median + IQr and range (n=4). ANOVA + Bonferroni P<0.0001. H) Cilia length of collecting ducts cells in wt and db/db mice at 8 and 24 weeks of age. Data is represented as mentioned above. Median + IQr and range (n=4). ANOVA + Bonferroni P<0.0001. I) Representative images of kidney sections (one stack) double stained with acetylated tubulin (green) for cilia measurement and Na^{+}-K^{+} ATPase (red) to identify distal tubules cells. Nuclei (blue) were counterstained with DAPI. I´ wt 8 weeks; I´´db/db 8 weeks; I´´´wt 24 weeks; I´´´´ db/db 24 weeks. J) Percentage of ciliated distal tubules cells in wt and db/db mice at 8 and 24 weeks of age. Data is represented as mentioned above. Median + IQr and range (n=4). ANOVA + Bonferroni P=0.0003. K) Cilia length of distal tubules cells in wt and db/db mice at 8 and 24 weeks of age. Data is represented as mentioned above. Median + IQr and range (n=4). ANOVA + Bonferroni P=0.33.

These results show that ciliogenesis or cilia maintenance are altered during diabetic nephropathy in at least two different cell types. Although a defective ciliogenesis have been found in neurons during hyperleptinemia (182, 183), in 8 weeks old db/db mice ciliogenesis was not impaired in the presence of leptin levels similar to 24 weeks old db/db mice. For the same reason, we also excluded altered lipid profile as possible causes of ciliary derangements. However, we cannot fully exclude a role for adiponectin and insulin in the phenotype we observed due to their decrease in 24 week old db/db mice (Sup.Fig.3B,C).

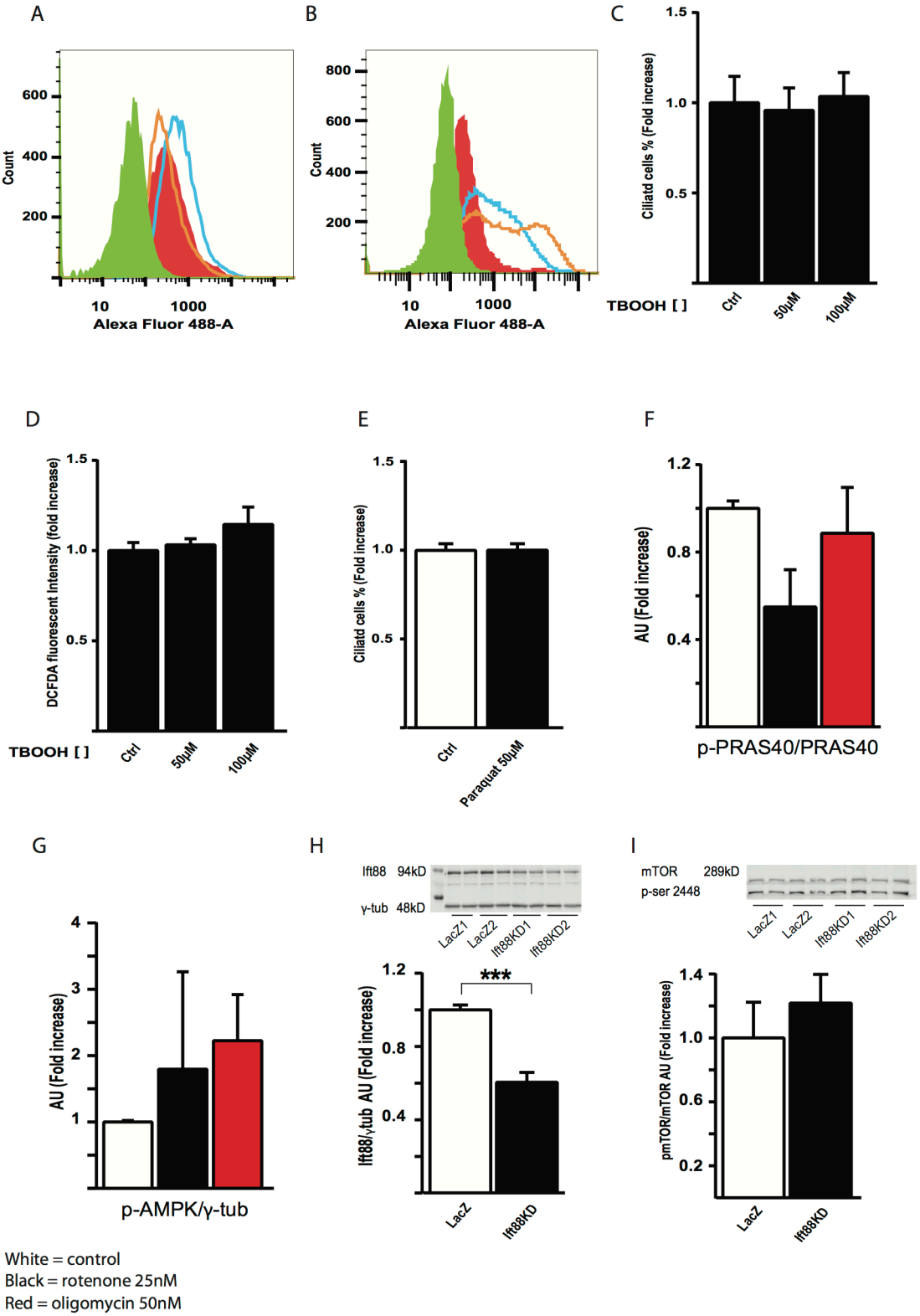

Supplementary Figure 1. A) Representation of flow cytometric histogram of IMCD3 stained with MitoSOX. Green: unstained, red: control, blue: rotenone, orange: oligomycin. B) Representation of flow cytometric histogram of IMCD3 stained with DCFDA. Green: unstained, red: control, blue: rotenone, orange: oligomycin. C) Quantification of dose dependent effect of TBOOH on number of ciliated IMCD3 cells. Data represent 3 experiments (n=14 with approximately 20 cells each). Mean ± s.e.m ANOVA P=0.69. D) Quantification of DCFDA intensity in IMCD3 cells after 48h treatment with different doses of TBOOH. Data represent 3 experiments (n=6). Mean ± s.e.m ANOVA P=0.28. E) Quantification of the effect of paraquat on number of ciliated IMCD3 cells. Data represent 3 experiments (n=14 with approximately 20 cells each). Mean ± s.e.m t-test P=0.99. F) Quantification of Fig.13E p-PRAS40 versus PRAS40 in IMCD3 treated for 48h with 25nM rotenone, 50nM oligomycin. Data represent 3 experiments (n>6). Mean + s.e.m ANOVA P=0.14. G) Quantification of Fig.13G p-AMPKα versus loading control in IMCD3 treated as above. Data represent 3 experiments (n>6). Median + IQr, Kruskal-Wallis P=0.08. H) Representative WB image of IFT88 protein from LacZ and *Ift88*KD stable IMCD3 and

quantification of IFT88 protein levels. Data represent 4 experiments (n=6). Mean ± s.e.m t-test P<0.001. I) Representative WB image of mTOR protein from LacZ and *Ift88*KD stable IMCD3 and quantification of pmTOR/mTOR ratio. Data represent 4 experiments (n=6). Mean ± s.e.m t-test P=0.12. The number 1 and 2 represent two different transductions used to generate *Ift88* stable cell lines.

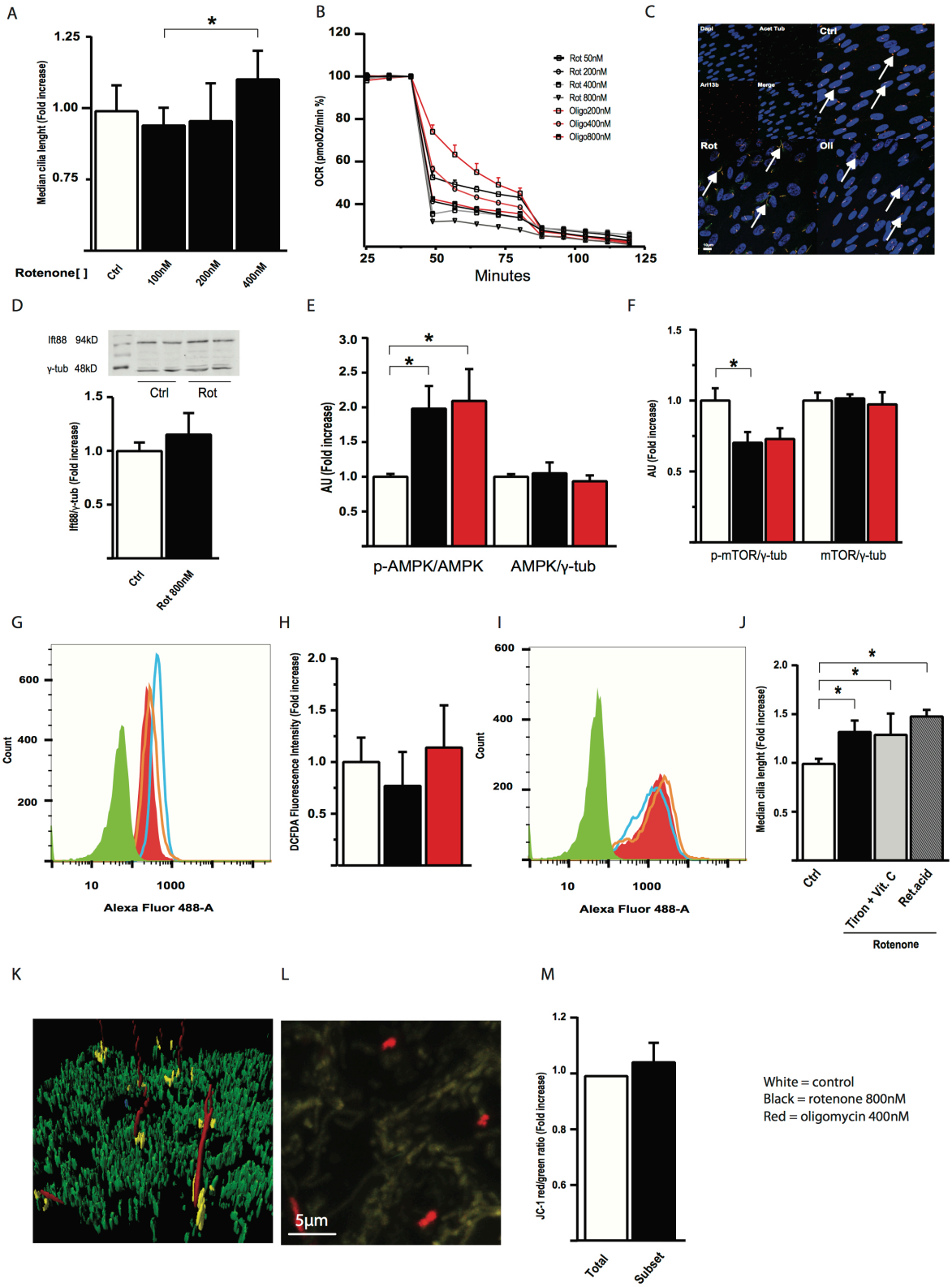

Supplementary Figure 2. A) Quantification of dose-dependent effect of rotenone on median cilia length in RPE1 cells treated 48h. Data represent 3 experiments (n>12 with >20 cells each). Median +IQr, Kruskal-Wallis + Tukey P=0.031. B) Representative experiment of cellular respiration (OCR) normalized to the baseline after addition of different doses of rotenone and oligomycin in RPE1. Mean ± s.e.m. C) Representative images of RPE1 cell line treated 48h with 800nM rotenone (rot) or 400nM oligomycin (oli). Examples of cilia are indicated with white arrows. The top left box represents the staining in single channels. D) Representative image of WB of IFT88 protein in RPE1 treated as above and quantification of

IFT88 protein levels. Data represent 3 experiments (n>6). Mean ± s.e.m. P=0.50. E) Quantification of Fig.15C in RPE1 cells. Median + IQr phospho-AMPKα/total AMPKα control 1.00 (0.96, 1.04); rotenone 1.86 (1.13, 2.28); oligomycin 2.14 (1.49, 2.26) Kruskal-Wallis + Tukey P=0.003; AMPKα/γtub Kruskal-Wallis P=0.3. Data represent 4 experiments (n=7). F) Quantification of Fig.15D in RPE1 cells. Mean ± s.e.m. phospho-mTOR/γtub control 1.00±0.09; rotenone 0.70±0.07; oligomycin 0.73±0.07. ANOVA + Tukey P=0.031; mTOR/γtub Kruskal-Wallis P=0.88. Data represent 4 experiments (n=7). G) Representation of flow cytometric histogram of RPE1 stained with MitoSOX. Green: unstained, red: control, blue: rotenone, orange: oligomycin. H) Quantification of DCFDA intensity in RPE1 cells treated as above. Data represent 3 experiments (n=6 of 50000 events). Mean ± s.e.m., ANOVA. P=0.27 I) Representation of flow cytometric histogram of RPE1 stained with DCFDA. Green: unstained, red: control, blue: rotenone, orange: oligomycin. J) Quantification of median ciliary length in RPE1 cells treated with 800nM of rotenone 48h in the presence of antioxidants (Tiron + Vit.C 1mM, retinoic acid 1uM). Data represent minimum 3 experiments (n>14). Median + IQr, Kruskal-Wallis + Dunn´s. P<0.001. K) Example of rendering with Imaris software used for JC1 and TMRE intensity quantification. Rendering colors: mitochondria (green), cilium (red), subset of selected mitochondria (yellow) within 2µM distance from the primary cilium. L) Representative cropped image of stable ARL13b-RFP-mito-PAGFP IMCD3 stained with JC1. M) Quantification of JC-1 red/green ratio normalized on the entire cell mitochondria (black) of the mitochondrial subset in proximity of the cilium (white). Data represent 2 experiments (n=8 approximately 20 cells each). Mitochondrial ciliary selected subset Mean + CI 0.98-1.12.

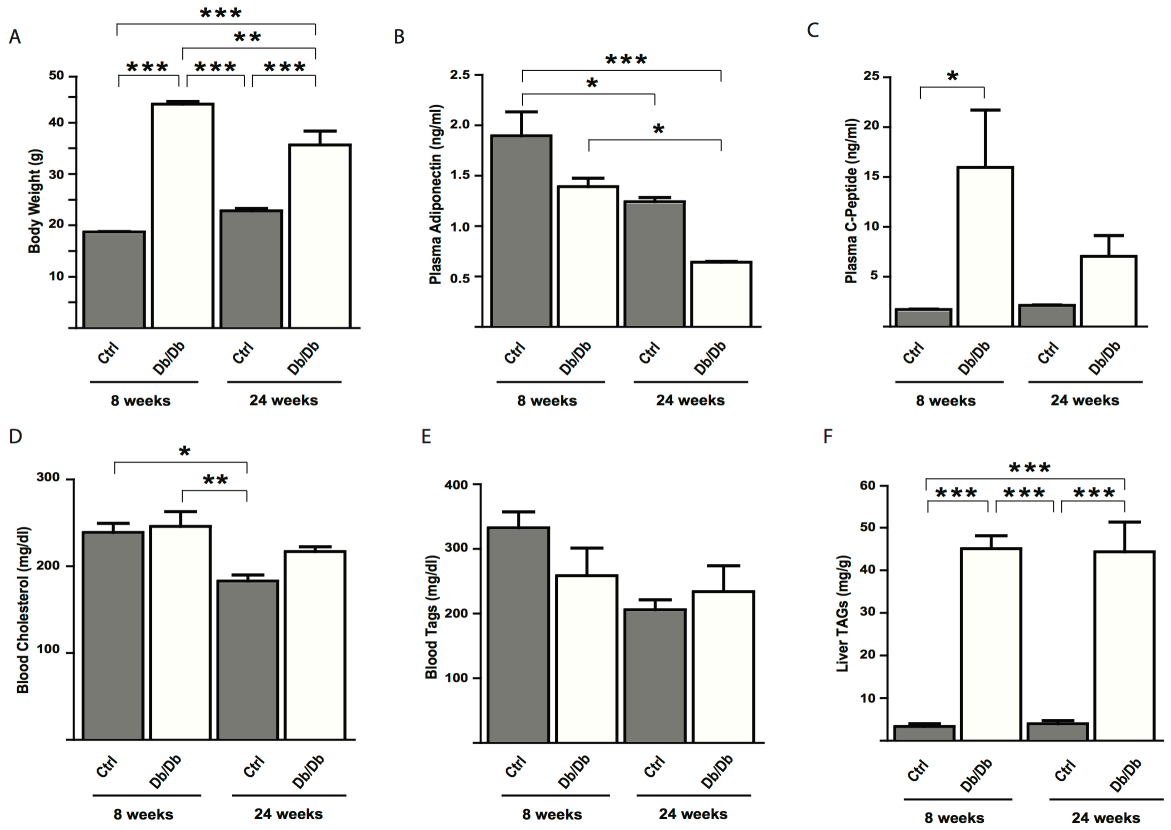

Supplementary Figure 3. A) Body weight of wt and db/db mice at 8 and 24 weeks of age (n=4 each group) P<0.0001. B) Plasma adiponectin in wt and db/db mice at 8 (n=4) and 24 weeks (n=3) of age. P=0.0011. C) Plasma C-Peptide in wt and db/db mice at 8 (n=4) and 24 weeks (n=3) of age. P=0.044. D) Blood cholesterol in wt and db/db mice at 8 (n=4) and 24 weeks (n=3) of age. P=0.0067. E) Blood triglycerides in wt and db/db mice at 8 (n=4) and 24 weeks (n=3) of age. P=0.086. F) Liver triglycerides in wt and db/db mice at 8 (n=4) and 24 weeks (n=3) of age. Data are presented as mean ± s.e.m ANOVA + Tukey P<0.0001.

4.5 PRELIMINARY RESULTS II: RELATIONSHIP BETWEEN $_{MT}$DNA COPY NUMBER AND CELLULAR ENERGY METABOLISM IN MIN6M9 AND IMCD3 CELL LINES

Mitochondrial DNA (mtDNA) copy number as well as mitochondrial mass are tissues specific and likely reflect different energy requirements (184). MtDNA depletion is a particular condition observed in cardiovascular disease, diabetes and cancer and might impair mitochondria and metabolic function of target tissues (49, 184). Moreover, a reduction in ATP production can be due to decrease in mtDNA in several tissues during aging (185).

As mentioned in the introduction (see 1.2.4), mtDNA and its transcription factor TFAM are in equilibrium with each other. Although much progress has been made in the understanding of the mtDNA replication, its mechanisms are still not clear. In this project we aimed to understand the relationship between the amount of mtDNA and mitochondrial bioenergetics.

4.5.1 Transient or Stable TFAM Knock Down Effects on Mitochondrial Respiration and ATP Levels in min6m9 and IMCD3 Cells

To investigate the relationship between mtDNA copy number and mitochondrial function, we generated shRNA (186) targeting *Tfam*. Using a commercially available adenoviral vector, we reduced *Tfam* mRNA in min6m9 and IMCD3 cells by 66.0 ± 3.2% and 71.5 ± 6.5% respectively (mean ± s.e.m.; Fig.18A). The reduction in gene expression was proportional to TFAM protein levels and mtDNA in min6m9 measured after one week of transduction (mean ± s.e.m. 53.9 ± 4.4% and 52.6 ± 4.3%, respectively) (Fig.18B,C).

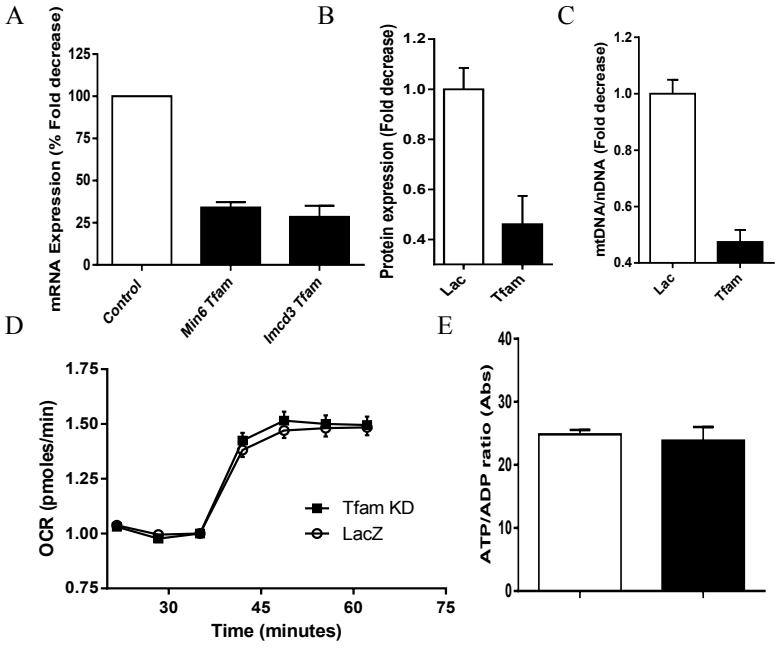

Figure 18. Adenoviral Transduction A) *Tfam* mRNA levels in min6m9 and IMCD3. Mean ± s.e.m 2 experiments n=4. B) TFAM protein expression in min6m9. Mean ± s.e.m 3 experiments n=6. D) mtDNA/nDNA ratio in min6m9. Mean ± s.e.m 2 experiments n=4 E) OCR normalized on baseline in glucose-stimulated min6m9. Mean + CI 1 experiment n=30. F) ATP/ADP ratio min6m9. Mean ± s.e.m 2 experiments n=3 White bar Lacz; black bar Tfam.

Despite the decrease of mtDNA in min6m9, which use almost exclusively mitochondria as energy source, we did not detect changes in the OCR upon glucose stimulation (Fig.18D) and ATP/ADP ratio *(mean ± s.e.m.: LacZ 25.2 ± 0.5, Tfam KD 24.5 ± 1.3)* (Fig.18E).

To overcome the limit of shRNA transient expression associated with adenoviral delivery, we generated cell lines stably expressing the shRNA targeting *Tfam*. This strategy has been successfully used to decrease mitochondrial energy production in human bone osteosarcoma cells and mouse embryonic cells (187, 188). Thus, we used lentivirus to integrate the shRNA into the cells genome. One month after transduction and blasticidin selection, IMCD3 cells showed decreased *Tfam* mRNA and protein as well as mtDNA levels *(mean ± s.e.m. decrease in Tfam: mRNA 49.8 ± 5.6%, protein 59.5 ± 3.9% and mtDNA COX vs S18 60.0 ± 2.7% and S12 vs S18 62.8 ± 7.2%)* (Fig.19A-C). Even more pronounced decline in protein expression was found in min6m9 stable cell line *(mean ± s.e.m. decrease in TFAM 78.2 ± 3.6%)* (Fig.19D).

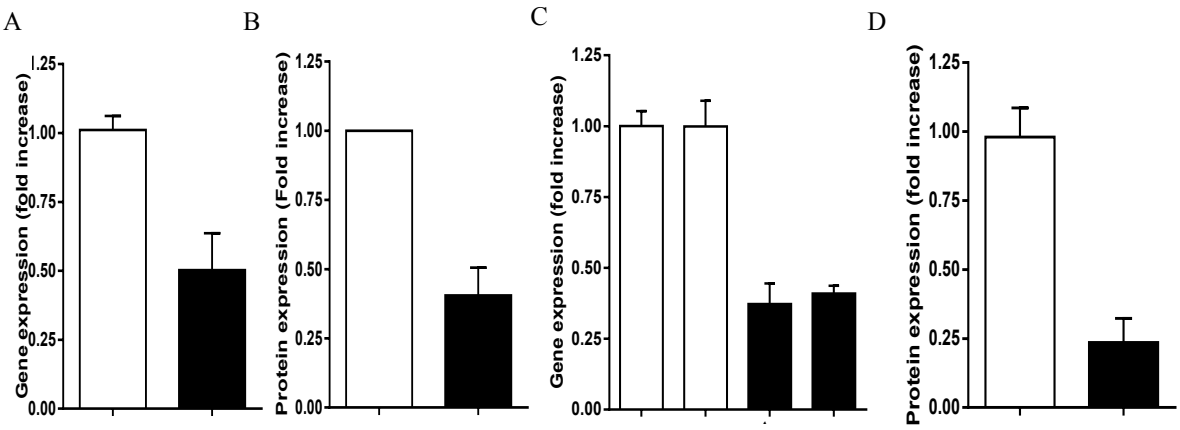

Figure 19. Stable cell lines. White = Control LacZ; Black *Tfam* KD. A) *Tfam* mRNA levels in IMCD3 stable KD. Mean ± s.e.m 3 experiments n=8. B) TFAM protein expression in IMCD3. Mean ± s.e.m 4 experiments n=6. C) mtDNA/nDNA in IMCD3. Left COX vs S18 and right S12 vs S18. Mean ± s.e.m 2 experiments n=3. D) TFAM protein expression levels in min6m9. Mean ± s.e.m 2 experiments n=7.

Surprisingly, the mitochondrial OCR was not altered in both min6m9 and IMCD3 stable cell lines compared to the control (Fig.20A,B) *(OCR normalized on LacZ. Mean + CI; IMCD3 cells: Basal LacZ 1.00 (0.98, 1.01); Tfam KD 0.96 (0.92, 0.99); Oligomycin LacZ 0.13 (0.12, 0.14), Tfam KD 0.16 (0.15, 0.17); FCCP LacZ 3.28 (3.13, 3,44) Tfam KD 3.45 (3.20, 3.70). Min6m9 cells: Basal LacZ 1.00 (0.96, 1.04); Tfam KD 1.12 (1.05, 1.19); Oligomycin LacZ 0.27 (0.24, 0.30), Tfam KD 0.28 (0.26, 0.30); FCCP LacZ 1.11 (1.03, 1.18) Tfam KD 1.48 (1.31, 1.69))*. To force IMCD3 cells to rely mainly on mitochondrial OXPHOS for ATP production we used a glucose-free media supplemented with galactose. It is worth to note that in this medium the cell growth was significantly reduced indicating a decrease in cellular energy. As expected, galactose culture decreased basal and maximum respiration (Fig.20B) *(OCR normalized on LacZ cultured in glucose media. Mean + CI; Basal LacZ 0.72 (0.67, 0.78); Tfam KD 0.84 (0.75, 0.92); Oligomycin LacZ 0.11 (0.09, 0.13), Tfam KD 0.11 (0.09, 0.13); FCCP LacZ 1.57 (1.47, 1.68) Tfam KD 1.70 (1.56, 1.85))*. However, the difference between cells expressing shRNA against *Tfam* and control (LacZ) was negligible. In line with

the respiration data, the ATP/ADP ratio was not changed compared to the control in IMCD3 (Fig.20D). Preliminary data from min6m9 showed a slight but significant decrease in ATP/ADP ratio suggesting that these cells might be affected by long-term depletion of mtDNA (Fig.20C) *(ATP/ADP ratio mean ± s.e.m.: LacZ 1.00 ± 0.05 and Tfam KD 0.76 ± 0.07)*.

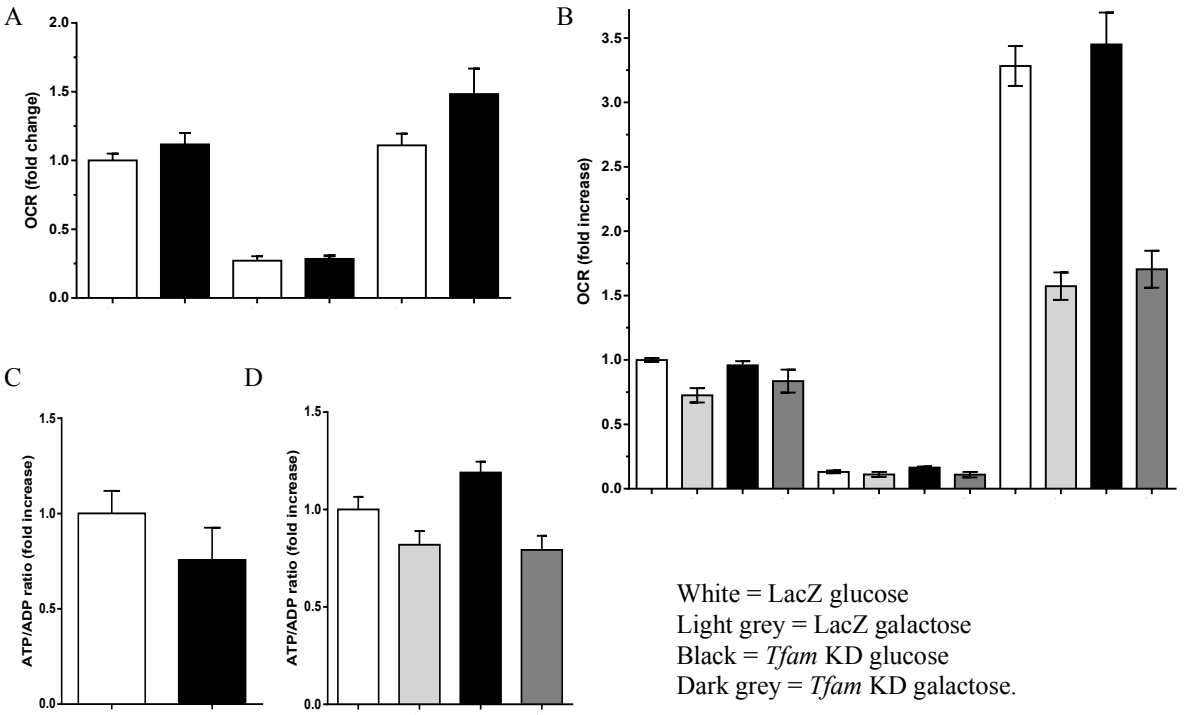

Figure 20. A) OCR in min6m9 stable cells normalized on basal respiration (left columns) after addition of 1μM oligomycin (central columns) and 7μM FCCP (right columns). Mean + CI 3 experiments. B) OCR in IMCD3 stable cells normalized on basal respiration and addition as above. Mean + CI 3 experiments. C) ATP/ADP ratio min6m9 stable cell. Mean ± s.e.m 2 experiments n=8. D) ATP/ADP ratio IMCD3 stable cell. Mean ± s.e.m 2 experiments n=8.

5 SUMMARY

1. Acute and long-term hyperglycemia caused a metabolic switch from oxidative phosphorylation to aerobic glycolysis in human healthy primary fibroblasts and endothelial cells. Transient acute alteration of mitochodrial respiration and intermembrane potential, as well as long-term reduction in cell proliferation, was due to hyperosmotic effect of high glucose. Prolonged exposure to high glucose decreased mitochondria steady-state and uncoupled respiration together with reduced ATP/ADP ratio without changes in mitochondria number, ROS production and cellular NAD^+/NADH ratio. Thus, in diabetes conditions, hyperglycemia in combination with hypoxia, inflammation and/or paracrine factors may be the cause of mitochondria dysfunction, ROS production and later complications.

2. In pancreatic islets, both high oxygen tension and hypoxia reduced mitochondria content and function, induced apoptosis and impaired glucose-stimulated insulin secretion. Preconditioning of pancretic islets using the K^+_{ATP} channel opener diazoxide protected against hypoxia. Thus, diazoxide preconditioning could improve transplanted pancreatic islets yield and function protecting them from the hypoxic environment during engrafment and revasculatization.

3. Primary cilia/basal body defect was associated with an impaired glucose-stimulated insulin release linked to the absent translocation of insulin receptor A to the cilium. Ciliary impairement had no effect on mitochondrial or cellular energy metabolism *in vitro*. A defective ciliogenesis was also found in β-cells of a diabetic rat model. Our *in vitro* studies indicated that decrease in ATP and increase in mitochondria ROS production impair cilia morphology and number. Altered cilia morphology and number was also found *in vivo* in diabetic nephropathy where the kidneys are characterized by increased ROS production and altered mitochondria metabolism. Conditions of decreased cellular energy levels and/or increased ROS production can potentially affect ciliary function. Dysfunctional cilia impairs insulin signaling and may also be associated with progression of diabetes complications.

4. mtDNA depletion by 60-80%, which in some extent has been found during diabetes, did not alter mitochondrial metabolism in two different cell types.

6 CONCLUSIONS AND FUTURE PERSPECTIVES

6.1 PAPER I

The pathogenic mechanisms leading to the complications of diabetes are yet to be clarified in order to develop strategies to counteract the progression of the disease. The primary cause triggering these deleterious pathways is hyperglycemia, which characterizes the diabetic disease. However, how high glucose levels are involved in the development of diabetes complications is still a matter of extensive research and debate. Several theories have been suggested in the last decades, the latest of which put mitochondria as source of metabolic and redox imbalance observed *in vivo*. Mitochondrial defects, overproduction of ROS and cellular redox imbalance are features of tissues exposed to the diabetic milieu but can either be cause or consequence of the disease.

Trying to unravel the pathogenic mechanism accounting for the metabolic defects during hyperglycemia, several works have been conducted using cell lines. In our work, we showed that healthy primary human cells exposed to hyperglycemia decrease their OXPHOS and shift their metabolism towards aerobic glycolysis. The increase in lactate levels due to hyperglycemia we found is in good agreement with previous works in cell lines and tissues (189, 190). Long-term hyperglycemia decreases cellular energy levels, maximal respiration without alteration in mitochondrial number or ROS production. These adjustments to the hyperglycemic milieu in healthy cells point out that other additive factors, such as time of exposure, hypoxia and paracrine mediators, might be necessary to exacerbate the deleterious effect of glucose. Moreover, the effect of these factors might be related to the characteristics of the cells composing that specific tissue.

In this work, we showed that hyperosmosis could alter acutely the cell metabolism, bioenergetics and growth. The intermittent negative effect of high osmotic pressure on mitochondrial and cellular function might be partly responsible for diabetes complications. In our opinion, our results help to better understand the mitochondrial and metabolic changes induced by high glucose. Monitoring cellular metabolic changes *in vivo* with novel technologies is necessary to reveal the primary mechanisms leading to the complications of diabetes in kidney, neurons, heart and vasculature, as well as during wound healing.

6.2 PAPER II AND III

In these two works we studied possible approaches to improve islets functionality and yield after transplantation using the K^+_{ATP} channel opener diazoxide or high oxygen tension

pretreatments. We sought first to confirm the deleterious metabolic effect of hypoxia in islets *in vitro*. Here, we found a decrease in mtDNA, mitochondrial complexes, glucose oxidation and ATP production following hypoxia and re-oxygenation.

Although hyperbaric chamber treatment and consequent hyperoxia is a valid coadjuvant treatment during transplantation, in our work pretreatment of isolated islets did not protect from the following hypoxia. The metabolic and mitochondrial impairments we found during hyperoxia are in agreement with other studies, in which decreased basal and spare respiratory capacity, and OXPHOS impairment *in vitro* were described (191, 192). Lastly, interpretation of hyperoxia and hypoxia regarding cellular respiration needs to be contextualized *in vivo*. In fact, *in vitro* measurements do not reflect the *in vivo* levels of oxygen in tissues and blood, especially regarding high oxygen tension (193).

Preconditioning of tissues or cells using different drugs has been proven to be effective against short periods of ischemia and thus hypoxia. In the current view, preconditioning activates cellular defenses against injuries, which depends on the energy metabolism and electrical activity of the cells. Although works on preconditioning effects have been carried out mostly in the heart, similar results have been obtained in brain, skeletal muscle, kidney and liver (161). One of the molecules mimicking preconditioning is the K^+_{ATP} channel opener diazoxide. This compound has been shown to activate K^+_{ATP} channels present both in the cellular surface and mitochondria, depending on cell type. Moreover, it can inhibit succinate dehydrogenase, ATP synthase and act as mitochondrial uncoupler (161). In line with works where diazoxide have been used during ischemia or ischemia/reperfusion, we found a protective effect of diazoxide preconditioning against hypoxia in pancreatic islets. This was due to a decrease in necrosis that we explained by a prolonged similar-resting state of the islets. The protective effect might be also *via* the induced increase in HIF1α and AMPK, which enable adaptation to hypoxia (30). Finally, in our work we found a positive effect of preconditioning with diazoxide, which has not been previously investigated, opening a new potential pretreatment to improve yield and function of transplanted islets.

6.3 PAPER IV

Ciliopathies are a heterogeneous class of genetic disorders that display different or similar phenotypes depending of the genes involved (see 1.3.2). Beside the most common manifestations of ciliopathies, Bardet-Biedl and Alström syndromes present obesity and high comorbidity with diabetes.

In our work we found that cilia/basal body impairment led to β-cells dysfunction, especially regarding first phase insulin secretion. We suggest that these impairments are due to the localization of IR-A isoform to the cilium in β-cells during insulin stimulation. When insulin signaling was disrupted due to ciliary defects, reduction of SNARE complex by decreased PI3K/FOXO1 transcriptional regulation affected the first-phase of insulin secretion. Corroborating this hypothesis, $Bbs4^{-/-}$ mice displayed impaired glucose tolerance at the moment in which they had the same weight compared to wild type littermates. Our findings are strictly related to the localization of the IR-A to the cilium after stimulation in insulin secreting cell, proved by the fact that depletion of a trafficking protein necessary for ciliary function (OFD1) produced results similar to BBS protein deficiency.

In the current work, we provide *in vivo* evidence of defective ciliogenesis in pancreatic islet of a rat model of diabetes (GK rats). The fact that other ciliopathies than Bardet-Biedl and Alström syndromes do not exhibit diabetes and/or obesity could be due to the gene and tissue involved in ciliary defects. However, it is also possible that diabetes or hyperglycemia is the cause of ciliary defect we found in β-cells. In this case, the ciliary impairment can establish a vicious cycle due to the recruitment of IR-A to the cilium during insulin stimulation. Further studies are needed to understand the IR-A specific signaling pathway through the cilium, in order to find novel strategy to increase insulin secretion from β-cells.

In conclusion, we found that cilia/basal body impairment led to β-cells dysfunction, and defective ciliogenesis in a rat model of diabetes. We suggest that these impairments are due to the localization of IR-A isoform at the cilium in β-cells upon insulin stimulation. However, the effect of diabetes *per se* and the activation of deleterious pathway that accompany the disease (e.g. ROS production or energy metabolism) in relation to the primary cilium should be studied not only in pancreas but also in other tissues to understand the cause/consequence relationship between diabetes and ciliary signaling.

6.4 PRELIMINARY RESULTS I

In the last decades the primary cilium has emerged as signaling organelle (113-117, 194). For its maintenance, it might be speculated that ciliary machinery requires a great amount of energy. However, to what extent energy depletion can affect ciliary assembly and morphology, thus potentially altering its functions, is not known.

Using two different cell lines (IMCD3 and RPE1), we found that interference with mitochondrial metabolism resulting in ATP depletion and ROS overproduction impairs primary cilium maintenance and morphology. Moreover, we found a subset of mitochondria

closer to the cilium, which displays a mitochondrial intermembrane potential similar compared to the one of the rest of the cell, indicating that this subset is in equilibrium with the intracellular mitochondrial network.

In line with *in vitro* findings, we showed ciliary impairment in at least two different kidney cell types in a diabetic mouse model (db/db mouse) during nephropathy. In db/db mice during diabetic nephropathy sustained ROS production and metabolic derangements have been previously described, thus supporting our hypothesis that cilia can be affected by these causes (67, 84, 102, 105, 180).

In conclusion, we described for the first time that interfering with the energy status of the cells impaired cilia formation or maintenance. We showed that ATP levels but not changes in ATP/ADP ratio could be critical to maintain primary cilia at least *via* protein synthesis. Moreover, we suggest that in both IMCD3 and RPE1 cell types, the impairment in ciliation could be due to a small amount of radicals for prolonged period of time acting as signaling molecules. The *in vivo* evidence of ciliary impairments in a mouse model that closely represents the human progression of diabetic nephropathy is also a novel finding. However, further studies would be needed to clarify the mechanisms by which ROS affects cilia and their functions in different cell types.

Since mitochondrial radical production and energy balance are impaired during aging and other disease states, it would be important to further study ciliary function and morphology in different disease models in order to understand whether or not ciliary signaling could contribute to disease progression and aging.

6.5 PRELIMINARY RESULTS II

MtDNA depletion is a particular condition observed in several pathological conditions such as cardiovascular disease, diabetes and cancer and might impair mitochondria and metabolic function of target tissues (49, 184). Mitochondrial and cellular metabolism is severely impaired when mtDNA is absent (e.g treatment with EtBr or *Tfam* knock out). Larsson and colleagues showed that homozygous knock out of *Tfam* is not compatible with life underlining that TFAM is necessary for development and survival (195). However, the mitochondrial metabolic alterations as a consequence of decreased mtDNA are not clear. In fact, in $Tfam^{+/-}$ mouse, where the TFAM and mtDNA levels are reduced to half, only a slight reduction of transcripts and single complex activities in the heart has been found, suggesting an excess of mitochondrial transcripts compared to cellular needs. In tissues such as the heart, the described phenotype might be related to a higher mtDNA turnover and abundance of

mitochondrial proteins. Corroborating the hypothesis of excess of transcripts, more than 60% reduction in TFAM and mtDNA in *Drosophila* affects only some mitochondrial transcripts turnover (mrRNA) (196).

Our preliminary data suggest that mitochondrial bioenergetics is only partially dependent on the amount of mtDNA. In fact, we demonstrated that stably decreasing mtDNA copies up to 60-80% in two metabolically different cell lines did not affect mitochondrial respiration. Our result is in line with a previous observation in cultured adipocytes (197). A possible explanation could be that there is a threshold for the amount of mtDNA under which the mitochondrial dysfunction leads to an impairment of cellular bioenergetics. It would be important in future research to understand the reason of the possible overabundance of mtDNA and the amount of mtDNA needed for different tissues to be metabolically healthy.

7 ACKNOWLEDGEMENTS

Firstly, I would like to express my sincere gratitude to my main supervisor **Prof. Kerstin Brismar**. Thank you for accepting me as student, for having believed in me, given me so much support and rescued me in difficult situations. You showed me how a world-known person in the academic field can be a great scientist and at the same time an understanding, patient and open-minded person with high moral values. You are the difference between a boss and a leader. I will always be thankful for having you as supervisor and to have known such an impressive person.

To my co-supervisors **Dr. Jacob Grünler**, **Dr. Michael Tekle**, **Dr. Chrsitian Bergamini** and **Dr. Ismael-Valladolid-Acebes** for the scientific and practical advices during all my studies, for teaching me and being always there in case of necessity. Thank you Jacob also for having helped me in my transition in Sweden and being there always for everybody. Together with Micke and his laughter it was great to have you on my side. Thank you Chris for all you taught me in the lab, the discussion and the friendship you demonstrated. It has been an honor and really fun for me to work with you. Ismael "hermano" there are no words to express my joy to have known you. Thank you for everything, inside and outside science.

Beside my advisors, I would like to thank my mentor **Dr. Slavena Mandic** for accepting this role and for having listened and given me advices when I needed.

I would like to thank also the people who instilled me the passion for science and mitochondria. In particular thanks to **Prof. Giovanna Parenti-Castelli** who with passion first introduced me to biochemistry, **Prof. Giorgio Lenaz** for your help from the bachelor thesis to the Ph.D. and for suggesting me to contact Prof. Kerstin Brismar. To **Prof. Romana Fato** who has been always supportive and an example of scientific professionalism and human values (and great cakes!!).

I would like to express my special appreciation and thanks to **Prof. P-O Berggren** and his group for the collaboration during my work and for being always prompt in his comment and replies whenever needed. To **Prof. Heiko Lickert** for the help and comprehension during the time I spent in Germany in your lab and for being a great scientist and sincere person and **Dr. Jantje Gerdes** for the possibility to work with the extremely interesting and expanding field of primary cilia.

A sincere thanks goes to the people in the administration and in particular **Ann-Britt and Katarina** who help me through all the "easy" applications needed during the doctoral

process. Big thanks also to the secretaries of Kerstin (**IngeBorg**) and Heiko at Helmholtz (**Donna**) for being always on top of things and ready to help. To **Jan Erik** for the extraordinary IT support.

I thank my fellow lab mates for the great help and good time during and after work. In particular **Charlotte Mattsson**, great friend and office mate for having spent times helping my acclimatization in Sweden and to introduce me to my girlfriend Sara. A special thank goes to "the Italian crew" **Teresa Daraio** and **Marianna Del Sole** for the jokes, fun time and "sometimes" serious discussions. I would like to thank **Prof. Gustav Dallner** for transmitting his passion for science, his enthusiasm and also for having found together with Jacob my first two amazing place to live in Sweden. My sincere thanks goes to **Yan Xiong**, lab mates and friend who helped me and taught me constantly in the lab with her experience and patience. Moreover, thank you to all the lab mates from Kerstin´s group **Ileana, Octavian, Xiaowei, David, Katrin, Åse, Ishtrath, Anette, Stina, Cristina, Elisabete, Magnus, Vivek, Jing, Inga-Lena, Elvi, Harvest, Sampath, Senthil** and P-O Berggren´s group **Meike, Karin, Subbu, Andrea, Erwin, Elisabetta, Essam, Lars, Lisa, Martin, Stefan, Thomas, Yue, Yixin, Jaeyoon, Tushita, Chris, Sergei, Irina, Galina, Ingo, Barbara, Tilo** for the help and the good time spent during science discussions, lunch and MF pub. A special thanks also goes to the lab mates at the Helmholtz-Center Munich **Anika, Donna, Feli, Lexi, Aurelia, Robert, Stefan, Ingo, Moritz, Pallawi, Erik, Michi, Amir, Toto, Marta, Kerstin, Anett, Julia**, the neighboring lab **Carmelo, Cristina, Fabio, MJ, Daniel, Uma, Dirij, Christian, Matthias, Beata**. In particular I want to express my gratitude to the office **Mostafa, Aimee, Dapeng, Lisann, Francesco** and **Adriana** and **Bader** for the friendship, support, discussions and experiences together.

To my closest friends from Italy **Steppa** and **Poz**. You are the ones, which even for one second I have lost contact with and it is not easy after so many years abroad. You have been always there and I consider you part of my family. To all my Italian (in particular **Vale, Fae, Linda, Davide, Pamela, Fil, Ale, Lucia, Jessica, Michele, Daria, Erica**) and German (**Jacob, Max, Flo, Michi, Peter**) and Poinger (**Ale, Eugenia**) friends for spending time and have fun together whenever possible.

Last but not least an immense thank to my family. Ai miei genitori **Mauro** e **Nadia** che mi hanno supportato e sopportato in molte difficili decisioni e che mi hanno dato l´opportuntitá di seguire il mio desiderio di studiare. Sebbene non sia molto bravo a esprimerlo a parole o nella vita reale, voi siete quelli a cui devo di piú. To **Sara,** thank you for being as you are.

You gave me joy, strength and balance in difficult moments. With you I grew as a person and now as father of our great joy Eliott and his brother or sister that will be with us soon.

This research was supported by grants from Family Erling-Persson Foundation, Medical Research Council, Magnus Bergvalls Stiftelse, Berth von Kantzows stiftelse and O.E och Edla Johansson vetenskapliga stiftelse.

8 REFERENCES

1. WHO. 2016 (http://www.who.int/features/factfiles /diabetes/facts/en/index8.html).
2. WHO. 2016. (http://www.euro.who.int/data/assets/pdf_file/0003/98391/E93348.pdf).
3. International Diabetes Federation B, Belgium. IDF Diabetes Atlas. 2009;4th edn. .
4. Pinhas-Hamiel O, Zeitler P. Type 2 diabetes in adolescents, no longer rare. Pediatr Rev. 1998;19(12):434-5.
5. American Diabetes A. Standards of medical care in diabetes--2013. Diabetes Care. 2013;36 Suppl 1:S11-66.
6. Perfetti R, Merkel P. Glucagon-like peptide-1: a major regulator of pancreatic beta-cell function. European journal of endocrinology / European Federation of Endocrine Societies. 2000;143(6):717-25.
7. Drucker DJ. Enhancing incretin action for the treatment of type 2 diabetes. Diabetes Care. 2003;26(10):2929-40.
8. Zhao C, Wilson MC, Schuit F, Halestrap AP, Rutter GA. Expression and distribution of lactate/monocarboxylate transporter isoforms in pancreatic islets and the exocrine pancreas. Diabetes. 2001;50(2):361-6.
9. Maechler P. Mitochondrial function and insulin secretion. Molecular and cellular endocrinology. 2013;379(1-2):12-8.
10. Reidy K, Kang HM, Hostetter T, Susztak K. Molecular mechanisms of diabetic kidney disease. J Clin Invest. 2014;124(6):2333-40.
11. Hippisley-Cox J, Coupland C. Predicting the risk of chronic Kidney Disease in men and women in England and Wales: prospective derivation and external validation of the QKidney Scores. BMC family practice. 2010;11:49.
12. Mogensen CE, Andersen MJ. Increased kidney size and glomerular filtration rate in early juvenile diabetes. Diabetes. 1973;22(9):706-12.
13. Forbes JM, Cooper ME. Mechanisms of diabetic complications. Physiol Rev. 2013;93(1):137-88.
14. Klein R, Klein BE, Moss SE, Davis MD, DeMets DL. The Wisconsin epidemiologic study of diabetic retinopathy. II. Prevalence and risk of diabetic retinopathy when age at diagnosis is less than 30 years. Arch Ophthalmol. 1984;102(4):520-6.
15. Antonetti DA, Barber AJ, Bronson SK, Freeman WM, Gardner TW, Jefferson LS, et al. Diabetic retinopathy: seeing beyond glucose-induced microvascular disease. Diabetes. 2006;55(9):2401-11.
16. Frank RN. The galactosemic dog. A valid model for both early and late stages of diabetic retinopathy. Arch Ophthalmol. 1995;113(3):275-6.
17. Kern TS, Engerman RL. Capillary lesions develop in retina rather than cerebral cortex in diabetes and experimental galactosemia. Arch Ophthalmol. 1996;114(3):306-10.
18. Stratton IM, Kohner EM, Aldington SJ, Turner RC, Holman RR, Manley SE, et al. UKPDS 50: risk factors for incidence and progression of retinopathy in Type II diabetes over 6 years from diagnosis. Diabetologia. 2001;44(2):156-63.
19. Klein R, Klein BE. Relation of glycemic control to diabetic complications and health outcomes. Diabetes Care. 1998;21 Suppl 3:C39-43.
20. Abbott CA, Malik RA, van Ross ER, Kulkarni J, Boulton AJ. Prevalence and characteristics of painful diabetic neuropathy in a large community-based diabetic population in the U.K. Diabetes Care. 2011;34(10):2220-4.
21. Said G. Diabetic neuropathy--a review. Nat Clin Pract Neurol. 2007;3(6):331-40.
22. Thamotharampillai K, Chan AK, Bennetts B, Craig ME, Cusumano J, Silink M, et al. Decline in neurophysiological function after 7 years in an adolescent diabetic cohort and the role of aldose reductase gene polymorphisms. Diabetes Care. 2006;29(9):2053-7.
23. Sumner CJ, Sheth S, Griffin JW, Cornblath DR, Polydefkis M. The spectrum of neuropathy in diabetes and impaired glucose tolerance. Neurology. 2003;60(1):108-11.
24. Cade WT. Diabetes-related microvascular and macrovascular diseases in the physical therapy setting. Phys Ther. 2008;88(11):1322-35.
25. The effect of intensive treatment of diabetes on the development and progression of long-term complications in insulin-dependent diabetes mellitus. The Diabetes Control and Complications Trial Research Group. N Engl J Med. 1993;329(14):977-86.
26. Godoy A, Ulloa V, Rodriguez F, Reinicke K, Yanez AJ, Garcia Mde L, et al. Differential subcellular distribution of glucose transporters GLUT1-6 and GLUT9 in human cancer: ultrastructural localization of GLUT1 and GLUT5 in breast tumor tissues. J Cell Physiol. 2006;207(3):614-27.

27. Carruthers A, DeZutter J, Ganguly A, Devaskar SU. Will the original glucose transporter isoform please stand up! Am J Physiol Endocrinol Metab. 2009;297(4):E836-48.
28. Jorneskog G, Brismar K, Fagrell B. Skin capillary circulation is more impaired in the toes of diabetic than non-diabetic patients with peripheral vascular disease. Diabetic medicine : a journal of the British Diabetic Association. 1995;12(1):36-41.
29. Jorneskog G, Brismar K, Fagrell B. Pronounced skin capillary ischemia in the feet of diabetic patients with bad metabolic control. Diabetologia. 1998;41(4):410-5.
30. Catrina SB. Impaired hypoxia-inducible factor (HIF) regulation by hyperglycemia. J Mol Med (Berl). 2014;92(10):1025-34.
31. Brownlee M. Biochemistry and molecular cell biology of diabetic complications. Nature. 2001;414(6865):813-20.
32. Du XL, Edelstein D, Rossetti L, Fantus IG, Goldberg H, Ziyadeh F, et al. Hyperglycemia-induced mitochondrial superoxide overproduction activates the hexosamine pathway and induces plasminogen activator inhibitor-1 expression by increasing Sp1 glycosylation. Proc Natl Acad Sci U S A. 2000;97(22):12222-6.
33. Nishikawa T, Edelstein D, Du XL, Yamagishi S, Matsumura T, Kaneda Y, et al. Normalizing mitochondrial superoxide production blocks three pathways of hyperglycaemic damage. Nature. 2000;404(6779):787-90.
34. Williamson JR, Chang K, Frangos M, Hasan KS, Ido Y, Kawamura T, et al. Hyperglycemic pseudohypoxia and diabetic complications. Diabetes. 1993;42(6):801-13.
35. Ido Y. Pyridine nucleotide redox abnormalities in diabetes. Antioxid Redox Signal. 2007;9(7):931-42.
36. Hung YP, Yellen G. Live-cell imaging of cytosolic NADH-NAD+ redox state using a genetically encoded fluorescent biosensor. Methods Mol Biol. 2014;1071:83-95.
37. Zhao Y, Yang Y. Profiling metabolic states with genetically encoded fluorescent biosensors for NADH. Curr Opin Biotechnol. 2015;31:86-92.
38. Christensen CE, Karlsson M, Winther JR, Jensen PR, Lerche MH. Non-invasive in-cell determination of free cytosolic [NAD+]/[NADH] ratios using hyperpolarized glucose show large variations in metabolic phenotypes. The Journal of biological chemistry. 2014;289(4):2344-52.
39. Nathan DM, Bayless M, Cleary P, Genuth S, Gubitosi-Klug R, Lachin JM, et al. Diabetes control and complications trial/epidemiology of diabetes interventions and complications study at 30 years: advances and contributions. Diabetes. 2013;62(12):3976-86.
40. Rekittke NE, Ang M, Rawat D, Khatri R, Linn T. Regenerative Therapy of Type 1 Diabetes Mellitus: From Pancreatic Islet Transplantation to Mesenchymal Stem Cells. Stem Cells Int. 2016;2016:3764681.
41. Johannesson B, Sui L, Freytes DO, Creusot RJ, Egli D. Toward beta cell replacement for diabetes. The EMBO journal. 2015;34(7):841-55.
42. Ramirez MA, Borja NL. Epalrestat: an aldose reductase inhibitor for the treatment of diabetic neuropathy. Pharmacotherapy. 2008;28(5):646-55.
43. Geraldes P, King GL. Activation of protein kinase C isoforms and its impact on diabetic complications. Circ Res. 2010;106(8):1319-31.
44. Ansurudeen I, Sunkari VG, Grunler J, Peters V, Schmitt CP, Catrina SB, et al. Carnosine enhances diabetic wound healing in the db/db mouse model of type 2 diabetes. Amino Acids. 2012;43(1):127-34.
45. Shi TJ, Zhang MD, Zeberg H, Nilsson J, Grunler J, Liu SX, et al. Coenzyme Q10 prevents peripheral neuropathy and attenuates neuron loss in the db-/db- mouse, a type 2 diabetes model. Proc Natl Acad Sci U S A. 2013;110(2):690-5.
46. Ceriello A, Testa R, Genovese S. Clinical implications of oxidative stress and potential role of natural antioxidants in diabetic vascular complications. Nutr Metab Cardiovasc Dis. 2016;26(4):285-92.
47. Wiesner RJ, Ruegg JC, Morano I. Counting target molecules by exponential polymerase chain reaction: copy number of mitochondrial DNA in rat tissues. Biochem Biophys Res Commun. 1992;183(2):553-9.
48. Seidel-Rogol BL, Shadel GS. Modulation of mitochondrial transcription in response to mtDNA depletion and repletion in HeLa cells. Nucleic Acids Res. 2002;30(9):1929-34.
49. Clay Montier LL, Deng JJ, Bai Y. Number matters: control of mammalian mitochondrial DNA copy number. Journal of genetics and genomics = Yi chuan xue bao. 2009;36(3):125-31.
50. Fisher RP, Clayton DA. A transcription factor required for promoter recognition by human mitochondrial RNA polymerase. Accurate initiation at the heavy- and light-strand promoters dissected and reconstituted in vitro. J Biol Chem. 1985;260(20):11330-8.

51. Furukawa R, Yamada Y, Matsushima Y, Goto Y, Harashima H. The manner in which DNA is packaged with TFAM has an impact on transcription activation and inhibition. FEBS open bio. 2012;2:145-50.
52. McCulloch V, Seidel-Rogol BL, Shadel GS. A human mitochondrial transcription factor is related to RNA adenine methyltransferases and binds S-adenosylmethionine. Molecular and cellular biology. 2002;22(4):1116-25.
53. Falkenberg M, Gaspari M, Rantanen A, Trifunovic A, Larsson NG, Gustafsson CM. Mitochondrial transcription factors B1 and B2 activate transcription of human mtDNA. Nature genetics. 2002;31(3):289-94.
54. Matsushima Y, Adan C, Garesse R, Kaguni LS. Drosophila mitochondrial transcription factor B1 modulates mitochondrial translation but not transcription or DNA copy number in Schneider cells. J Biol Chem. 2005;280(17):16815-20.
55. Matsushima Y, Garesse R, Kaguni LS. Drosophila mitochondrial transcription factor B2 regulates mitochondrial DNA copy number and transcription in schneider cells. J Biol Chem. 2004;279(26):26900-5.
56. Scarpulla RC. Transcriptional paradigms in mammalian mitochondrial biogenesis and function. Physiol Rev. 2008;88(2):611-38.
57. Wredenberg A, Freyer C, Sandstrom ME, Katz A, Wibom R, Westerblad H, et al. Respiratory chain dysfunction in skeletal muscle does not cause insulin resistance. Biochem Biophys Res Commun. 2006;350(1):202-7.
58. Zabielski P, Lanza IR, Gopala S, Heppelmann CJ, Bergen HR, 3rd, Dasari S, et al. Altered Skeletal Muscle Mitochondrial Proteome As the Basis of Disruption of Mitochondrial Function in Diabetic Mice. Diabetes. 2016;65(3):561-73.
59. Sleigh A, Raymond-Barker P, Thackray K, Porter D, Hatunic M, Vottero A, et al. Mitochondrial dysfunction in patients with primary congenital insulin resistance. J Clin Invest. 2011;121(6):2457-61.
60. Karakelides H, Asmann YW, Bigelow ML, Short KR, Dhatariya K, Coenen-Schimke J, et al. Effect of insulin deprivation on muscle mitochondrial ATP production and gene transcript levels in type 1 diabetic subjects. Diabetes. 2007;56(11):2683-9.
61. Ritov VB, Menshikova EV, He J, Ferrell RE, Goodpaster BH, Kelley DE. Deficiency of subsarcolemmal mitochondria in obesity and type 2 diabetes. Diabetes. 2005;54(1):8-14.
62. Kelley DE, He J, Menshikova EV, Ritov VB. Dysfunction of mitochondria in human skeletal muscle in type 2 diabetes. Diabetes. 2002;51(10):2944-50.
63. Patti ME, Butte AJ, Crunkhorn S, Cusi K, Berria R, Kashyap S, et al. Coordinated reduction of genes of oxidative metabolism in humans with insulin resistance and diabetes: Potential role of PGC1 and NRF1. Proc Natl Acad Sci U S A. 2003;100(14):8466-71.
64. Morino K, Petersen KF, Dufour S, Befroy D, Frattini J, Shatzkes N, et al. Reduced mitochondrial density and increased IRS-1 serine phosphorylation in muscle of insulin-resistant offspring of type 2 diabetic parents. J Clin Invest. 2005;115(12):3587-93.
65. Chattopadhyay M, Guhathakurta I, Behera P, Ranjan KR, Khanna M, Mukhopadhyay S, et al. Mitochondrial bioenergetics is not impaired in nonobese subjects with type 2 diabetes mellitus. Metabolism. 2011;60(12):1702-10.
66. Anderson EJ, Kypson AP, Rodriguez E, Anderson CA, Lehr EJ, Neufer PD. Substrate-specific derangements in mitochondrial metabolism and redox balance in the atrium of the type 2 diabetic human heart. J Am Coll Cardiol. 2009;54(20):1891-8.
67. Sharma K, Karl B, Mathew AV, Gangoiti JA, Wassel CL, Saito R, et al. Metabolomics reveals signature of mitochondrial dysfunction in diabetic kidney disease. J Am Soc Nephrol. 2013;24(11):1901-12.
68. Kang HM, Ahn SH, Choi P, Ko YA, Han SH, Chinga F, et al. Defective fatty acid oxidation in renal tubular epithelial cells has a key role in kidney fibrosis development. Nat Med. 2015;21(1):37-46.
69. Lee HK, Song JH, Shin CS, Park DJ, Park KS, Lee KU, et al. Decreased mitochondrial DNA content in peripheral blood precedes the development of non-insulin-dependent diabetes mellitus. Diabetes research and clinical practice. 1998;42(3):161-7.
70. Reiling E, Ling C, Uitterlinden AG, Van't Riet E, Welschen LM, Ladenvall C, et al. The association of mitochondrial content with prevalent and incident type 2 diabetes. J Clin Endocrinol Metab. 2010;95(4):1909-15.
71. Widlansky ME, Wang J, Shenouda SM, Hagen TM, Smith AR, Kizhakekuttu TJ, et al. Altered mitochondrial membrane potential, mass, and morphology in the mononuclear cells of humans with type 2 diabetes. Translational research : the journal of laboratory and clinical medicine. 2010;156(1):15-25.

72. Avila C, Huang RJ, Stevens MV, Aponte AM, Tripodi D, Kim KY, et al. Platelet mitochondrial dysfunction is evident in type 2 diabetes in association with modifications of mitochondrial anti-oxidant stress proteins. Exp Clin Endocrinol Diabetes. 2012;120(4):248-51.
73. Shen X, Zheng S, Thongboonkerd V, Xu M, Pierce WM, Jr., Klein JB, et al. Cardiac mitochondrial damage and biogenesis in a chronic model of type 1 diabetes. Am J Physiol Endocrinol Metab. 2004;287(5):E896-905.
74. Tomita M, Mukae S, Geshi E, Umetsu K, Nakatani M, Katagiri T. Mitochondrial respiratory impairment in streptozotocin-induced diabetic rat heart. Jpn Circ J. 1996;60(9):673-82.
75. Boveris AA, Cattaneo de Peralta R, Stoppani AO, Foglia VG. Phosphorylation, oxidation, and ubiquinone content in diabetic mitochondria. Proc Soc Exp Biol Med. 1969;132(1):171-4.
76. Coughlan MT, Thorburn DR, Penfold SA, Laskowski A, Harcourt BE, Sourris KC, et al. RAGE-induced cytosolic ROS promote mitochondrial superoxide generation in diabetes. J Am Soc Nephrol. 2009;20(4):742-52.
77. Rosca MG, Mustata TG, Kinter MT, Ozdemir AM, Kern TS, Szweda LI, et al. Glycation of mitochondrial proteins from diabetic rat kidney is associated with excess superoxide formation. Am J Physiol Renal Physiol. 2005;289(2):F420-30.
78. Munusamy S, Saba H, Mitchell T, Megyesi JK, Brock RW, Macmillan-Crow LA. Alteration of renal respiratory Complex-III during experimental type-1 diabetes. BMC Endocr Disord. 2009;9:2.
79. Bugger H, Chen D, Riehle C, Soto J, Theobald HA, Hu XX, et al. Tissue-specific remodeling of the mitochondrial proteome in type 1 diabetic akita mice. Diabetes. 2009;58(9):1986-97.
80. Chang JH, Gurley SB. Assessment of diabetic nephropathy in the Akita mouse. Methods Mol Biol. 2012;933:17-29.
81. Tan AL, Sourris KC, Harcourt BE, Thallas-Bonke V, Penfold S, Andrikopoulos S, et al. Disparate effects on renal and oxidative parameters following RAGE deletion, AGE accumulation inhibition, or dietary AGE control in experimental diabetic nephropathy. Am J Physiol Renal Physiol. 2010;298(3):F763-70.
82. Cortes P, Dumler F, Goldman J, Levin NW. Relationship between renal function and metabolic alterations in early streptozocin-induced diabetes in rats. Diabetes. 1987;36(1):80-7.
83. Zhang H, Zhang HM, Wu LP, Tan DX, Kamat A, Li YQ, et al. Impaired mitochondrial complex III and melatonin responsive reactive oxygen species generation in kidney mitochondria of db/db mice. J Pineal Res. 2011;51(3):338-44.
84. Persson MF, Franzen S, Catrina SB, Dallner G, Hansell P, Brismar K, et al. Coenzyme Q10 prevents GDP-sensitive mitochondrial uncoupling, glomerular hyperfiltration and proteinuria in kidneys from db/db mice as a model of type 2 diabetes. Diabetologia. 2012;55(5):1535-43.
85. Boudina S, Sena S, Theobald H, Sheng X, Wright JJ, Hu XX, et al. Mitochondrial energetics in the heart in obesity-related diabetes: direct evidence for increased uncoupled respiration and activation of uncoupling proteins. Diabetes. 2007;56(10):2457-66.
86. Holmstrom MH, Iglesias-Gutierrez E, Zierath JR, Garcia-Roves PM. Tissue-specific control of mitochondrial respiration in obesity-related insulin resistance and diabetes. Am J Physiol Endocrinol Metab. 2012;302(6):E731-9.
87. Choo HJ, Kim JH, Kwon OB, Lee CS, Mun JY, Han SS, et al. Mitochondria are impaired in the adipocytes of type 2 diabetic mice. Diabetologia. 2006;49(4):784-91.
88. Rong JX, Qiu Y, Hansen MK, Zhu L, Zhang V, Xie M, et al. Adipose mitochondrial biogenesis is suppressed in db/db and high-fat diet-fed mice and improved by rosiglitazone. Diabetes. 2007;56(7):1751-60.
89. Bonnard C, Durand A, Peyrol S, Chanseaume E, Chauvin MA, Morio B, et al. Mitochondrial dysfunction results from oxidative stress in the skeletal muscle of diet-induced insulin-resistant mice. J Clin Invest. 2008;118(2):789-800.
90. Turrens JF. Mitochondrial formation of reactive oxygen species. J Physiol. 2003;552(Pt 2):335-44.
91. Slater TF. Free-radical mechanisms in tissue injury. Biochem J. 1984;222(1):1-15.
92. Cadenas E. Biochemistry of oxygen toxicity. Annu Rev Biochem. 1989;58:79-110.
93. Monig J, Asmus KD, Forni LG, Willson RL. On the reaction of molecular oxygen with thiyl radicals: a re-examination. Int J Radiat Biol Relat Stud Phys Chem Med. 1987;52(4):589-602.
94. Pacher P, Beckman JS, Liaudet L. Nitric oxide and peroxynitrite in health and disease. Physiol Rev. 2007;87(1):315-424.
95. Chen SX, Schopfer P. Hydroxyl-radical production in physiological reactions. A novel function of peroxidase. Eur J Biochem. 1999;260(3):726-35.
96. Brand MD. Mitochondrial Generation of Superoxide and Hydrogen Peroxide as the Source of Mitochondrial Redox Signaling. Free Radic Biol Med. 2016.

97. St-Pierre J, Buckingham JA, Roebuck SJ, Brand MD. Topology of superoxide production from different sites in the mitochondrial electron transport chain. J Biol Chem. 2002;277(47):44784-90.
98. Hoeldtke RD, Bryner KD, McNeill DR, Warehime SS, Van Dyke K, Hobbs G. Oxidative stress and insulin requirements in patients with recent-onset type 1 diabetes. J Clin Endocrinol Metab. 2003;88(4):1624-8.
99. Marra G, Cotroneo P, Pitocco D, Manto A, Di Leo MA, Ruotolo V, et al. Early increase of oxidative stress and reduced antioxidant defenses in patients with uncomplicated type 1 diabetes: a case for gender difference. Diabetes Care. 2002;25(2):370-5.
100. Collins AR, Raslova K, Somorovska M, Petrovska H, Ondrusova A, Vohnout B, et al. DNA damage in diabetes: correlation with a clinical marker. Free Radic Biol Med. 1998;25(3):373-7.
101. Dandona P, Thusu K, Cook S, Snyder B, Makowski J, Armstrong D, et al. Oxidative damage to DNA in diabetes mellitus. Lancet. 1996;347(8999):444-5.
102. Forbes JM, Coughlan MT, Cooper ME. Oxidative stress as a major culprit in kidney disease in diabetes. Diabetes. 2008;57(6):1446-54.
103. Dugan LL, You YH, Ali SS, Diamond-Stanic M, Miyamoto S, DeCleves AE, et al. AMPK dysregulation promotes diabetes-related reduction of superoxide and mitochondrial function. J Clin Invest. 2013;123(11):4888-99.
104. Coughlan MT, Sharma K. Challenging the dogma of mitochondrial reactive oxygen species overproduction in diabetic kidney disease. Kidney Int. 2016.
105. Brezniceanu ML, Liu F, Wei CC, Chenier I, Godin N, Zhang SL, et al. Attenuation of interstitial fibrosis and tubular apoptosis in db/db transgenic mice overexpressing catalase in renal proximal tubular cells. Diabetes. 2008;57(2):451-9.
106. Cameron NE, Cotter MA, Maxfield EK. Anti-oxidant treatment prevents the development of peripheral nerve dysfunction in streptozotocin-diabetic rats. Diabetologia. 1993;36(4):299-304.
107. Kanwar M, Chan PS, Kern TS, Kowluru RA. Oxidative damage in the retinal mitochondria of diabetic mice: possible protection by superoxide dismutase. Invest Ophthalmol Vis Sci. 2007;48(8):3805-11.
108. Gerdes JM, Davis EE, Katsanis N. The vertebrate primary cilium in development, homeostasis, and disease. Cell. 2009;137(1):32-45.
109. Huangfu D, Liu A, Rakeman AS, Murcia NS, Niswander L, Anderson KV. Hedgehog signalling in the mouse requires intraflagellar transport proteins. Nature. 2003;426(6962):83-7.
110. Corbit KC, Aanstad P, Singla V, Norman AR, Stainier DY, Reiter JF. Vertebrate Smoothened functions at the primary cilium. Nature. 2005;437(7061):1018-21.
111. Corbit KC, Shyer AE, Dowdle WE, Gaulden J, Singla V, Chen MH, et al. Kif3a constrains beta-catenin-dependent Wnt signalling through dual ciliary and non-ciliary mechanisms. Nature cell biology. 2008;10(1):70-6.
112. Gerdes JM, Liu Y, Zaghloul NA, Leitch CC, Lawson SS, Kato M, et al. Disruption of the basal body compromises proteasomal function and perturbs intracellular Wnt response. Nature genetics. 2007;39(11):1350-60.
113. Cardenas-Rodriguez M, Irigoin F, Osborn DP, Gascue C, Katsanis N, Beales PL, et al. The Bardet-Biedl syndrome-related protein CCDC28B modulates mTORC2 function and interacts with SIN1 to control cilia length independently of the mTOR complex. Human molecular genetics. 2013;22(20):4031-42.
114. Boehlke C, Kotsis F, Patel V, Braeg S, Voelker H, Bredt S, et al. Primary cilia regulate mTORC1 activity and cell size through Lkb1. Nature cell biology. 2010;12(11):1115-22.
115. Zimmerman K, Yoder BK. SnapShot: Sensing and Signaling by Cilia. Cell. 2015;161(3):692-2 e1.
116. Pampliega O, Orhon I, Patel B, Sridhar S, Diaz-Carretero A, Beau I, et al. Functional interaction between autophagy and ciliogenesis. Nature. 2013;502(7470):194-200.
117. Wang S, Livingston MJ, Su Y, Dong Z. Reciprocal regulation of cilia and autophagy via the MTOR and proteasome pathways. Autophagy. 2015;11(4):607-16.
118. Bisgrove BW, Yost HJ. The roles of cilia in developmental disorders and disease. Development. 2006;133(21):4131-43.
119. Rosenbaum JL, Moulder JE, Ringo DL. Flagellar elongation and shortening in Chlamydomonas. The use of cycloheximide and colchicine to study the synthesis and assembly of flagellar proteins. J Cell Biol. 1969;41(2):600-19.
120. Hsiao YC, Tuz K, Ferland RJ. Trafficking in and to the primary cilium. Cilia. 2012;1(1):4.
121. Czarnecki PG, Shah JV. The ciliary transition zone: from morphology and molecules to medicine. Trends in cell biology. 2012;22(4):201-10.
122. Garcia-Gonzalo FR, Reiter JF. Scoring a backstage pass: mechanisms of ciliogenesis and ciliary access. J Cell Biol. 2012;197(6):697-709.

123. Kee HL, Verhey KJ. Molecular connections between nuclear and ciliary import processes. Cilia. 2013;2(1):11.
124. Broekhuis JR, Leong WY, Jansen G. Regulation of cilium length and intraflagellar transport. International review of cell and molecular biology. 2013;303:101-38.
125. Colicelli J. Human RAS superfamily proteins and related GTPases. Science's STKE : signal transduction knowledge environment. 2004;2004(250):RE13.
126. Fan S, Margolis B. The Ran importin system in cilia trafficking. Organogenesis. 2011;7(3):147-53.
127. Yoshimura S, Egerer J, Fuchs E, Haas AK, Barr FA. Functional dissection of Rab GTPases involved in primary cilium formation. J Cell Biol. 2007;178(3):363-9.
128. Forsythe E, Beales PL. Bardet-Biedl syndrome. European journal of human genetics : EJHG. 2013;21(1):8-13.
129. Beales PL, Elcioglu N, Woolf AS, Parker D, Flinter FA. New criteria for improved diagnosis of Bardet-Biedl syndrome: results of a population survey. Journal of medical genetics. 1999;36(6):437-46.
130. Green JS, Parfrey PS, Harnett JD, Farid NR, Cramer BC, Johnson G, et al. The cardinal manifestations of Bardet-Biedl syndrome, a form of Laurence-Moon-Biedl syndrome. N Engl J Med. 1989;321(15):1002-9.
131. Waters AM, Beales PL. Ciliopathies: an expanding disease spectrum. Pediatr Nephrol. 2011;26(7):1039-56.
132. Li G, Vega R, Nelms K, Gekakis N, Goodnow C, McNamara P, et al. A role for Alstrom syndrome protein, alms1, in kidney ciliogenesis and cellular quiescence. PLoS Genet. 2007;3(1):e8.
133. Marshall JD, Bronson RT, Collin GB, Nordstrom AD, Maffei P, Paisey RB, et al. New Alstrom syndrome phenotypes based on the evaluation of 182 cases. Arch Intern Med. 2005;165(6):675-83.
134. Winyard P, Jenkins D. Putative roles of cilia in polycystic kidney disease. Biochim Biophys Acta. 2011;1812(10):1256-62.
135. Willey CJ, Blais JD, Hall AK, Krasa HB, Makin AJ, Czerwiec FS. Prevalence of autosomal dominant polycystic kidney disease in the European Union. Nephrol Dial Transplant. 2016.
136. Pietrzak-Nowacka M, Safranow K, Byra E, Nowosiad M, Marchelek-Mysliwiec M, Ciechanowski K. Glucose metabolism parameters during an oral glucose tolerance test in patients with autosomal dominant polycystic kidney disease. Scandinavian journal of clinical and laboratory investigation. 2010;70(8):561-7.
137. Vareesangthip K, Tong P, Wilkinson R, Thomas TH. Insulin resistance in adult polycystic kidney disease. Kidney Int. 1997;52(2):503-8.
138. Karbowski M, Arnoult D, Chen H, Chan DC, Smith CL, Youle RJ. Quantitation of mitochondrial dynamics by photolabeling of individual organelles shows that mitochondrial fusion is blocked during the Bax activation phase of apoptosis. J Cell Biol. 2004;164(4):493-9.
139. Jones DP. Determination of pyridine dinucleotides in cell extracts by high-performance liquid chromatography. J Chromatogr. 1981;225(2):446-9.
140. Lowry OH, Rosebrough NJ, Farr AL, Randall RJ. Protein measurement with the Folin phenol reagent. J Biol Chem. 1951;193(1):265-75.
141. Bellin C, de Wiza DH, Wiernsperger NF, Rosen P. Generation of reactive oxygen species by endothelial and smooth muscle cells: influence of hyperglycemia and metformin. Horm Metab Res. 2006;38(11):732-9.
142. Ihnat MA, Thorpe JE, Kamat CD, Szabo C, Green DE, Warnke LA, et al. Reactive oxygen species mediate a cellular 'memory' of high glucose stress signalling. Diabetologia. 2007;50(7):1523-31.
143. Inoguchi T, Li P, Umeda F, Yu HY, Kakimoto M, Imamura M, et al. High glucose level and free fatty acid stimulate reactive oxygen species production through protein kinase C--dependent activation of NAD(P)H oxidase in cultured vascular cells. Diabetes. 2000;49(11):1939-45.
144. Xiao X, Dong Y, Zhong J, Cao R, Zhao X, Wen G, et al. Adiponectin protects endothelial cells from the damages induced by the intermittent high level of glucose. Endocrine. 2011;40(3):386-93.
145. Paltauf-Doburzynska J, Malli R, Graier WF. Hyperglycemic conditions affect shape and Ca2+ homeostasis of mitochondria in endothelial cells. J Cardiovasc Pharmacol. 2004;44(4):423-36.
146. Yu T, Robotham JL, Yoon Y. Increased production of reactive oxygen species in hyperglycemic conditions requires dynamic change of mitochondrial morphology. Proc Natl Acad Sci U S A. 2006;103(8):2653-8.

147. Al-Kafaji G, Sabry MA, Skrypnyk C. Time-course effect of high-glucose-induced reactive oxygen species on mitochondrial biogenesis and function in human renal mesangial cells. Cell Biol Int. 2016;40(1):36-48.
148. Busik JV, Mohr S, Grant MB. Hyperglycemia-induced reactive oxygen species toxicity to endothelial cells is dependent on paracrine mediators. Diabetes. 2008;57(7):1952-65.
149. Fink BD, Herlein JA, O'Malley Y, Sivitz WI. Endothelial cell and platelet bioenergetics: effect of glucose and nutrient composition. PLoS One. 2012;7(6):e39430.
150. Zhang L, Yu C, Vasquez FE, Galeva N, Onyango I, Swerdlow RH, et al. Hyperglycemia alters the schwann cell mitochondrial proteome and decreases coupled respiration in the absence of superoxide production. J Proteome Res. 2010;9(1):458-71.
151. Chiong M, Parra V, Eisner V, Ibarra C, Maldonado C, Criollo A, et al. Parallel activation of Ca(2+)-induced survival and death pathways in cardiomyocytes by sorbitol-induced hyperosmotic stress. Apoptosis : an international journal on programmed cell death. 2010;15(8):887-903.
152. Brocker C, Thompson DC, Vasiliou V. The role of hyperosmotic stress in inflammation and disease. Biomol Concepts. 2012;3(4):345-64.
153. Brem H, Tomic-Canic M. Cellular and molecular basis of wound healing in diabetes. The Journal of clinical investigation. 2007;117(5):1219-22.
154. Rutter GA, Burnett P, Rizzuto R, Brini M, Murgia M, Pozzan T, et al. Subcellular imaging of intramitochondrial Ca2+ with recombinant targeted aequorin: significance for the regulation of pyruvate dehydrogenase activity. Proc Natl Acad Sci U S A. 1996;93(11):5489-94.
155. Sakata N, Chan NK, Ostrowski RP, Chrisler J, Hayes P, Kim S, et al. Hyperbaric oxygen therapy improves early posttransplant islet function. Pediatr Diabetes. 2010;11(7):471-8.
156. Vijayasarathy C, Damle S, Prabu SK, Otto CM, Avadhani NG. Adaptive changes in the expression of nuclear and mitochondrial encoded subunits of cytochrome c oxidase and the catalytic activity during hypoxia. Eur J Biochem. 2003;270(5):871-9.
157. Heerlein K, Schulze A, Hotz L, Bartsch P, Mairbaurl H. Hypoxia decreases cellular ATP demand and inhibits mitochondrial respiration of a549 cells. Am J Respir Cell Mol Biol. 2005;32(1):44-51.
158. Kulkarni AC, Kuppusamy P, Parinandi N. Oxygen, the lead actor in the pathophysiologic drama: enactment of the trinity of normoxia, hypoxia, and hyperoxia in disease and therapy. Antioxid Redox Signal. 2007;9(10):1717-30.
159. Zhu L, Wang Q, Zhang L, Fang Z, Zhao F, Lv Z, et al. Hypoxia induces PGC-1alpha expression and mitochondrial biogenesis in the myocardium of TOF patients. Cell Res. 2010;20(6):676-87.
160. Gutsaeva DR, Carraway MS, Suliman HB, Demchenko IT, Shitara H, Yonekawa H, et al. Transient hypoxia stimulates mitochondrial biogenesis in brain subcortex by a neuronal nitric oxide synthase-dependent mechanism. J Neurosci. 2008;28(9):2015-24.
161. Hanley PJ, Daut J. K(ATP) channels and preconditioning: a re-examination of the role of mitochondrial K(ATP) channels and an overview of alternative mechanisms. J Mol Cell Cardiol. 2005;39(1):17-50.
162. Wang Y, Wang S, Harvat T, Kinzer K, Zhang L, Feng F, et al. Diazoxide, a K(ATP) channel opener, prevents ischemia-reperfusion injury in rodent pancreatic islets. Cell Transplant. 2015;24(1):25-36.
163. Huang Q, Bu S, Yu Y, Guo Z, Ghatnekar G, Bu M, et al. Diazoxide prevents diabetes through inhibiting pancreatic beta-cells from apoptosis via Bcl-2/Bax rate and p38-beta mitogen-activated protein kinase. Endocrinology. 2007;148(1):81-91.
164. Ritzel RA, Hansen JB, Veldhuis JD, Butler PC. Induction of beta-cell rest by a Kir6.2/SUR1-selective K(ATP)-channel opener preserves beta-cell insulin stores and insulin secretion in human islets cultured at high (11 mM) glucose. J Clin Endocrinol Metab. 2004;89(2):795-805.
165. Hausenloy D, Wynne A, Duchen M, Yellon D. Transient mitochondrial permeability transition pore opening mediates preconditioning-induced protection. Circulation. 2004;109(14):1714-7.
166. Rahmouni K, Fath MA, Seo S, Thedens DR, Berry CJ, Weiss R, et al. Leptin resistance contributes to obesity and hypertension in mouse models of Bardet-Biedl syndrome. J Clin Invest. 2008;118(4):1458-67.
167. Feuillan PP, Ng D, Han JC, Sapp JC, Wetsch K, Spaulding E, et al. Patients with Bardet-Biedl syndrome have hyperleptinemia suggestive of leptin resistance. J Clin Endocrinol Metab. 2011;96(3):E528-35.
168. Kim JC, Badano JL, Sibold S, Esmail MA, Hill J, Hoskins BE, et al. The Bardet-Biedl protein BBS4 targets cargo to the pericentriolar region and is required for microtubule anchoring and cell cycle progression. Nature genetics. 2004;36(5):462-70.
169. Kulkarni RN, Bruning JC, Winnay JN, Postic C, Magnuson MA, Kahn CR. Tissue-specific knockout of the insulin receptor in pancreatic beta cells creates an insulin secretory defect similar to that in type 2 diabetes. Cell. 1999;96(3):329-39.

170. Leibiger B, Leibiger IB, Moede T, Kemper S, Kulkarni RN, Kahn CR, et al. Selective insulin signaling through A and B insulin receptors regulates transcription of insulin and glucokinase genes in pancreatic beta cells. Molecular cell. 2001;7(3):559-70.
171. Szewczyk A, Wojtczak L. Mitochondria as a pharmacological target. Pharmacol Rev. 2002;54(1):101-27.
172. Gilkerson RW, Selker JM, Capaldi RA. The cristal membrane of mitochondria is the principal site of oxidative phosphorylation. FEBS letters. 2003;546(2-3):355-8.
173. Umberger NL, Caspary T. Ciliary transport regulates PDGF-AA/alphaalpha signaling via elevated mammalian target of rapamycin signaling and diminished PP2A activity. Molecular biology of the cell. 2015;26(2):350-8.
174. Broekhuis JR, Verhey KJ, Jansen G. Regulation of cilium length and intraflagellar transport by the RCK-kinases ICK and MOK in renal epithelial cells. PLoS One. 2014;9(9):e108470.
175. Yuan S, Li J, Diener DR, Choma MA, Rosenbaum JL, Sun Z. Target-of-rapamycin complex 1 (Torc1) signaling modulates cilia size and function through protein synthesis regulation. Proc Natl Acad Sci U S A. 2012;109(6):2021-6.
176. Laplante M, Sabatini DM. mTOR signaling at a glance. Journal of cell science. 2009;122(Pt 20):3589-94.
177. Lu L, Hackett SF, Mincey A, Lai H, Campochiaro PA. Effects of different types of oxidative stress in RPE cells. J Cell Physiol. 2006;206(1):119-25.
178. Arnaiz O, Malinowska A, Klotz C, Sperling L, Dadlez M, Koll F, et al. Cildb: a knowledgebase for centrosomes and cilia. Database : the journal of biological databases and curation. 2009;2009:bap022.
179. Kim JI, Kim J, Jang HS, Noh MR, Lipschutz JH, Park KM. Reduction of oxidative stress during recovery accelerates normalization of primary cilia length that is altered after ischemic injury in murine kidneys. Am J Physiol Renal Physiol. 2013;304(10):F1283-94.
180. Sharma K. Obesity and Diabetic Kidney Disease: Role of Oxidant Stress and Redox Balance. Antioxid Redox Signal. 2016;25(4):208-16.
181. Sharma K, McCue P, Dunn SR. Diabetic kidney disease in the db/db mouse. Am J Physiol Renal Physiol. 2003;284(6):F1138-44.
182. Han YM, Kang GM, Byun K, Ko HW, Kim J, Shin MS, et al. Leptin-promoted cilia assembly is critical for normal energy balance. J Clin Invest. 2014;124(5):2193-7.
183. Kang GM, Han YM, Ko HW, Kim J, Oh BC, Kwon I, et al. Leptin Elongates Hypothalamic Neuronal Cilia via Transcriptional Regulation and Actin Destabilization. J Biol Chem. 2015;290(29):18146-55.
184. D'Erchia AM, Atlante A, Gadaleta G, Pavesi G, Chiara M, De Virgilio C, et al. Tissue-specific mtDNA abundance from exome data and its correlation with mitochondrial transcription, mass and respiratory activity. Mitochondrion. 2015;20:13-21.
185. Picca A, Pesce V, Fracasso F, Joseph AM, Leeuwenburgh C, Lezza AM. A comparison among the tissue-specific effects of aging and calorie restriction on TFAM amount and TFAM-binding activity to mtDNA in rat. Biochim Biophys Acta. 2014;1840(7):2184-91.
186. Paddison PJ, Caudy AA, Bernstein E, Hannon GJ, Conklin DS. Short hairpin RNAs (shRNAs) induce sequence-specific silencing in mammalian cells. Genes & development. 2002;16(8):948-58.
187. Vernochet C, Mourier A, Bezy O, Macotela Y, Boucher J, Rardin MJ, et al. Adipose-specific deletion of TFAM increases mitochondrial oxidation and protects mice against obesity and insulin resistance. Cell metabolism. 2012;16(6):765-76.
188. Jeng JY, Yeh TS, Lee JW, Lin SH, Fong TH, Hsieh RH. Maintenance of mitochondrial DNA copy number and expression are essential for preservation of mitochondrial function and cell growth. J Cell Biochem. 2008;103(2):347-57.
189. Nyengaard JR, Ido Y, Kilo C, Williamson JR. Interactions between hyperglycemia and hypoxia: implications for diabetic retinopathy. Diabetes. 2004;53(11):2931-8.
190. Hehenberger K, Heilborn JD, Brismar K, Hansson A. Inhibited proliferation of fibroblasts derived from chronic diabetic wounds and normal dermal fibroblasts treated with high glucose is associated with increased formation of l-lactate. Wound Repair Regen. 1998;6(2):135-41.
191. Scatena R, Messana I, Martorana GE, Gozzo ML, Lippa S, Maccaglia A, et al. Mitochondrial damage and metabolic compensatory mechanisms induced by hyperoxia in the U-937 cell line. J Biochem Mol Biol. 2004;37(4):454-9.
192. Das KC. Hyperoxia decreases glycolytic capacity, glycolytic reserve and oxidative phosphorylation in MLE-12 cells and inhibits complex I and II function, but not complex IV in isolated mouse lung mitochondria. PLoS One. 2013;8(9):e73358.
193. Gnaiger E, Kuznetsov AV. Mitochondrial respiration at low levels of oxygen and cytochrome c. Biochem Soc Trans. 2002;30(2):252-8.

194. Gerdes JM, Christou-Savina S, Xiong Y, Moede T, Moruzzi N, Karlsson-Edlund P, et al. Ciliary dysfunction impairs beta-cell insulin secretion and promotes development of type 2 diabetes in rodents. Nat Commun. 2014;5:5308.
195. Larsson NG, Wang J, Wilhelmsson H, Oldfors A, Rustin P, Lewandoski M, et al. Mitochondrial transcription factor A is necessary for mtDNA maintenance and embryogenesis in mice. Nature genetics. 1998;18(3):231-6.
196. Goto A, Matsushima Y, Kadowaki T, Kitagawa Y. Drosophila mitochondrial transcription factor A (d-TFAM) is dispensable for the transcription of mitochondrial DNA in Kc167 cells. Biochem J. 2001;354(Pt 2):243-8.
197. Stankov MV, Lucke T, Das AM, Schmidt RE, Behrens GM, German Competence Network HA. Relationship of mitochondrial DNA depletion and respiratory chain activity in preadipocytes treated with nucleoside reverse transcriptase inhibitors. Antiviral therapy. 2007;12(2):205-16.